AUTOMATIC AIRSPACE AVOIDANCE USING ADVANCED FLIGHT CONTROL SYSTEM

A Thesis by

Yakup Gunbatar

Bachelor of Sciences in Aerospace Engineering, Middle East Technical University, 2003

Submitted to the Department of Aerospace Engineering

and the faculty of the Graduate School of

Wichita State University

in partial fulfillment of

the requirements for the degree of

Master of Science

December 2006

AUTOMATIC AIRSPACE AVOIDANCE USING ADVANCED FLIGHT CONTROL SYSTEM

I have examined the final copy of this Thesis for form and content and recommend that it be accepted in partial fulfillment of the requirement for the degree of Master of Science with a major in Aerospace Engineering.

_____

Kamran Rokhsaz, Committee Chair

We have read this Thesis and recommend its acceptance:

_____

James E. Steck, Committee Member

_____

M. Bayram Yildirim, Committee Member

DEDICATION

To my parents

Sadik, Ayten, Selcuk, Sercan, and Aslihan

ACKNOWLEDGEMENTS

I would like to express my sincere thanks and appreciation to my supervisor Prof.Dr. Kamran Rokhsaz for his support, guidance and understanding during the preparation of this thesis.

ABSTRACT

An algorithm is developed and validated for automatic avoidance of restricted airspaces. This method is devised specifically for implementation with an advanced flight control system designed for general aviation application. The algorithm presented here implements two inputs to the aircraft; the bank angle, and the airspeed, while the control system always ensures coordinated maneuvers. Unlike collision avoidance systems, the current method is not designed to serve in an advisory role, but to assume complete control of the aircraft is necessary.

It is demonstrated that in order to implement this technique, the aircraft must be assigned an immediate domain whose size would have to depend on the aircraft performance and flight conditions. The strategy is designed such that as the domain surrounding the aircraft approaches that of the restricted airspace, aircraft control would switch gradually away from the pilot and to the controller, which would initiate an evasive maneuver. The degree of relative control is made dependant on the level of the threat defined by the steepness of trajectory and the extent of the overlap between the aircraft domain and the restricted space. While the algorithm is formulated primarily for avoiding a single zone, its application to multiple zones is also explored.

Application of the method on a light single-engine general aviation aircraft is demonstrated. Simulations are made using a six-degree of freedom model that includes the effects of wind. Results are presented for six cases involving single zones and one case involving of multiple zones. The aircraft is made to approach the restricted zones with various airspeeds and attitudes with and without crosswind. It is shown that the controller can effectively prevent the aircraft from penetrating the prohibited area, while

leaving the pilot some level of control. Recommendations are made to refine the strategy by employing a more sophisticated switching strategy and by implementing a multi-variable optimization of the control inputs.

TABLE OF CONTENTS

TABLE OF CONTENTS (CONT.)

LIST OF TABLES

LIST OF FIGURES

LIST OF FIGURES (CONT.)

LIST OF FIGURES (CONT.)

LIST OF FIGURES (CONT.)

LIST OF FIGURES (CONT.)

NOMENCLATURE

$\vec{a}_c$	Centripetal acceleration
b	Span
c	Chord
C_D	Drag coefficient
C_{D_o}	Drag coefficient at zero lift coefficient
C_{D_α}	$\partial C_D / \partial \alpha$
$C_{D_{\dot{\alpha}}}$	$\left(\partial C_D / \partial \dot{\alpha}\right)\left(2V_\infty / c\right)$
$C_{D_{\delta_e}}$	$\left(\partial C_D / \partial \delta_e\right)$
C_{D_u}	$\partial C_D / \partial \left(u / V_\infty\right)$
C_F	Force coefficient
C_l	Rolling moment coefficient
C_{l_o}	Rolling moment coefficient for zero sideslip angle and zero control surface deflections
C_{l_v}	$\left(\partial C_l / \partial v\right)$
C_{l_β}	$\left(\partial C_l / \partial \beta\right)$
C_{l_p}	$\left(\partial C_l / \partial p\right)\left(2V_\infty / b\right)$
C_{l_r}	$\left(\partial C_l / \partial r\right)\left(2V_\infty / b\right)$
$C_{l_{\delta_r}}$	$\left(\partial C_D / \partial \delta_r\right)$

NOMENCLATURE (CONT.)

$C_{l_{\delta_a}}$	$\left(\partial C_D / \partial \delta_a\right)$
C_{L_o}	Lift coefficient for zero angle of attack
$C_{L_{\delta_e}}$	$\left(\partial C_L / \partial \delta_e\right)$
C_L	Lift coefficient
C_{L_u}	$\partial C_L / \partial\left(u / V_\infty\right)$
C_{L_α}	$\partial C_L / \partial \alpha$
$C_{L_{\dot{\alpha}}}$	$\left(\partial C_L / \partial \dot{\alpha}\right)\left(2V_\infty / c\right)$
C_{L_q}	$\left(\partial C_L / \partial q\right)\left(2V_\infty / c\right)$
$C_{L_{\max}}$	Maximum lift coefficient
$C_{L_{trim}}$	Trim lift coefficient
C_m	Pitching moment coefficient
C_{m_o}	Pitching moment coefficient for zero angle of attack
C_{m_u}	$\partial C_m / \partial\left(u / V_\infty\right)$
C_{m_w}	$\partial C_m / \partial w$
$C_{m_{\dot{w}}}$	$\partial C_m / \partial \dot{w}$
C_{m_q}	$\left(\partial C_m / \partial q\right)\left(2V_\infty / c\right)$
$C_{m_{\delta_e}}$	$\left(\partial C_m / \partial \delta_e\right)$
C_n	Yawing moment coefficient

NOMENCLATURE (CONT.)

C_{n_o}	Yawing moment coefficient for zero sideslip angle and zero control surface deflections
C_{n_v}	$\left(\partial C_n / \partial v\right)$
C_{n_β}	$\left(\partial C_n / \partial \beta\right)$
C_{n_p}	$\left(\partial C_n / \partial p\right)\left(2V_\infty / b\right)$
C_{n_r}	$\left(\partial C_n / \partial r\right)\left(2V_\infty / b\right)$
$C_{n_{\delta_a}}$	$\left(\partial C_n / \partial \delta_a\right)$
$C_{n_{\delta_r}}$	$\left(\partial C_n / \partial \delta_r\right)$
C_x	Force coefficient along X_B axis
C_{x_o}	Force coefficient along X_B axis for zero angle of attack
C_{x_α}	$\partial C_x / \partial \alpha$
$C_{x_{\dot\alpha}}$	$\left(\partial C_x / \partial \dot\alpha\right)\left(2V_\infty / c\right)$
C_{x_u}	$\partial C_x / \partial\left(u / V_\infty\right)$
C_{x_w}	$\partial C_x / \partial w$
$C_{x_{\dot w}}$	$\left(\partial C_x / \partial \dot w\right)\left(2V_\infty / c\right)$
$C_{x_{\delta_e}}$	$\left(\partial C_x / \partial \delta_e\right)$
C_y	Side force coefficient

NOMENCLATURE (CONT.)

C_{y_o}	Side force coefficient for zero sideslip angle and zero control surface deflections
C_{y_v}	$\left(\partial C_y / \partial v\right)$
C_{y_β}	$\left(\partial C_y / \partial \beta\right)$
C_{y_p}	$\left(\partial C_y / \partial p\right)\left(2V_\infty / b\right)$
C_{y_r}	$\left(\partial C_y / \partial r\right)\left(2V_\infty / b\right)$
$C_{y_{\delta_r}}$	$\left(\partial C_y / \partial \delta_r\right)$
$C_{y_{\delta_a}}$	$\left(\partial C_y / \partial \delta_a\right)$
C_z	Force coefficient along Z_B-axis
C_{z_o}	Force coefficient along Z_B-axis for zero angle of attack
C_{z_α}	$\partial C_z / \partial \alpha$
$C_{z_{\dot\alpha}}$	$\left(\partial C_z / \partial \dot\alpha\right)\left(2V_\infty / c\right)$
C_{z_u}	$\partial C_z / \partial \left(u / V_\infty\right)$
C_{z_w}	$\partial C_z / \partial w$
$C_{z_{\dot w}}$	$\left(\partial C_z / \partial \dot w\right)\left(2V_\infty / c\right)$
C_{z_q}	$\left(\partial C_z / \partial q\right)\left(2V_\infty / c\right)$
$C_{z_{\delta_e}}$	$\left(\partial C_z / \partial \delta_e\right)$

NOMENCLATURE (CONT.)

$F_{A_x}, F_{A_y}, F_{A_z}$	Aerodynamic force components along $X_B Y_B Z_B$
$F_{T_x}, F_{T_y}, F_{T_z}$	Thrust force components along $X_B Y_B Z_B$
$F_o(O)$	Earth-fixed frame
$F_b(C)$	Body-fixed frame
$\vec{F}$	Force
$\vec{g}$	Acceleration of gravity
h	Altitude
h_T	Restricted zone's ceiling
I_{xx}, I_{yy}, I_{zz}	Aircraft moments of inertia about $X_B Y_B Z_B$
I_{zx}	Aircraft product of inertia about $X_B Y_B Z_B$
$\vec{l}$	Distance vector from aircraft to center of a restricted area
l_{decel}	Required distance to slow down the aircraft from its flight speed to 170 ft/s
L_A, M_A, N_A	Aerodynamic moment components about $X_B Y_B Z_B$
L_T, M_T, N_T	Thrust moment components about $X_B Y_B Z_B$
m	Aircraft mass
$\vec{M}$	Moment
n	Load factor, the ratio of an external load to the weight of the aircraft
$n_{structural}$	Structural load factor
P, Q, R	Aircraft angular velocity components about $X_B Y_B Z_B$

NOMENCLATURE (CONT.)

P_w, Q_w, R_w	Wind angular velocity components about $X_B Y_B Z_B$
p, q, r	Perturbed values of P, Q, R
P_{PC}	Pilot command penalty function
P_{CC}	Controller command penalty function
$\vec{r}$	Vector which defines the position of any mass element dm with respect to body-fixed frame
$\vec{r}_p$	Vector which defines the position of any mass element dm with respect to Earth-fixed frame
$\vec{r}_c$	Vector which defines the position of center of the gravity of the aircraft with respect to Earth-fixed frame
q_∞	Dynamic pressure, $q_\infty = 0.5\rho V_\infty^{\ 2}$
R_{sf}	Safety margin
R_T	Radius of restricted zone
R_{AC}	Radius of aircraft domain
S	Area
U, V, W	Velocity components of aircraft along $X_B Y_B Z_B$
U_w, V_w, W_w	Wind velocity components along $X_B Y_B Z_B$
u, v, w	Perturbed values of U, V, W
V_∞	Free stream velocity
$\vec{V}_{wind}$	Wind linear velocity

NOMENCLATURE (CONT.)

$\vec{V}_{AC}$	Aircraft velocity with respect to inertial frame
$X_E Y_E Z_E$	Earth-fixed frame axes set
$X_B Y_B Z_B$	Body-fixed frame axes set

Greek Symbols

α	Angle of attack
$\dot{\alpha}$	Rate of change of angle of attack
β	Sideslip angle
$\dot{\beta}$	Rate of change of sideslip angle
ζ	Minimum angle between aircraft velocity vector and distance vector defined in Earth-fixed frame
ξ	Wind angle
δ_a	Aileron deflection angle
δ_e	Elevator deflection angle
δ_r	Rudder deflection angle
ρ	Air density
φ	Bank angle command
φ_{PC}	Pilot bank angle command
φ_{CC}	Controller bank angle command
Θ	Pitch angle
Φ	Roll angle

NOMENCLATURE (CONT.)

Ψ	Yaw angle
$\vec{\omega}_{wind}$	Wind angular velocity

Abbreviations

AFCS	Advanced Flight Control System
CFIT	Controlled Flight Into Terrain
GCAS	Ground Collision Avoidance System
SafAS	Safety Augmentation System
TCAS	Traffic Alert and Collision Avoidance Systems

CHAPTER 1

INTRODUCTION

With the advent of hijacking, the importance of the pilot's authority in aircraft control became controversial. As long as the control of the aircraft is in the hands of the right person, there is no problem. However, if aircraft is hijacked or controlled by malevolent people, it can play the role of a powerful weapon like a missile. Therefore, it is easy to imagine cases where the pilot's authority must be diminished in favor of some other form of aircraft control to prevent using the aircraft as a weapon. Some examples are flying over government centers, military areas, nuclear power plants, etc. that are surrounded by no-fly zones.

The concepts of restricted airspace and temporary flight restriction in sensitive areas are not new in civil aviation. However, after the events of September 11, 2001, preventing penetration of such airspace has assumed a much higher importance in the interest of security. Although pilot training can help avert such incursions, novice pilots occasionally breach the boundaries of such regions, resulting in a great deal of alarm, expense, and inconvenience.[1] The Federal Aviation Administration reported about 3,400 violations of restricted airspace from September 12, 2001, to December 31, 2004, most of which were committed by general aviation pilots.[2]

The aircraft industry has always been searching for means of minimizing the risk of direct flying into restricted zones or aircraft collisions. There are examples of systems developed for this purpose, some of which are used in transport aircraft. However, these systems act in an advisory role and only recommend the required maneuver to the pilot to

prevent collision or penetrating of restricted areas. Ground-Proximity-Warning-System, Enhanced-Ground-Proximity-Warning-System, Traffic-alert-and-Collision-Avoidance-System are some examples to these types of devices. [3]

Especially after September 11 attacks on the World Trade Center in New York, avoidance systems that would take the control from pilot or modify the pilot's input to refrain from collision or the threat of Controlled Flight Into Terrain (CFIT) became the subject of new research.[4, 5] The Automatic Ground Collision Avoidance System (Auto-GCAS) is one example.[6] This is an experimental safety system for military aircraft to prevent CFIT. In this scheme, a maximum 5-g pull-up maneuver is initiated automatically when the system determines that an escape maneuver is needed within 5 seconds to stay away from terrain. However, if flight path is pointed above the threatening terrain, Auto-GCAS leaves the control to the pilot. The Robolander System is another approach relying on taking the control from the pilot. [7, 8] This system is activated by the pilot in an emergency such as hijacking. This approach relies on transferring of the control to a ground controller to take the aircraft to a predestined area. Robolander System uses a digital ground-to-air data link. Owing to financial implications and the very strict safety requirements for a ground-to-air data link these types of systems have not been employed yet.

In late 2001, Edward A. Lee[9] proposed the concept of "Soft Walls" in which the control of an aircraft would be shifted away gently from the pilot and on to the flight control system in the event of approaching a no-fly zone. The system, as envisioned in this article was for application in airliners and would rely on the aircraft carrying a three-dimensional model of the Earth, annotated with the topology of the surface. In his

proposal, each restricted airspace would be surrounded by a soft boundary which would trigger the safety system in case of penetration by an aircraft. While this article outlined the ideas governing such a system, it was void of any specific theoretical formulation. The first formulations were offered by Cataldo.[10, 11] Fundamentally, this system works by adding a bias to the pilot input. A pilot approaching a restricted zone while trying to hold steady will be turned away from the zone until it is safe to let the aircraft fly straight. A pilot preferring to turn away faster can do so. A pilot trying to enter the restricted zone will be unsuccessful. In Ref. 10, the author presented the two-dimensional form of the scheme in which the aircraft was treated as a point mass with heading rate and speed as the input. The motion was considered to be planar and the restricted airspace was represented by a flat wall. In this article, the authors introduced some of the fundamental aspects of such systems, including control blending and criticality measures. In Ref. 11, the author focused on evading of a restricted zone as a collision avoidance issue, adapted from the method presented in Ref. 12. The aircraft was again modeled as a point mass with the three degrees of freedom (i.e. position vector and heading angle). The speed was assumed to be constant, so the only control input would be the change in the heading.

Another approach in controlling the aircraft in case of emergency is called Safety Augmentation System (SafAS), developed at Delft Aerospace.[13] This arrangement, designed for commercial aircraft is an on-board system avoiding intrusion of restricted zones via warning the pilot ahead of time. Interface with the pilot is applied through the communication channels which are aural, visual and haptic. This system warns the pilot concerning the possibility of intrusion of restricted zone, and if pilot does not respond, system takes over full control and banks the aircraft away from the zone boundary.

In all of the above approaches, the emphasis was placed on applications in the military and or airline transport environments. In such applications, the economics are of a different scale from those of general aviation industry that is the main focus of this thesis. Specific attention is paid here to keeping the cost to a minimum by not employing systems requiring multiple levels of redundancy. Of specific interest is implementation of an automatic avoidance system in the context of Advanced Flight Control System (AFCS).[14, 15] This system was aimed at making flying more acceptable for the general public by reducing the labor and cost intensity of flight training. It is natural to expect that such systems would attract less experienced pilots, which in turn increases the possibility of their inadvertent penetration of restricted airspaces. Therefore, safeguards are needed to assist the pilots in avoiding such incidents.

The goal of this thesis is to offer a system in conjunction with advanced flight control system to keep a general aviation aircraft away from restricted zones. Differently from other studies explained above, airspace avoidance system presented here has two inputs to the aircraft. One of them is the bank angle required for a coordinated level turn, while the second one is the velocity command. The technique borrows certain elements from Traffic Alert and Collision Avoidance Systems (TCAS). The aircraft is assigned an immediate domain whose size depends on the aircraft performance and flight conditions. As the domain surrounding the aircraft begins to overlap with the restricted airspace, aircraft control is switched gradually away from the pilot and to that of the controller, which undertakes an evasive maneuver. The degree of relative control is made dependant on the steepness of approach and the extent of the overlap between the aircraft domain and the restricted space. With this aim, the algorithm is developed first for avoidance of

a single zone. Later, the algorithm is modified to handle simultaneous multiple zones. Furthermore, wind effect is also taken into account in the control system.

The algorithms are implemented in Matlab/Simulink™ environment for validation. Results are presented from simulation for a number of single zone maneuvers and one case in the presence of multiple zones. A light single-engine general aviation aircraft is modeled in six degrees of freedom. The aircraft is made to approach the restricted zones with various airspeeds and attitudes with and without crosswind. It is shown that the controller effectively prevents the aircraft from penetrating the prohibited area, while leaving the pilot some level of control.

The above material will be presented in the following order. Chapter 2 is dedicated to the development of the equations of motion. Although the bulk of the programming was accomplished during previous phases of this project, the effect of wind was never built into the equations of motion. This is shown in detail in Chapter 2. The details of the avoidance algorithm are presented in Chapter 3, while the results are presented and discussed in Chapter 4.

CHAPTER 2

EQUATIONS OF MOTION & WIND EFFECT

2.1. Introduction

The aircraft is assumed to be a rigid-body. Moreover, equations of motion are expressed in body-fixed axis system and Earth is taken to be a fixed point in space. The motion of the aircraft is described via twelve non-linear equations, composed of three each for forces, moments, kinematics, and Euler equations.

2.2. The Equations of Motion of a Rigid Body Aircraft

Equations for motion of a rigid aircraft in body-fixed coordinates, developed in Ref. 16, are:

$$m\left(\dot{U} + QW - VR\right) = -mg\sin\Theta + F_{A_x} + F_{T_x} \tag{2.1}$$

$$m\left(\dot{V} + UR - PW\right) = mg\cos\Theta\sin\Phi + F_{A_y} + F_{T_y} \tag{2.2}$$

$$m\left(\dot{W} + PV - UQ\right) = mg\cos\Theta\cos\Phi + F_{A_z} + F_{T_z} \tag{2.3}$$

$$I_{xx}\dot{P} - I_{zx}\left(\dot{R} + PQ\right) - \left(I_{yy} - I_{zz}\right)RQ = L_A + L_T \tag{2.4}$$

$$I_{yy}\dot{Q} - I_{zx}\left(R^2 - P^2\right) - \left(I_{zz} - I_{xx}\right)RP = M_A + M_T \tag{2.5}$$

$$I_{zz}\dot{R} - I_{zx}\left(\dot{P} - QR\right) - \left(I_{xx} - I_{yy}\right)PQ = N_A + N_T \tag{2.6}$$

$$P = \dot{\Phi} - \dot{\Psi}\sin\Theta \tag{2.7}$$

$$Q = \dot{\Theta}\cos\Phi + \dot{\Psi}\cos\Theta\sin\Phi \tag{2.8}$$

$$R = \dot{\Psi}\cos\Theta\cos\Phi - \dot{\Theta}\sin\Phi \tag{2.9}$$

$$\dot{\Psi} = \left(R\cos\Phi + Q\sin\Phi\right)\sec\Theta \tag{2.10}$$

$$\dot{\Theta} = Q\cos\Phi - R\sin\Phi \tag{2.11}$$

$$\dot{\Phi} = P + \left(R\cos\Phi + Q\sin\Phi\right)\tan\Theta \tag{2.12}$$

Through successive Euler rotations, equations of motion in the Earth-fixed coordinates become:

$$\begin{aligned}\dot{X}_E = {} & U\left(\cos\Theta\cos\Psi\right) + V\left(\sin\Phi\sin\Theta\cos\Psi - \cos\Phi\sin\Psi\right) \\ & + W\left(\cos\Phi\sin\Theta\cos\Psi + \sin\Phi\sin\Psi\right)\end{aligned} \tag{2.13}$$

$$\begin{aligned}\dot{Y}_E = {} & U\left(\cos\Theta\sin\Psi\right) + V\left(\sin\Phi\sin\Theta\sin\Psi + \cos\Phi\cos\Psi\right) \\ & + W\left(\cos\Phi\sin\Theta\sin\Psi - \sin\Phi\cos\Psi\right)\end{aligned} \tag{2.14}$$

$$\dot{Z}_E = U\left(-\sin\Theta\right) + V\left(\sin\Phi\cos\Theta\right) + W\left(\cos\Phi\cos\Theta\right) \tag{2.15}$$

2.3. Wind Effect

The Advanced Flight Control System (AFCS) as it stood, did not include the effect of wind. This had to be added to the simulations to ensure proper ground tracking in the presence of wind. The main effect of the wind is on the aerodynamic forces and moments. Thrust forces and moments are also affected by wind if the engine is an air-breathing type. However, in the present research, we are only concerned with the aerodynamic effects. The notation and the associated direction for the wind are shown in Figure 2-1. In this figure, $X_E Y_E Z_E$ is Earth-fixed axis system, $F_o(O)$, while $X_B Y_B Z_B$ stands for body-fixed coordinates, $F_b(C)$. Wind is defined in Earth-fixed frame and has angular and translational velocity components, which are defined as follows:

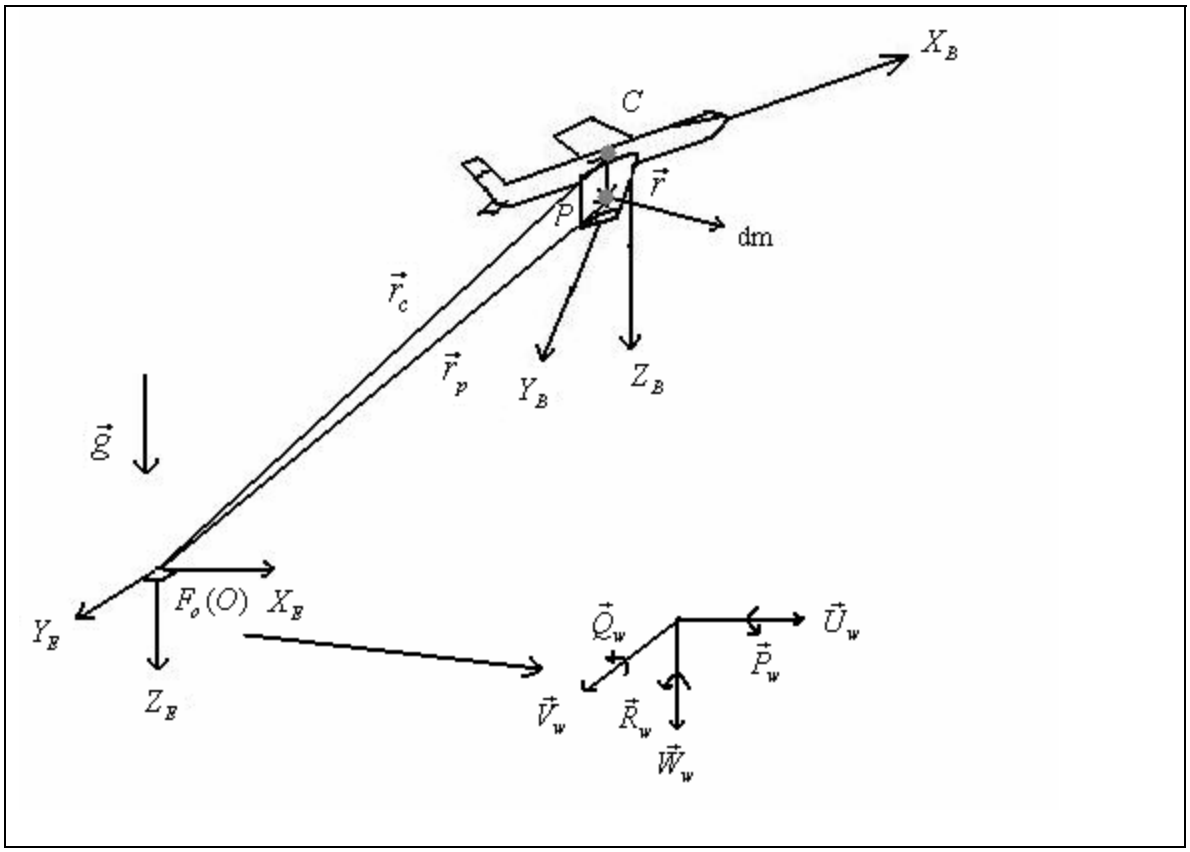

Figure 2-1 Wind described in Earth-fixed frame

$$\vec{V}_{wind} = \begin{bmatrix} \vec{U}_w \\ \vec{V}_w \\ \vec{W}_w \end{bmatrix} \tag{2.16}$$

$$\vec{\omega}_{wind} = \begin{bmatrix} \vec{P}_w \\ \vec{Q}_w \\ \vec{R}_w \end{bmatrix} \tag{2.17}$$

In order to incorporate the effects of wind in the equations of motion, wind velocity must be expressed in the body-fixed coordinate system. This is accomplished using Euler rotations, which results in:

$$\bar{V}_{wind} = \begin{bmatrix} U_{wb} \\ V_{wb} \\ W_{wb} \end{bmatrix} \tag{2.18}$$

$$\bar{V}_{wind} = \begin{bmatrix} U_w \cos\Theta\cos\Psi + V_w \cos\Theta\sin\Psi - W_w \sin\Theta \\ U_w\left(\sin\Phi\sin\Theta\cos\Psi - \cos\Phi\sin\Psi\right) + V_w\left(\sin\Phi\sin\Theta\sin\Psi + \cos\Phi\cos\Psi\right) + W_w\left(\sin\Phi\cos\Theta\right) \\ U_w\left(\cos\Phi\sin\Theta\cos\Psi + \sin\Phi\sin\Psi\right) + V_w\left(\cos\Phi\sin\Theta\sin\Psi - \sin\Phi\cos\Psi\right) + W_w\left(\cos\Phi\cos\Theta\right) \end{bmatrix} \tag{2.19}$$

$$\bar{\omega}_{wind} = \begin{bmatrix} P_{wb} \\ Q_{wb} \\ R_{wb} \end{bmatrix} \tag{2.20}$$

$$\bar{\omega}_{wind} = \begin{bmatrix} P_w \cos\Theta\cos\Psi + Q_w \cos\Theta\sin\Psi - R_w \sin\Theta \\ P_w\left(\sin\Phi\sin\Theta\cos\Psi - \cos\Phi\sin\Psi\right) + Q_w\left(\sin\Phi\sin\Theta\sin\Psi + \cos\Phi\cos\Psi\right) + R_w\left(\sin\Phi\cos\Theta\right) \\ P_w\left(\cos\Phi\sin\Theta\cos\Psi + \sin\Phi\sin\Psi\right) + Q_w\left(\cos\Phi\sin\Theta\sin\Psi - \sin\Phi\cos\Psi\right) + R_w\left(\cos\Phi\cos\Theta\right) \end{bmatrix} \tag{2.21}$$

In the present research, the wind is assumed to be rectilinear and parallel to the Earth's surface. Therefore, its rotational components are neglected. As shown in Figure 2-2, the wind is defined in Earth-fixed frame.

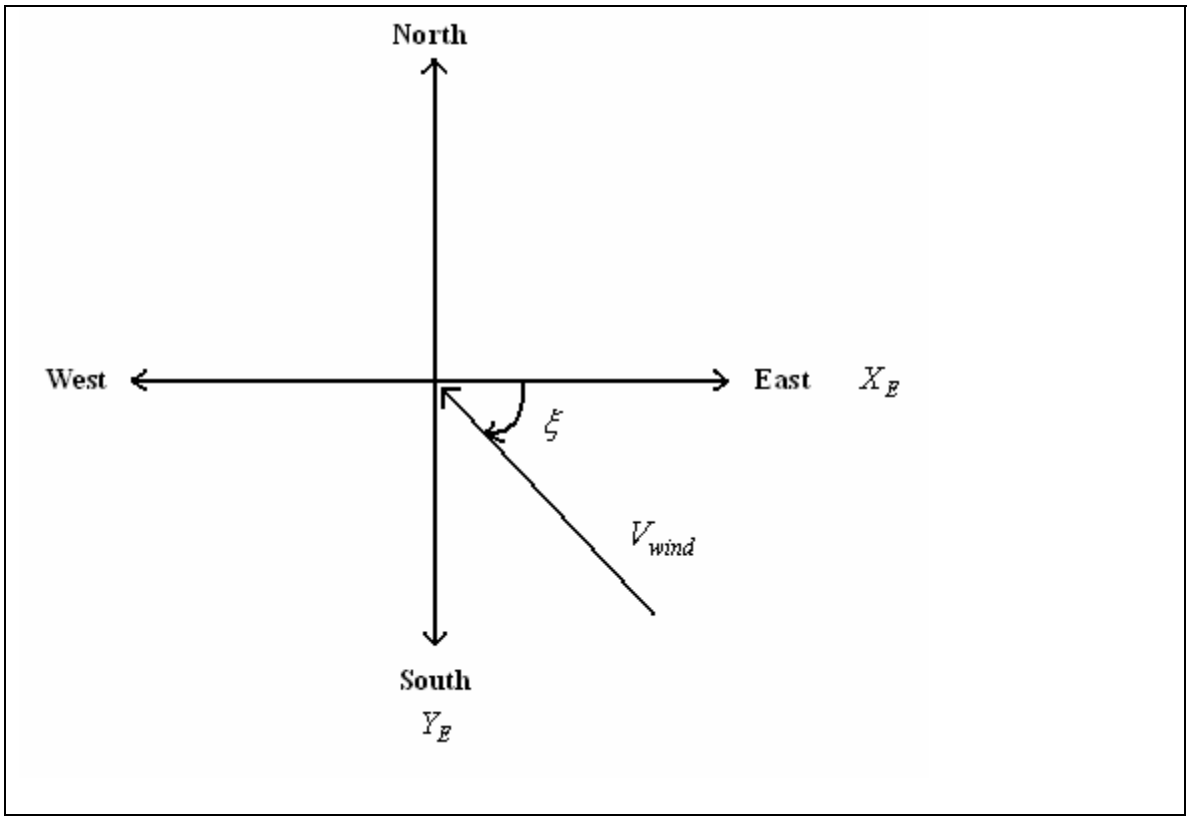

Figure 2-2 Expression of wind in Earth-fixed frame.

2.4. Stability Derivatives

Aerodynamic and thrust forces and moments are expressed in terms of their coefficients as:

$$F = C_F q_\infty S \tag{2.22}$$

$$M = C_M q_\infty S l \tag{2.23}$$

The airspeed of the aircraft can be expressed as a combination of its inertial speed and the wind speed. Consistent with the notation of Reference 16, the inertial speed is assumed to be composed of a steady state term and a small time-dependent perturbation. Therefore:

$$V_\infty = \sqrt{\left(U + u - U_{wb}\right)^2 + \left(V + v - V_{wb}\right)^2 + \left(W + w - W_{wb}\right)^2} \tag{2.24}$$

In Equations (2.25)-(2.30) aerodynamic forces and moments are written with respect to their coefficients:

$$F_{A_x} = C_x q_\infty S \tag{2.25}$$

$$F_{A_y} = C_y q_\infty S \tag{2.26}$$

$$F_{A_z} = C_z q_\infty S \tag{2.27}$$

$$L_A = C_l q_\infty S b \tag{2.28}$$

$$M_A = C_m q_\infty S c \tag{2.29}$$

$$N_A = C_n q_\infty S b \tag{2.30}$$

Aerodynamic coefficients can be expanded via their derivatives vis-à-vis $u, v, w, p, q, r, \dot{w}$ and control deflections consisting of aileron, rudder and elevator.

$$C_x = C_{x_o} + C_{x_u} u + C_{x_w} w + C_{x_{\dot{w}}} \dot{w} + C_{x_{\delta_e}} \delta_e \tag{2.31}$$

$$C_y = C_{y_o} + C_{y_v} v + C_{y_p} p + C_{y_r} r + C_{y_{\delta_r}} \delta_r \tag{2.32}$$

$$C_z = C_{z_o} + C_{z_u} u + C_{z_w} w + C_{z_{\dot{w}}} \dot{w} + C_{z_q} q + C_{z_{\delta_e}} \delta_e \tag{2.33}$$

$$C_l = C_{l_o} + C_{l_v} v + C_{l_p} p + C_{l_r} r + C_{l_{\delta_a}} \delta_a + C_{l_{\delta_r}} \delta_r \tag{2.34}$$

$$C_m = C_{m_o} + C_{m_u} u + C_{m_w} w + C_{m_{\dot{w}}} \dot{w} + C_{m_q} q + C_{m_{\delta_e}} \delta_e \tag{2.35}$$

$$C_n = C_{n_o} + C_{n_v} v + C_{n_p} p + C_{n_r} r + C_{n_{\delta_a}} \delta_a + C_{n_{\delta_r}} \delta_r \tag{2.36}$$

The aerodynamic coefficients, C_x, C_y, C_z, C_l, C_m, and C_n depend on velocity perturbations that are in turn related to wind speed. The effect of the wind on the angle of attack becomes clear when considering:

$$\alpha = \arctan\left(\frac{W + w - W_{wb}}{U + u - U_{wb}}\right) \tag{2.37}$$

resulting in:

$$w = \tan(\alpha)\left(U + u - U_{wb}\right) - \left(W - W_{wb}\right) \tag{2.38}$$

Also, the sideslip angle is given by:

$$\beta = \arctan\left(\frac{V + v - V_{wb}}{\sqrt{\left(U + u - U_{wb}\right)^2 + \left(W + w - W_{wb}\right)^2}}\right) \approx \arctan\left(\frac{V + v - V_{wb}}{U + u - U_{wb}}\right) \tag{2.39}$$

resulting in:

$$v = \tan(\beta)\left(U + u - U_{wb}\right) - \left(V - V_{wb}\right) \tag{2.40}$$

Hence:

$$\dot{\alpha} = \frac{\dfrac{\left(\dot{w}\right)}{\left(U + u - U_{wb}\right)} - \dfrac{\left(W + w - W_{wb}\right)\dot{u}}{\left(U + u - U_{wb}\right)^2}}{1 + \dfrac{\left(W + w - W_{wb}\right)^2}{\left(U + u - U_{wb}\right)^2}} \tag{2.41}$$

and

$$\dot{\beta} = \frac{\frac{(\dot{v})}{(U+u-U_{wb})} - \frac{(V+v-V_{wb})\dot{u}}{(U+u-U_{wb})^2}}{1+\frac{(V+v-V_{wb})^2}{(U+u-U_{wb})^2}} \tag{2.42}$$

Then:

$$C_{x_w} = \frac{\partial C_x}{\partial w} = \frac{\partial C_x}{\partial \alpha}\frac{\partial \alpha}{\partial w} = C_{x_\alpha}\frac{1}{(U+u-U_{wb})\left(1+\frac{(W+w-W_{wb})^2}{(U+u-U_{wb})^2}\right)} \tag{2.43}$$

$$C_{x_w} \cong \frac{1}{U+u-U_{wb}} C_{x_\alpha} \tag{2.44}$$

Since:

$$(U+u-U_{wb})^2 >> (W+w-W_{wb})^2 \tag{2.45}$$

and

$$(U+u-U_{wb})^2 >> (V+v-V_{wb})^2 \tag{2.46}$$

one obtains $\dot{w}$ and $\dot{v}$ as:

$$\dot{w} = \dot{\alpha}(U+u-U_{wb}) \tag{2.47}$$

and

$$\dot{v} = \dot{\beta}(U+u-U_{wb}) \tag{2.48}$$

With the same procedure, stability derivatives take the following forms:

$$C_{y_v} = \frac{1}{U+u-U_{wb}} C_{y_\beta} \tag{2.49}$$

$$C_{z_w} = \frac{1}{U+u-U_{wb}} C_{z_\alpha} \tag{2.50}$$

$$C_{x_{\dot{w}}} = \frac{1}{U + u - U_{wb}} C_{x_{\dot{\alpha}}} \tag{2.51}$$

$$C_{z_{\dot{w}}} = \frac{1}{U + u - U_{wb}} C_{z_{\dot{\alpha}}} \tag{2.52}$$

$$C_{l_v} = \frac{1}{U + u - U_{wb}} C_{l_\beta} \tag{2.53}$$

$$C_{n_v} = \frac{1}{U + u - U_{wb}} C_{n_\beta} \tag{2.54}$$

$$C_{m_w} = \frac{1}{U + u - U_{wb}} C_{m_\alpha} \tag{2.55}$$

$$C_{m_{\dot{w}}} = \frac{1}{U + u - U_{wb}} C_{m_{\dot{\alpha}}} \tag{2.56}$$

The stability derivatives $C_{x_{\dot{\alpha}}}$, $C_{z_{\dot{\alpha}}}$, C_{z_q}, C_{m_q}, and $C_{m_{\dot{\alpha}}}$ are dimensionless, so their respective derivatives are divided by $\frac{c}{2V_\infty}$. Likewise, the stability derivatives C_{y_p}, C_{y_r}, C_{l_p}, C_{l_r}, C_{n_p}, C_{n_r} are made nondimensional by dividing their respective derivatives with $\frac{b}{2V_\infty}$. Whereas C_{x_u} C_{m_u} and C_{z_u} are obtained by dividing the derivatives by $1/V_\infty$. For instance:

$$C_{m_{\dot{\alpha}}} = \frac{1}{\frac{c}{2V_\infty}} C_{m_{\dot{\alpha}}} \tag{2.57}$$

Then:

$$C_x = C_{x_o} + C_{x_u}\frac{u}{V_\infty} + \frac{1}{U+u-U_{wb}} C_{x_\alpha}\left(\tan(\alpha)(U+u-U_{wb})-(W-W_{wb})\right) + C_{x_{\dot\alpha}}\dot\alpha\frac{c}{2V_\infty} + C_{x_{\delta_e}}\delta_e \tag{2.58}$$

$$C_y = C_{y_o} + \frac{1}{U+u-U_{wb}} C_{y_\beta}\left(\tan(\beta)(U+u-U_{wb})-(V-V_{wb})\right) + C_{y_p}p\frac{b}{2V_\infty} + C_{y_r}r\frac{b}{2V_\infty} + C_{y_{\delta_r}}\delta_r \tag{2.59}$$

$$C_z = C_{z_o} + C_{z_u}\frac{u}{V_\infty} + \frac{1}{U+u-U_{wb}} C_{z_\alpha}\left(\tan(\alpha)(U+u-U_{wb})-(W-W_{wb})\right) + C_{z_{\dot\alpha}}\dot\alpha\frac{c}{2V_\infty} + C_{z_q}q\frac{c}{2V_\infty} + C_{z_{\delta_e}}\delta_e \tag{2.60}$$

$$C_l = C_{l_o} + \frac{1}{U+u-U_{wb}} C_{l_\beta}\left(\tan(\beta)(U+u-U_{wb})-(V-V_{wb})\right) + C_{l_p}p\frac{b}{2V_\infty} + C_{l_r}r\frac{b}{2V_\infty} + C_{l_{\delta_a}}\delta_a + C_{l_{\delta_r}}\delta_r \tag{2.61}$$

$$C_m = C_{m_o} + C_{m_u}\frac{u}{V_\infty} + \frac{1}{U+u-U_{wb}} C_{m_\alpha}\left(\tan(\alpha)(U+u-U_{wb})-(W-W_{wb})\right) + C_{m_{\dot\alpha}}\dot\alpha\frac{c}{2V_\infty} + C_{m_q}q\frac{c}{2V_\infty} + C_{m_{\delta_e}}\delta_e \tag{2.62}$$

$$C_n = C_{n_o} + \frac{1}{U+u-U_{wb}} C_{n_\beta}\left(\tan(\beta)(U+u-U_{wb})-(V-V_{wb})\right) + C_{n_p}p\frac{b}{2V_\infty} + C_{n_r}r\frac{b}{2V_\infty} + C_{n_{\delta_a}}\delta_a + C_{n_{\delta_r}}\delta_r \tag{2.63}$$

For small α and β as a matter of experience and convenience the following approximations can be made:

$$\frac{1}{U+u-U_{wb}} C_{x_\alpha}\left(\tan(\alpha)(U+u-U_{wb})-(W-W_{wb})\right) = C_{x_\alpha}\alpha \tag{2.64}$$

$$\frac{1}{U+u-U_{wb}} C_{y_\beta}\left(\tan(\beta)(U+u-U_{wb})-(V-V_{wb})\right) = C_{y_\beta}\beta \tag{2.65}$$

$$\frac{1}{U+u-U_{wb}} C_{z_\alpha} \left(\tan(\alpha)\left(U+u-U_{wb}\right) - \left(W-W_{wb}\right)\right) = C_{z_\alpha}\alpha \tag{2.66}$$

$$\frac{1}{U+u-U_{wb}} C_{l_\beta} \left(\tan(\beta)\left(U+u-U_{wb}\right) - \left(V-V_{wb}\right)\right) = C_{l_\beta}\beta \tag{2.67}$$

$$\frac{1}{U+u-U_{wb}} C_{m_\alpha} \left(\tan(\alpha)\left(U+u-U_{wb}\right) - \left(W-W_{wb}\right)\right) = C_{m_\alpha}\alpha \tag{2.68}$$

$$\frac{1}{U+u-U_{wb}} C_{n_\beta} \left(\tan(\beta)\left(U+u-U_{wb}\right) - \left(V-V_{wb}\right)\right) = C_{n_\beta}\beta \tag{2.69}$$

Therefore, Equations (2.58) to (2.63) become:

$$C_x = C_{x_o} + C_{x_u}\frac{u}{V_\infty} + C_{x_\alpha}\alpha + C_{x_{\dot\alpha}}\dot\alpha\frac{c}{2V_\infty} + C_{x_{\delta_e}}\delta_e \tag{2.70}$$

$$C_y = C_{y_o} + C_{y_\beta}\beta + C_{y_p}p\frac{b}{2V_\infty} + C_{y_r}r\frac{b}{2V_\infty} + C_{y_{\delta_r}}\delta_r \tag{2.71}$$

$$C_z = C_{z_o} + C_{z_u}\frac{u}{V_\infty} + C_{z_\alpha}\alpha + C_{z_{\dot\alpha}}\dot\alpha\frac{c}{2V_\infty} + C_{z_q}q\frac{c}{2V_\infty} + C_{z_{\delta_e}}\delta_e \tag{2.72}$$

$$C_l = C_{l_o} + C_{l_\beta}\beta + C_{l_p}p\frac{b}{2V_\infty} + C_{l_r}r\frac{b}{2V_\infty} + C_{l_{\delta_a}}\delta_a + C_{l_{\delta_r}}\delta_r \tag{2.73}$$

$$C_m = C_{m_o} + C_{m_u}\frac{u}{V_\infty} + C_{m_\alpha}\alpha + C_{m_{\dot\alpha}}\dot\alpha\frac{c}{2V_\infty} + C_{m_q}q\frac{c}{2V_\infty} + C_{m_{\delta_e}}\delta_e \tag{2.74}$$

$$C_n = C_{n_o} + C_{n_\beta}\beta + C_{n_p}p\frac{b}{2V_\infty} + C_{n_r}\mathrm{r}\frac{b}{2V_\infty} + C_{n_{\delta_a}}\delta_a + C_{n_{\delta_r}}\delta_r\,. \tag{2.75}$$

The coefficients C_x and C_z given in Equations (2.70) and (2.71) can be related to C_L and C_D through α, as shown in Figure 2-3.

$$F_{A_x} = C_x q_\infty S = L\sin\alpha - D\cos\alpha \tag{2.76}$$

$$F_{A_z} = C_z q_\infty S = -L\cos\alpha - D\sin\alpha \tag{2.77}$$

Then:

$$C_x = C_L \sin\alpha - C_D \cos\alpha \tag{2.78}$$

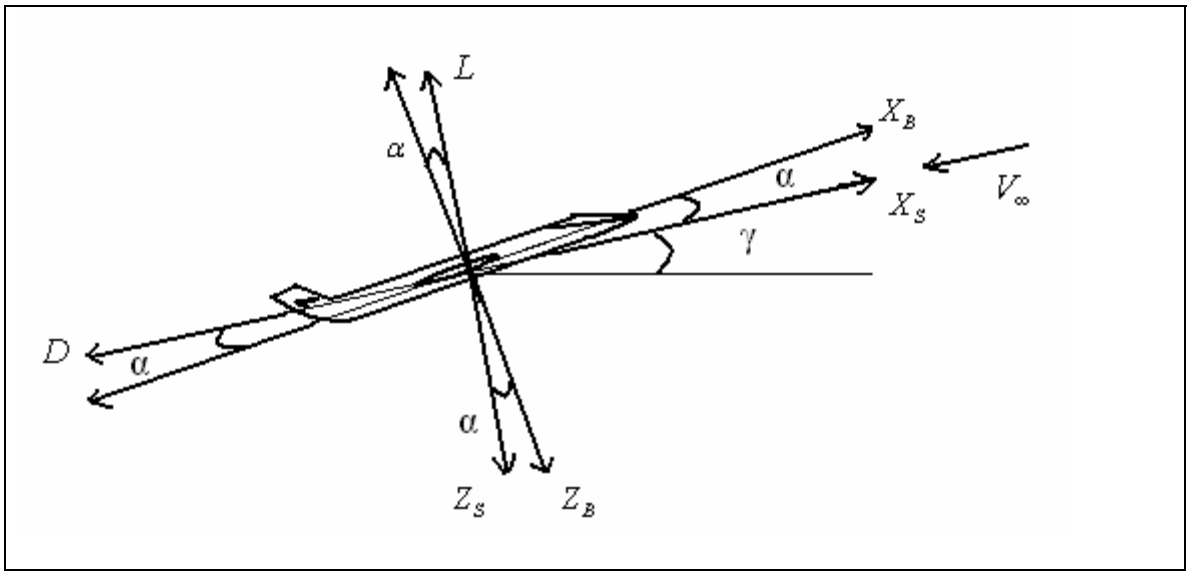

Figure 2-3 Stability and body-fixed axis systems

and

$$C_z = -C_L \cos\alpha - C_D \sin\alpha \tag{2.79}$$

Dynamic pressure includes airspeed. Therefore, aerodynamic forces should include the variation of dynamic pressure with respect to the components of velocity in the body-fixed frame. The effects if the vertical and the side velocity components are included primarily in angle of attack and sideslip angle. However, changes in the forward velocity must be included as perturbations in the magnitude of the velocity, resulting in variations of dynamic pressure. Therefore,

$$\frac{\partial F_{A_x}}{\partial\left(\frac{U}{V_\infty}\right)} = C_{x_u} q_\infty S + C_x q_{\infty_u} S V_\infty \tag{2.80}$$

where:

$$q_{\infty_u} = \rho\left(U - U_{wb}\right) \tag{2.81}$$

$$\rho\left(U - U_{wb}\right)V_{\infty} \approx 2q_{\infty} \tag{2.82}$$

Then:

$$\frac{\partial F_{A_x}}{\partial\left(\frac{U}{V_{\infty}}\right)} = C_{x_u} q_{\infty} S + 2C_x q_{\infty} S \,. \tag{2.83}$$

Using the same approach, the following equations are also obtained:

$$\frac{\partial F_{A_z}}{\partial\left(\frac{U}{V_{\infty}}\right)} = C_{z_u} q_{\infty} S + 2C_z q_{\infty} S \tag{2.84}$$

$$\frac{\partial M_A}{\partial\left(\frac{U}{V_{\infty}}\right)} = C_{m_u} q_{\infty} S + 2C_m q_{\infty} S \,. \tag{2.85}$$

Moreover other stability derivatives can be approximated for small angles as follows:

$$C_{x_o} \approx -C_{D_o} \tag{2.86}$$

$$C_{x_{\delta_e}} \approx -C_{D_{\delta_e}} \tag{2.87}$$

$$C_{z_o} \approx -C_{L_o} \tag{2.88}$$

$$C_{z_{\delta_e}} \approx -C_{L_{\delta_e}} \tag{2.89}$$

$$C_{x_u} \approx -C_{D_u} \tag{2.90}$$

$$C_x \approx -C_D \tag{2.91}$$

$$C_{z_u} \approx -C_{L_u} \tag{2.92}$$

$$C_z \approx -C_L \tag{2.93}$$

$$C_{x_\alpha} \approx \left(C_L - C_{D_\alpha}\right) \tag{2.94}$$

$$C_{x_{\dot{\alpha}}} \approx \left(-C_{D_{\dot{\alpha}}}\right) \tag{2.95}$$

$$C_{z_{\alpha}} \approx \left(-C_{L_{\alpha}} - C_{D}\right) \tag{2.96}$$

$$C_{z_{\dot{\alpha}}} \approx \left(-C_{L_{\dot{\alpha}}}\right) \tag{2.97}$$

$$C_{z_{q}} \approx -C_{L_{q}} \tag{2.98}$$

The effects of the wind, which was described above, were implemented in the simulations that were developed earlier in the process of developing the AFCS. These codes, written in Matlab/Simulink environment, were used to test the restricted airspace avoidance strategies that form the basis of the present thesis.

CHAPTER 3

RESTRICTED ZONE APPROACH

3.1. Introduction

The strategy for automatic avoidance of a restricted airspace is described in this chapter. In the first section, the formulation is limited to that for a single zone. Later, the technique is extended to deal with multiple zones. In the course of developing the single-zone approach, issues such as safety margins and the relative level of control to be assigned to the pilot and the controller, respectively, are discussed. Throughout, the primary aim has been not to take the control away from the pilot, but to minimize his/her authority in entering a restricted zone intentionally.

3.2. Single-Zone Approach

3.2.1. Preliminaries

The strategy described in this section is based on gradual shifting of the control authority away from the pilot and over to a collision avoidance algorithm based on the level of threat associated with the flight path. This level of threat depends on the magnitude and the direction of the aircraft's velocity vector and its proximity relative to the center of the restricted zone. The more eminent the threat is, the stronger the actions will be from the controller.

In the following development, the restricted zone is defined by a cylinder whose floor is centered at (X_T, Y_T, Z_T) with a radius, R_T, extending from surface to a predefined

ceiling, h_T. In most practical cases, the last parameter is larger than the ceiling of a general aviation aircraft. This is the assumption used throughout this document. Therefore, the strategies outlined here do not address cases of approach from above.

A cylinder centered on the aircraft with radius R_{AC} defines the aircraft domain. The parameter, R_{AC}, is the turn radius for a coordinated level turn. For the present research, this parameter was determined for a 45-degree-bank turn at 170 ft/s. These zones are shown schematically in Figure 3-1. This figure also shows the additional parameters that enter the method under discussion. These include, the separation between the centers of the two zones, $\vec{l}$ the aircraft velocity vector, $\vec{V}_{AC}$, and the angle defining the steepness of the approach, ζ.

All maneuvers are forced to be coordinated and the aircraft is assumed to be equipped with the decoupled flight control system described in Ref. 14 and 15.

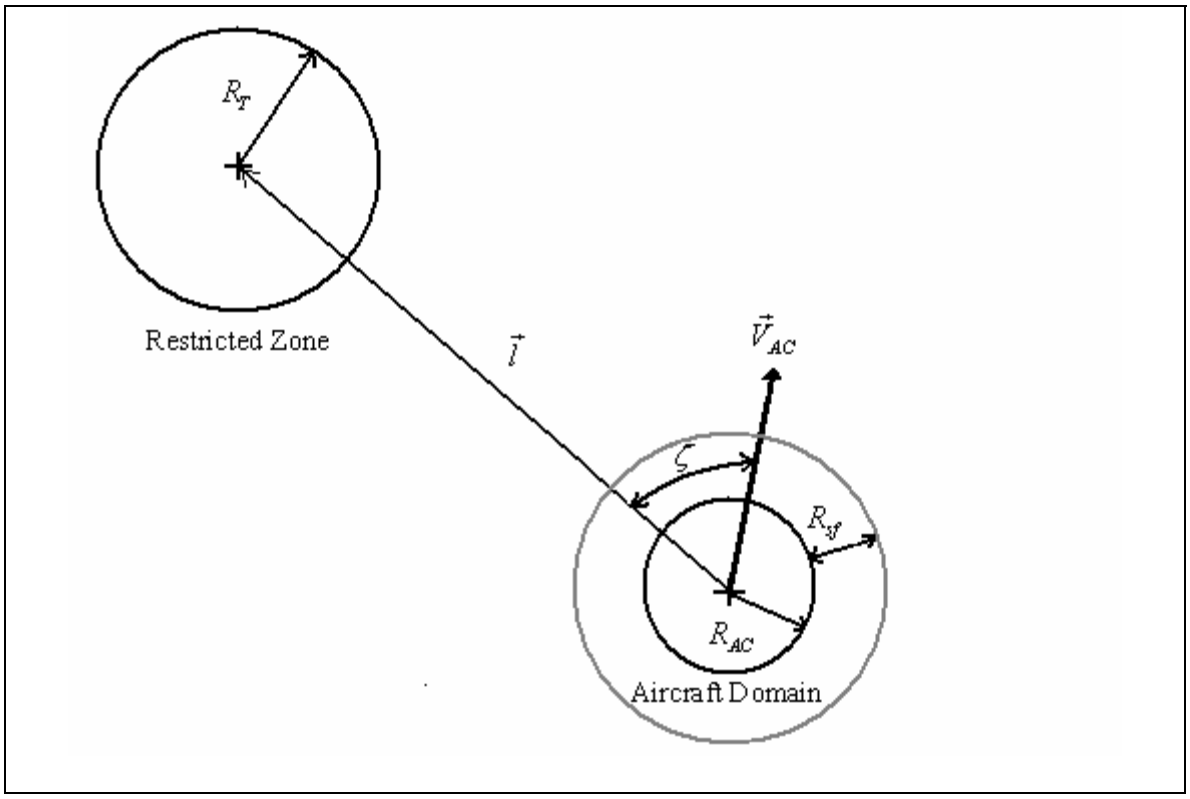

Figure 3-1 Schematic view of the restricted zone and aircraft domain.

The only difference in the present case is that artificial neural networks were not used to compensate for the differences between the aircraft and its inverse model. Therefore, the primary control input is in the form of a commanded bank angle. Later, it will be shown that it may be necessary to also limit the airspeed to keep the turn radius as small as possible.

The aircraft domain must be large enough to allow executing a turn without entering the restricted zone. If the aircraft could be banked from level flight to its maximum bank angle instantaneously, it would be sufficient to let R_{AC} be the same as the turn radius. However, due to the dynamics of the aircraft and the servos, a certain length of time is required for the aircraft to reach its maximum bank angle, starting from level flight. This time depends on the roll response of the aircraft. This can be made proportional to the time to bank to maximum bank angle from the roll approximation. During this time period, the aircraft continues to approach the restricted zone and will be closer to its perimeter that the turn radius by the time it achieves its maximum bank angle. Therefore, as a measure of safety, a small distance is added to the calculated value of R_{AC}, which is termed "safety radius" or R_{sf}. For the aircraft under consideration in this report, the length of this distance was determined by trial and error to be approximately 1000 feet. This parameter also enters in the calculations of the weights of inputs coming from pilot and controller. This penalty function is explained in detail in Section 3.2.3.

3.2.2. Coordinated Turn

The turn radius is that for a coordinated turn at a prescribed bank angle and airspeed. The maneuver is called as coordinated turn when lateral acceleration, $a_{y_{cg}}$ is

zero. This means that, in a coordinated turn the lift force must lie entirely perpendicular to the aircraft's wing span, as in Figure 3-2.

Assuming level flight, from Ref. 17, the turn radius can be approximated by

$$r = \frac{V_{AC}^{\ 2}}{g\sqrt{n^2 - 1}} \tag{3.1}$$

which can be shown to be the same as

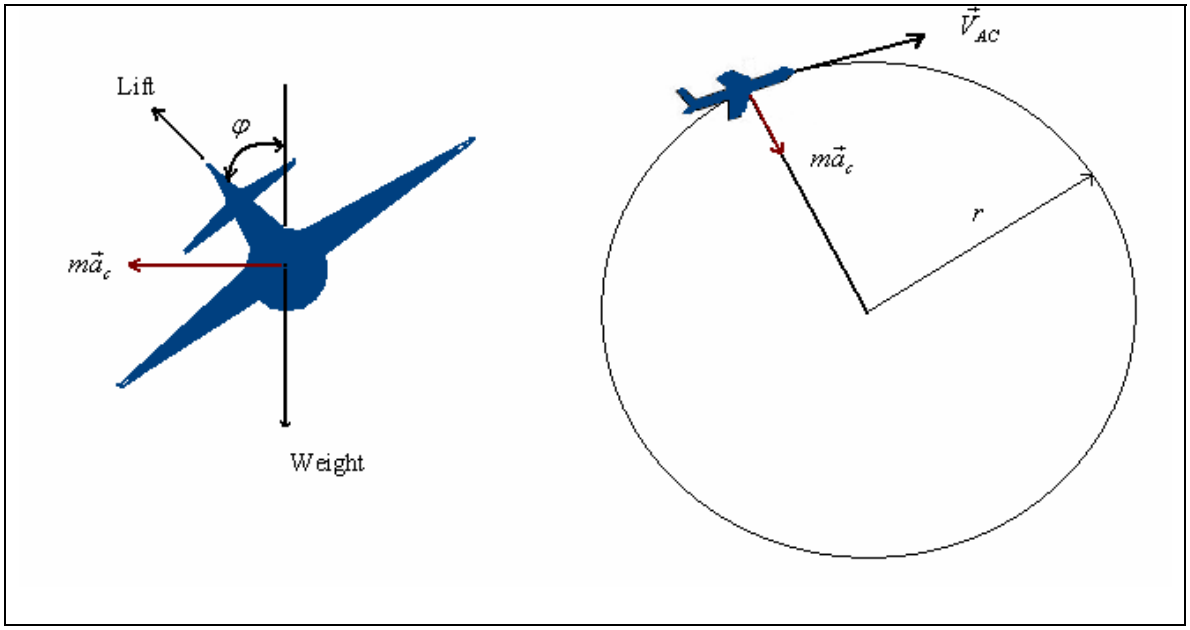

Figure 3-2 Coordinated turn

$$r = \frac{V_{AC}^{\ 2}}{g\tan(\varphi)} \tag{3.2}$$

The exact expression for the turn radius, using the six-degree-of-freedom model of the aircraft is

$$r = \left(\frac{V_{AC}^2}{g}\right)\left[\frac{\cos(\varphi)\cos^2(\theta) + \sin^2(\theta)}{\cos(\theta)\sin(\varphi)}\right] \tag{3.3}$$

However, under normal circumstances, this equation results in values that are extremely close to that from Equation (3.2) because θ is generally very small for this aircraft.

Using either model, it is obvious that the two variables of significance in determining the turn radius are velocity and angle of bank. In the absence of wind, V_{AC} is equal to airspeed.

There are additional constraints that restrict the turn radius. The combination of the maximum lift coefficient and airspeed imposes a limit on the load factor that can be created before the aircraft stalls. There is also a structural load factor limit that should not be exceeded to protect the structural integrity of the airframe. Finally, the flight control system enforces a limit on the bank angle for the purpose of safety. In light of the combination of these constraints, the maximum allowable load factor during an evasive maneuver is then defined by

$$n = \min(n_{structural}, \frac{C_{L_{\max}}}{C_{L_{trim}}}, \frac{1}{\cos(\varphi)}) \tag{3.4}$$

From Equation (3.2) , the minimum turn radius is associated with maximum bank angle, and therefore, the maximum possible load factor, Equation (3.1). However the latter quantity is subject to the constraints that were discussed earlier and must be determined from Equation (3.4).

Obviously, to avoid entering a restricted zone expeditiously, the aircraft should not be allowed to assume a position from which it would not be able to bypass the restricted zone using a level turn. The nearest distance to the restricted zone that the aircraft should be allowed to reach in a head-on direction is the smallest possible turn radius. This parameter, as discussed earlier, depends on the allowable load factor.

For a general aviation aircraft of the category under discussion here, the structural load factor limit ($n_{structural}$) is 3.8. The second restriction on load factor arises from the ratio of maximum lift coefficient to trim lift coefficient, where $C_{L_{trim}}$ is defined by

$$C_{L_{trim}} = \frac{Weight}{qS} \tag{3.5}$$

Obviously, $C_{L_{trim}}$ increases as dynamic pressure decreases, reducing the allowable load factor above which the aircraft stalls. The third limit on the load factor is related to the bank angle for a coordinated turn. The AFCS has a safety limit of 60 degrees on the bank angle in that the maximum lateral deflection of the control column would bank the aircraft to this limit regardless of the flight conditions.

It can be shown easily from Equation (3.2) the turn radius is greatly reduced by increasing the angle of bank from zero to 45 degrees. However, beyond 45 degrees, increasing the bank angle, while increasing the load factor, does not reduce the turn radius appreciably. Therefore, by limiting the bank angle to 45 degrees, the vertical load factor is limited. This also allows for a much more comfortable ride for the passengers. Based on this reasoning, 45 degrees was used as the maximum bank angle to perform an evasive maneuver, avoiding a collision with the restricted zone.

In the implementation phase of this project, the need for controlling the flight speed also became obvious. As indicated in Equations (3.1) and (3.2), the turn radius depends on the square of the aircraft speed. Through trial and error, it was determined that a combination of maximum speed of 170 ft/s and safety zone width of 1,000 ft would result in the smoothest avoidance maneuvers. Therefore, an upper limit was placed on the aircraft speed if it approached the region where

$$l < R_T + R_{sf} + R_{AC} + l_{decel} \tag{3.6}$$

The last parameter, l_{decel}, was the distance required to slow down the aircraft from its flight speed to 170 ft/s, and therefore, varied for different maneuvers. Again, for the aircraft under consideration in this report, based on previous experience, a deceleration of 2.5 ft/s^2 was assumed in determining this parameter. At this airspeed, limiting the maximum bank angle to 45 degrees resulted in a turn radius of approximately 900 ft. Therefore, R_{AC} was set to a fixed value of 1,000 ft.

3.2.3. Penalty Function

When the aircraft is outside of the restricted zone and

$$l \geq R_T + R_{AC} + R_{sf} \text{ or } \zeta \geq \pi / 2 \tag{3.7}$$

the pilot must have complete control authority. On the other hand, if the border of aircraft domain is on the perimeter of the restricted zone and $\zeta < \pi / 2$, complete control authority should be switched to the controller. To accomplish this, one can define two penalty functions, PPC (pilot command) and PCC (controller command). Both penalty functions will be in effect at all times while also requiring

$$P_{PC} + P_{CC} = 1 \tag{3.8}$$

However,

$$P_{PC} = 1 \text{ and } P_{CC} = 0 \tag{3.9}$$

for $$l > R_T + R_{AC} + R_{sf} \text{ or } \zeta \geq \pi / 2 \tag{3.10}$$

while $$P_{PC} = 0 \text{ and } P_{CC} = 1 \tag{3.11}$$

for $$l \leq R_T + R_{AC} \text{ and } \zeta < \pi / 2 \tag{3.12}$$

In the Advanced Flight Control System (AFCS), the pilot and the controller both command bank angle, φ, to perform a turning maneuver. The commanded bank angle communicated to the aircraft is the sum of the two, each multiplied by its penalty function, if evasive action is needed. Therefore,

$$\varphi = \begin{cases} \varphi_{PC} P_{PC} + \varphi_{CC} P_{CC} & \text{if evasive action is needed} \\ \varphi_{PC} & \text{otherwise} \end{cases} \tag{3.13}$$

The penalty functions could be simple ramps starting at the point, where $l = R_T + R_{AC} + R_{sf}$. Therefore, one example would be that shown in Figure 3-1.

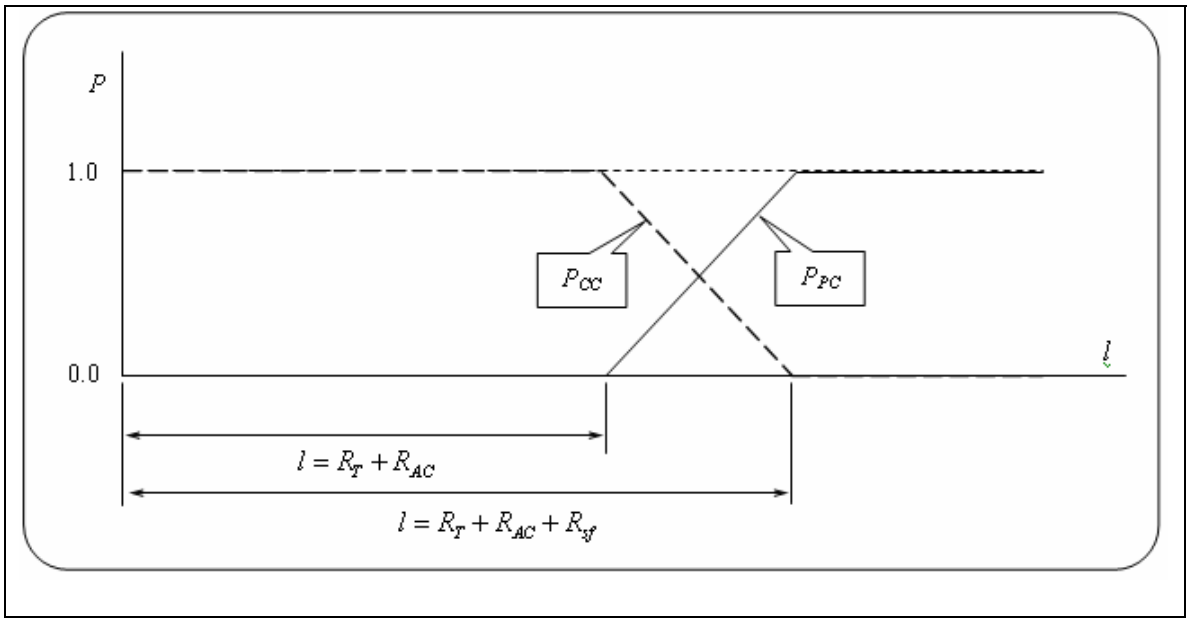

Figure 3-3 Schematic variation of the penalty functions with distance for $\zeta \le \pi/2$

3.2.4. Algorithm

The algorithm used in this document can be summarized in the following steps:

- If $l > R_T + R_{AC} + R_{sf}$, no action is necessary because the aircraft is well outside of the vicinity of the restricted zone.

- If $l < R_T + R_{AC} + R_{sf}$ and $\zeta \geq \frac{\pi}{2}$, no action is necessary because even though the aircraft is in the neighborhood of the restricted zone, it is leaving it.
- If $l \leq R_T + R_{AC}$ and $\zeta < \frac{\pi}{2}$, then the safety controller must command a bank angle, φ that would force $\zeta \to \frac{\pi}{2}$ till satisfying $\zeta \geq \frac{\pi}{2}$.

An outline of the operational algorithm of the approach is given in Figure 3-4.

When the aircraft approaches the restricted zone, the controller needs to determine the direction of the bank angle that would result in the fastest diversion. This is determined from cross product of the velocity vector and distance vector from the aircraft to the center of the zone as

$$(-).sign\left(\vec{k}\ component\ of\left(\vec{V}_{AC} \times \vec{l}\right)\right) \tag{3.14}$$

Of course, in the case of a head-on approach, banking to either side would have the same effect. Therefore, a left turn is chosen arbitrarily.

As long as the approach angle, ζ, remains greater than 90 degrees, the aircraft poses no threat to the restricted zone, even while flying on its boundary or inside it. Therefore, the pilot should have full control of the aircraft. This would allow the pilot to fly around the zone or exit it if placed there inadvertently. This is necessary to allow the pilot to take off and land at an airport on the edge of the restricted zone. For safety, within a 50-ft band of the restricted zone, the controller is designed to nullify any pilot input resulting in turning towards the restricted zone.

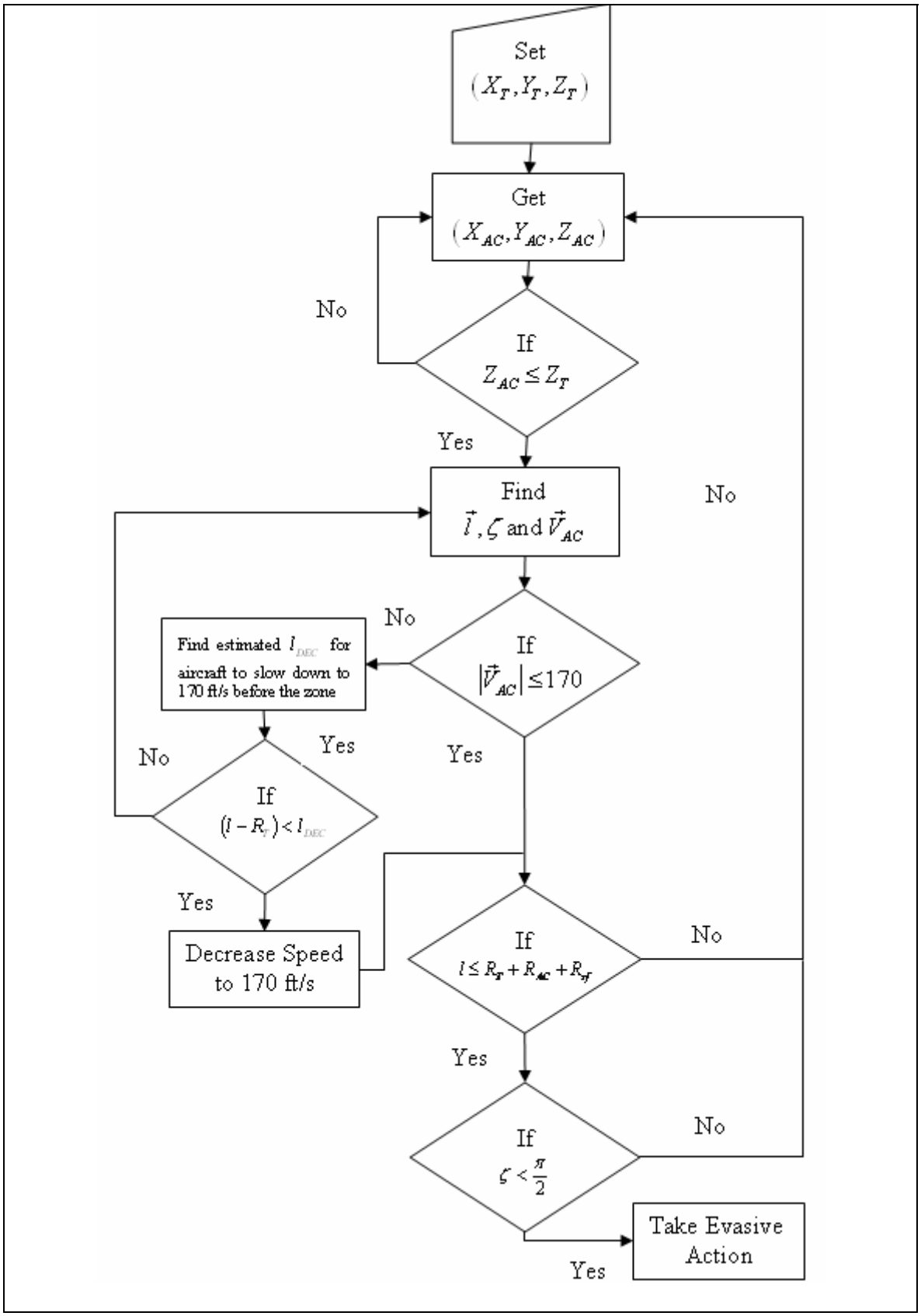

Figure 3-4 Outline of the decision making process

The intent to turn towards or away from the prohibited area is determined from

$$\begin{aligned} &sign\left(\vec{k}\ component\ of\left(\vec{V}_{AC}\times\vec{l}\right)\right).sign\left(\varphi_{PC}\right)=1 \quad \Rightarrow \quad \text{aircraft turns towards to zone} \\ &sign\left(\vec{k}\ component\ of\left(\vec{V}_{AC}\times\vec{l}\right)\right).sign\left(\varphi_{PC}\right)=-1 \quad \Rightarrow \quad \text{aircraft turns away from zone} \end{aligned} \tag{3.15}$$

This additional logic in the algorithm can be summarized as

- If $l > R_T + 50$, no output from controller.
- If $l \le R_T + 50$ and aircraft turns away from the zone, no output from controller.
- If $l \le R_T + 50$ and aircraft turns into the zone, output from controller is needed.

3.3. Multiple Zone

The algorithm described in the previous section was designed to avoid a single restricted zone. In practice, it may be necessary to avoid a number of such zones simultaneously. As it stands, the proposed scheme can be modified slightly to accommodate multiple zones, as long as they do not overlap, even if they are tangent to each other. Avoidance of multiple overlapping zones involves a different level of trajectory optimization of the aircraft and will be addressed in the future.

All zones have to be defined in the aircraft's information bank. The system must be updated periodically in case of changes in properties of the restricted zones. The idea is that the controller would have to prioritize the level of risk associated with each zone and try to avoid the one that is most likely to result in a collision.

It is assumed that there are *n* zones to be avoided with $\vec{l}_i$ representing the distance between the aircraft and the center of each zone and R_{T_i} standing for the radius of each. The algorithm continuously monitors the distance, $\left|l - R_{T_i}\right|$ from the center of aircraft to

the edge of each zone. The nearest zone is assigned the highest priority and is marked for avoidance, subject to the same conditions used for the single zone, which are the angle of approach and the distance. The flowchart for multiple-zone approach is presented in Figure 3-5.

3.4. Implementation

The algorithm described in the previous section was programmed in Matlab/Simulink™ environment for validation. A generic single-engine general aviation aircraft model using Advanced Flight Control System (AFCS) was employed for demonstration.

The flight control system, modeled after that of Watanabe et al.[18] uses a dynamic inverse controller, assisted by Artificial Neural Networks (ANN) for compensating for errors. The handling qualities chosen for the aircraft are those of decoupled flight controls. In this context, the longitudinal stick commands climb angle, the lateral stick commands bank angle, and the speed lever controller commands the desired airspeed. The collision avoidance algorithm was employed within this system in a manner very similar to those for envelope protection. A Graphical User Interface (GUI) was also designed to facilitate user interface with the codes. The results of this implementation will be discussed in the next chapter.

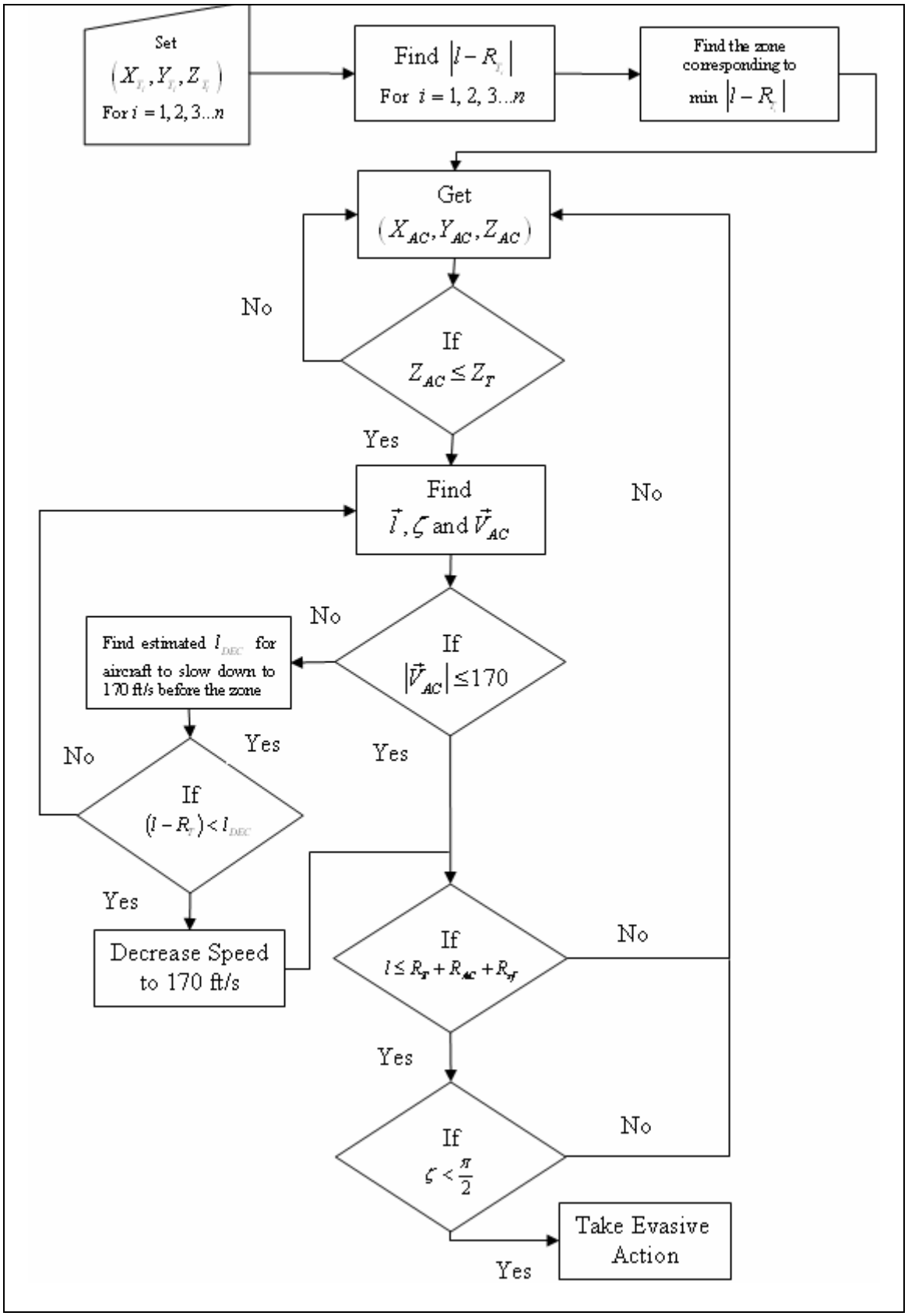

Figure 3-5 Outline of the decision making process for multiple zones

CHAPTER 4

RESULTS AND DISCUSSION

4.1. Introduction

A number of cases were investigated involving single and multiple zones. In the interest of brevity, only some of these cases are presented here. This chapter contains the results of the following cases:

Case 1: Aircraft approaching a single zone on a rectilinear flight path, slightly to the left of the center of the zone

Case 2: Aircraft approaching a single zone on a rectilinear flight path, slightly to the right of the center of the zone

Case 3: Aircraft approaching a single zone on a rectilinear flight path with some crosswind

Case 4: Aircraft approaching a single zone on a rectilinear flight path with high speed

Case 5: Aircraft approaching a single zone on a curvilinear flight path while the pilot tries to turn into the zone at maximum commanded turn rate

Case 6: Aircraft approaching a single zone on a curvilinear flight path at high speed while the pilot tries to turn into the zone at maximum commanded turn rate

Case 7: Maneuvering through multiple zones

4.2. Single Zone

For single zone, the cases from which results are obtained, are listed in Table 4-1

Case	$\lvert\vec{V}_{AC}\rvert$ (ft/s)	h (ft)	$\lvert\vec{V}_{wind}\rvert$ (ft/s)	ξ (deg)	φ_{PC} (deg)	φ_{PC} time(s)	X_T (ft)	Y_T (ft)	h_T (ft)	R_{AC} (ft)	R_T (ft)
1	170	2000	0	0	0	0	40000	100	5100	1000	25000
2	170	2000	0	0	0	0	40000	-100	5100	1000	25000
3	170	2000	50	90	0	0	40000	-100	5100	1000	25000
4	250	2000	0	0	0	0	40000	100	5100	1000	25000
5	170	2000	0	0	45	77	40000	-500	5100	1000	25000
6	250	2000	0	0	45	72	40000	-500	5100	1000	25000

Table 4-1 Cases for single-zone.

4.2.1. Case 1

Figures 4-1(a) and (b) show the top view of the aircraft trajectory in comparison with the location of the restricted zone. In this case, there was no wind and the commanded flight path was rectilinear with airspeed of 170 ft/s. Initially aircraft was flying to the east approaching the zone from the left as shown in Figure 4-1. When the distance between the aircraft and the zone reached 2000 ft, the controller started to command a bank angle to prevent penetrating the restricted zone. From Figure 4-1 (a) and (b) it is seen that controller commanded a negative bank angle because the center of the restricted zone was slightly on the right side of aircraft. In this case, the minimum distance between the edge of the restricted zone and the aircraft reached approximately 300 feet.

Time histories of the other variables are given in Figures 4-1(c) through 4-1(m). From Figures 4-1(c) through (e), it is obvious that the angle of attack, the sideslip angle,

and the elevator deflection angle remained reasonable. Figure 4-1(f) and (g) indicate that even though the bank angle exceeded 40 degrees, aileron deflection angle remained below 5 degrees that is a reasonable value for this airspeed. Likewise the rudder deflection angle remained well below its limits as shown in Figure 4-1(h) with a corresponding change in the heading angle. It is evident from Figures 4-1(j) through (l) that the AFCS performed this maneuver within 50 feet of the original altitude, while maintaining a nearly constant airspeed. This was accomplished by increasing the thrust almost to its limit, as shown in Figure 4-1(m).

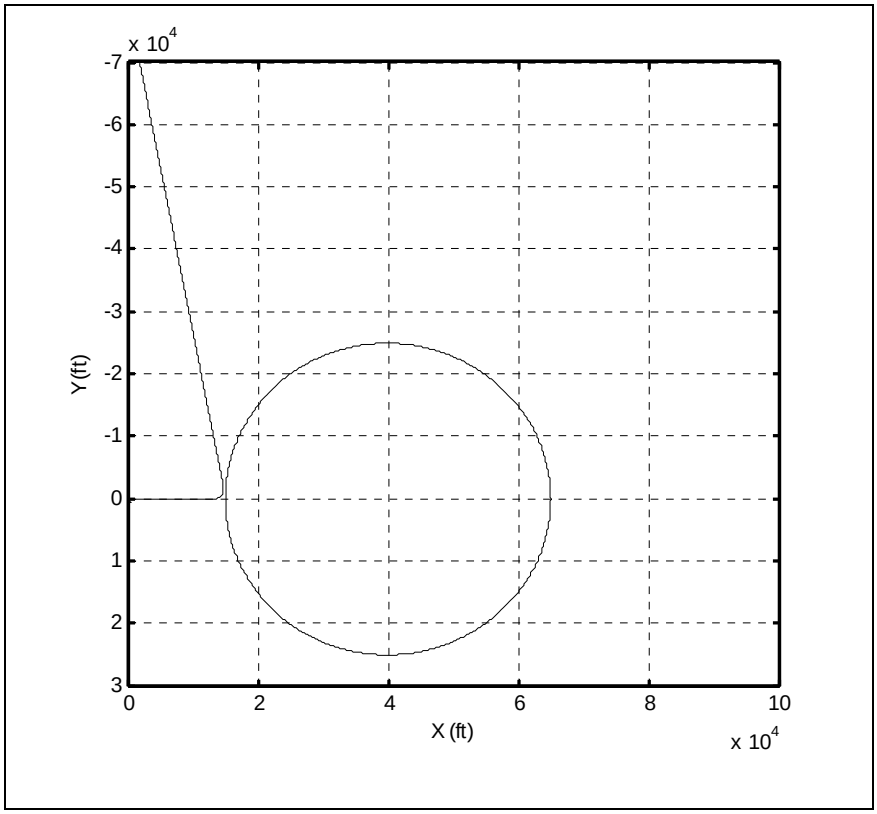

(a) Trajectory and restricted zone

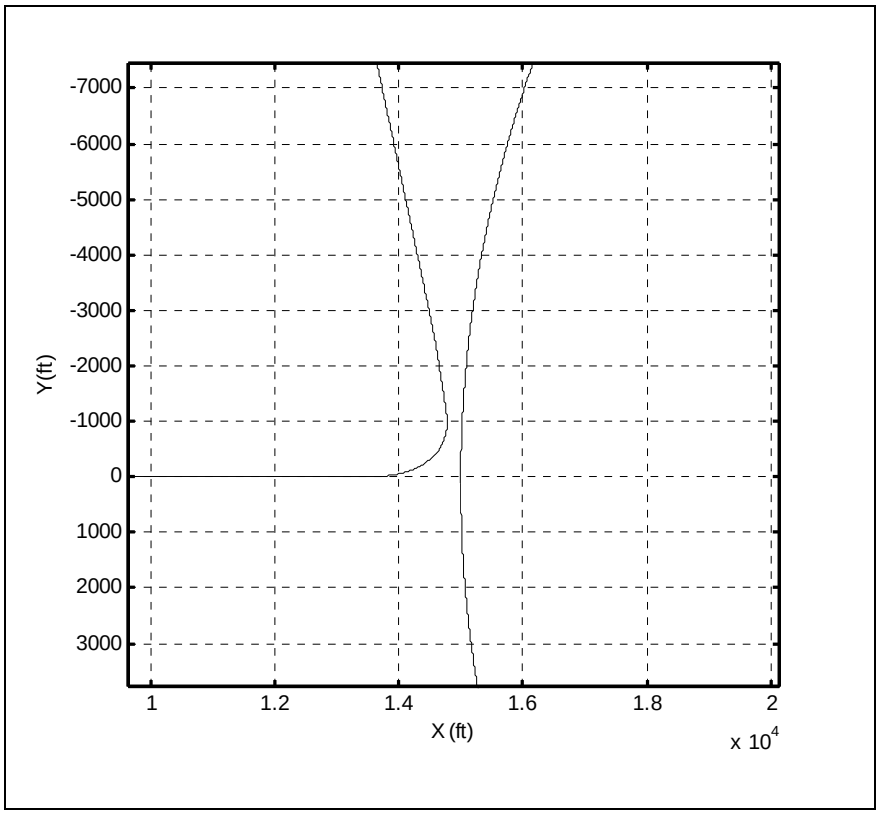

(b) Closeup view

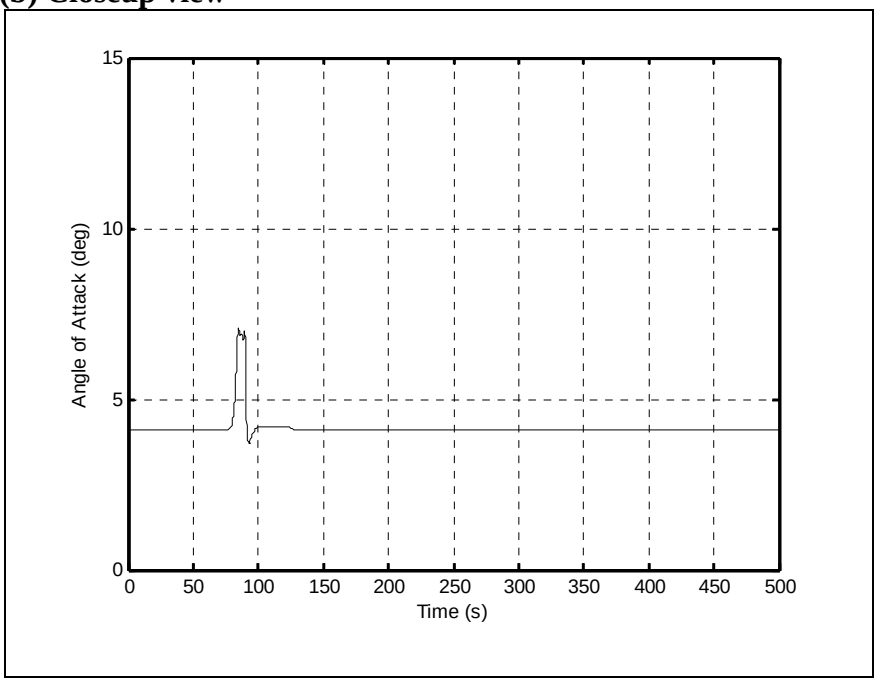

(c) Angle of Attack (deg)

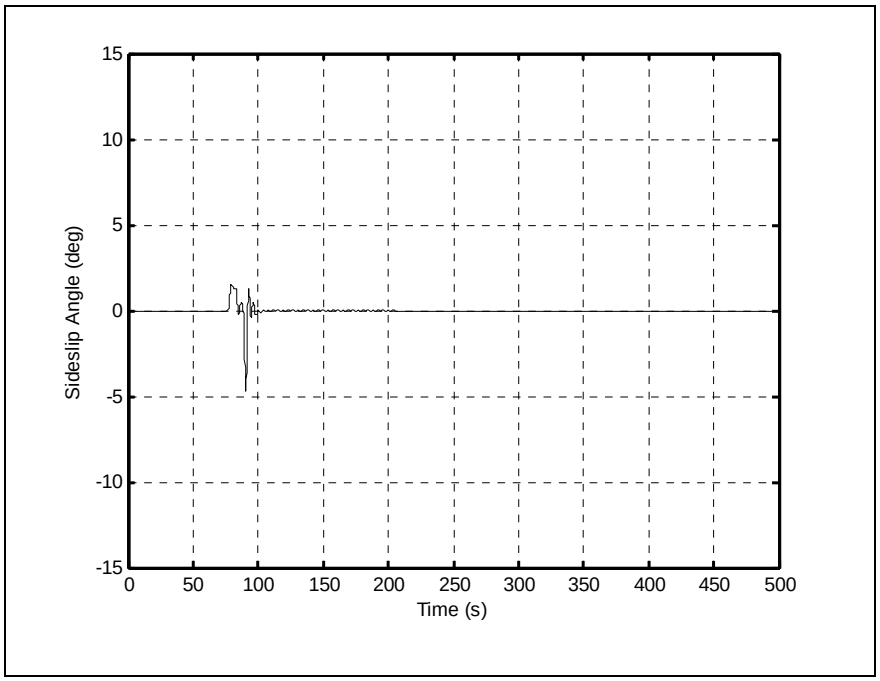

(d) Sideslip Angle (deg)

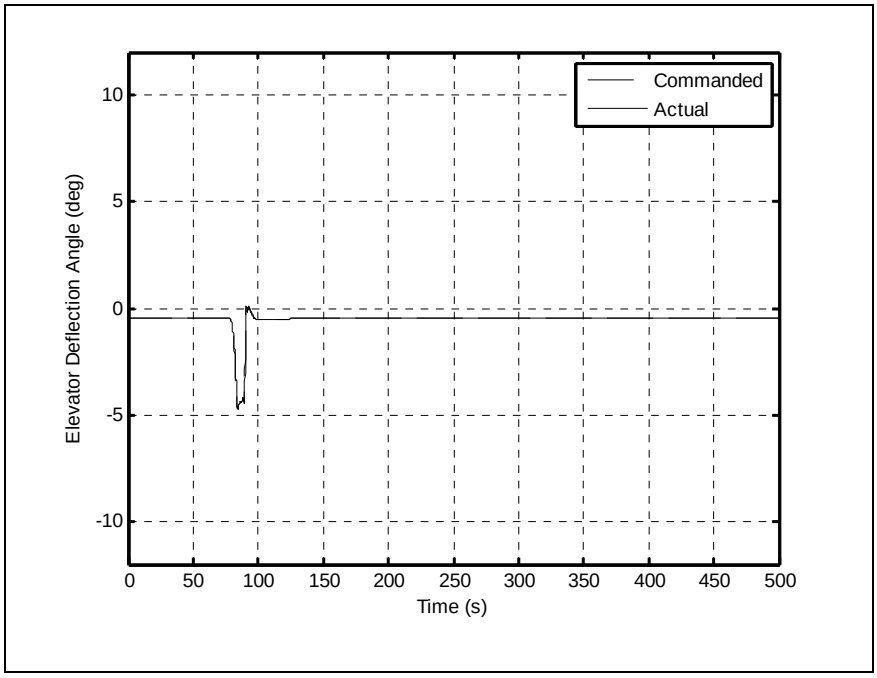

(e) Elevator Deflection Angle (deg)

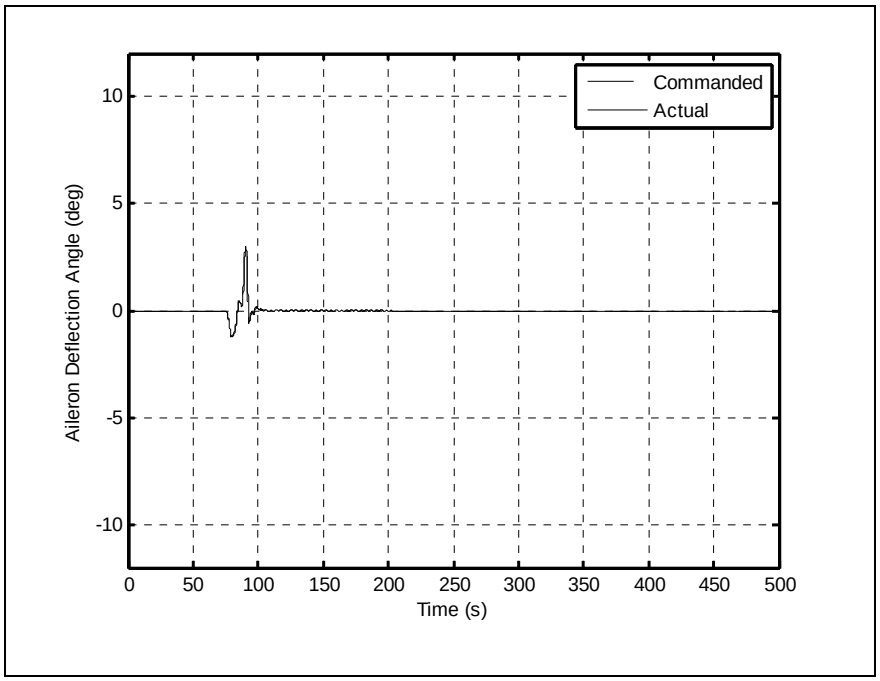

(f) Aileron Deflection Angle (deg)

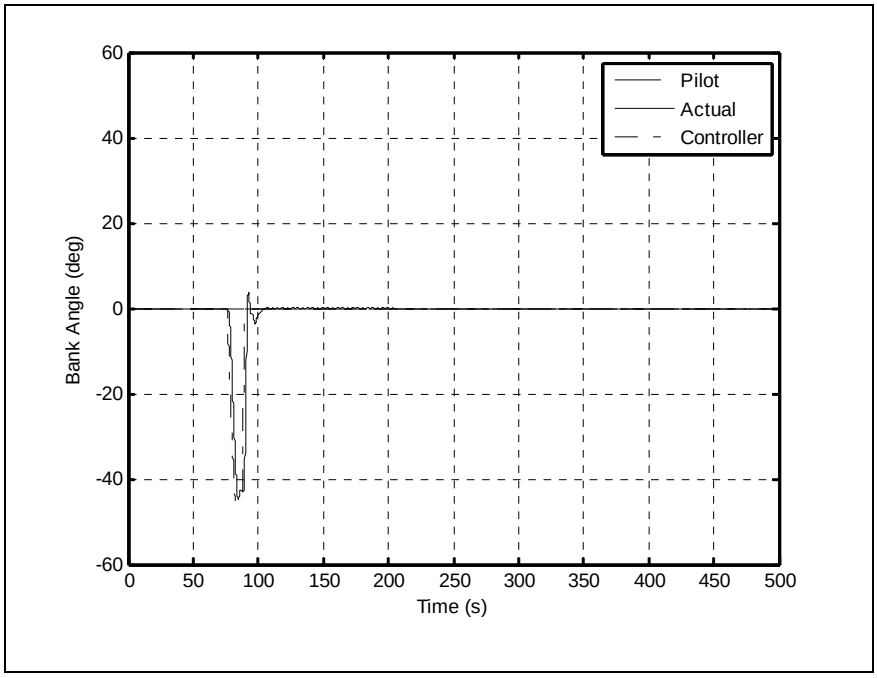

(g) Bank Angle (deg)

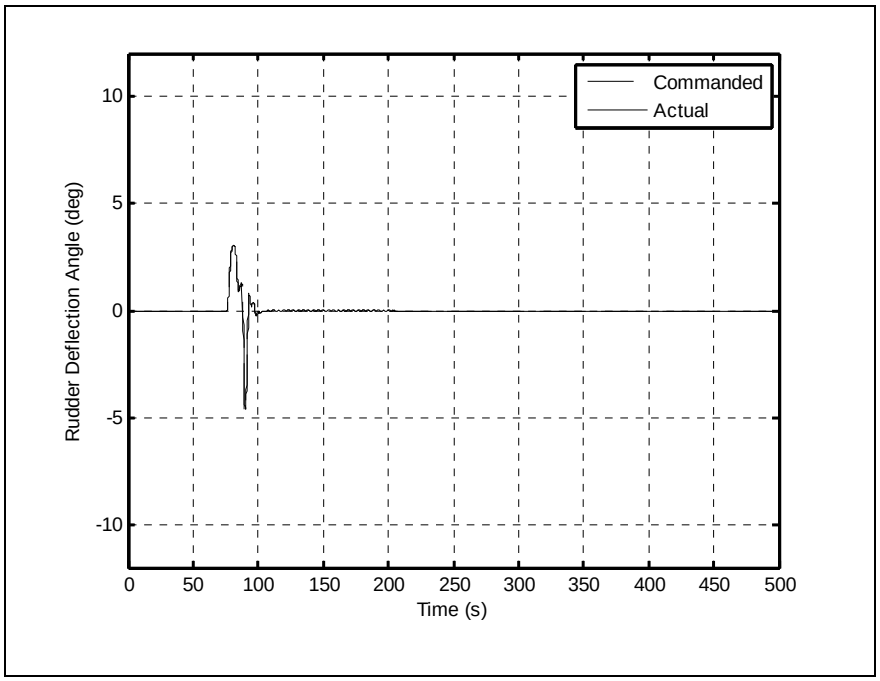

(h) Rudder Deflection Angle (deg)

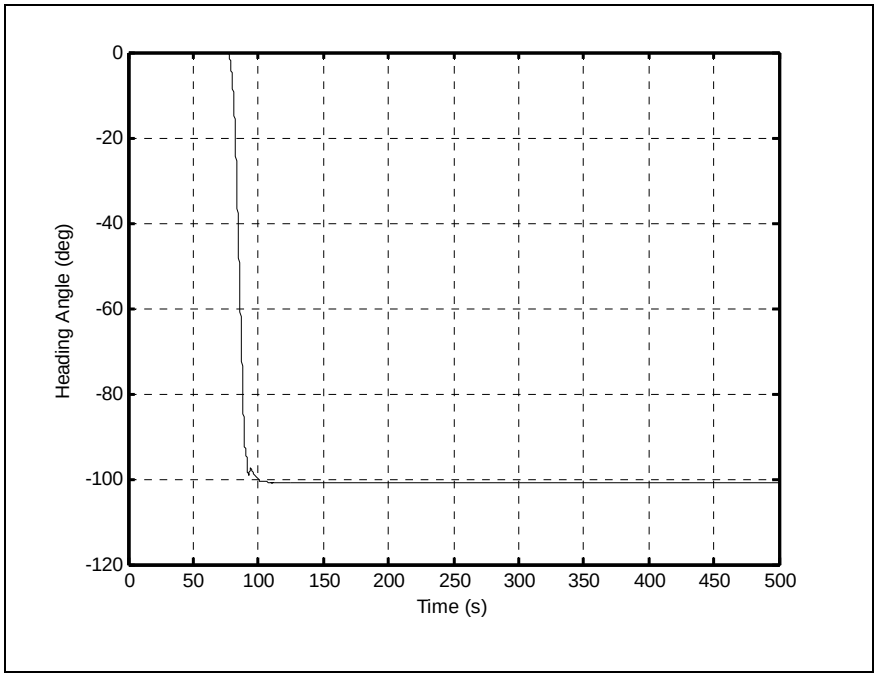

(i) Heading Angle (deg)

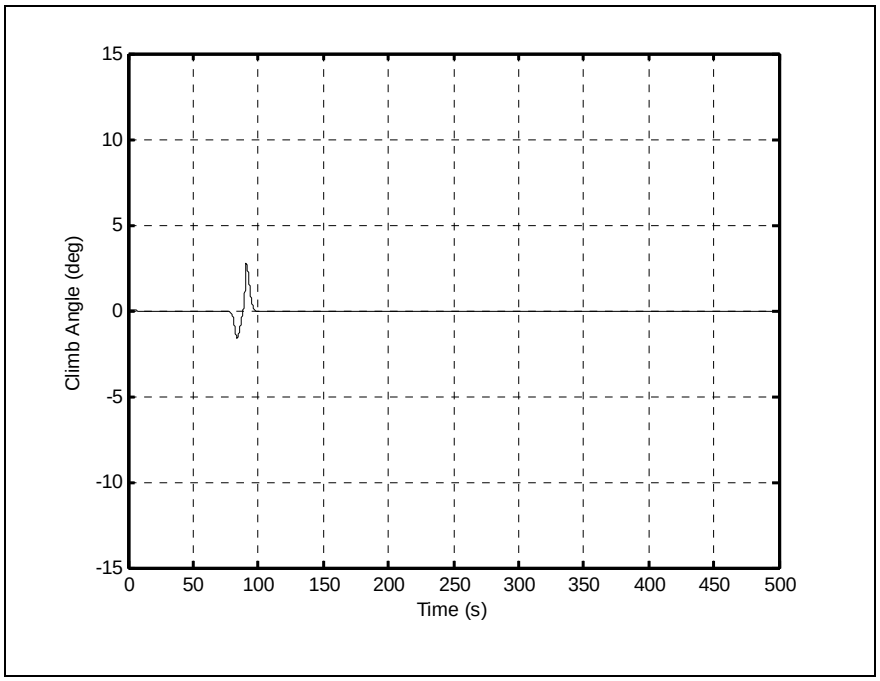

(j) Climb Angle (deg)

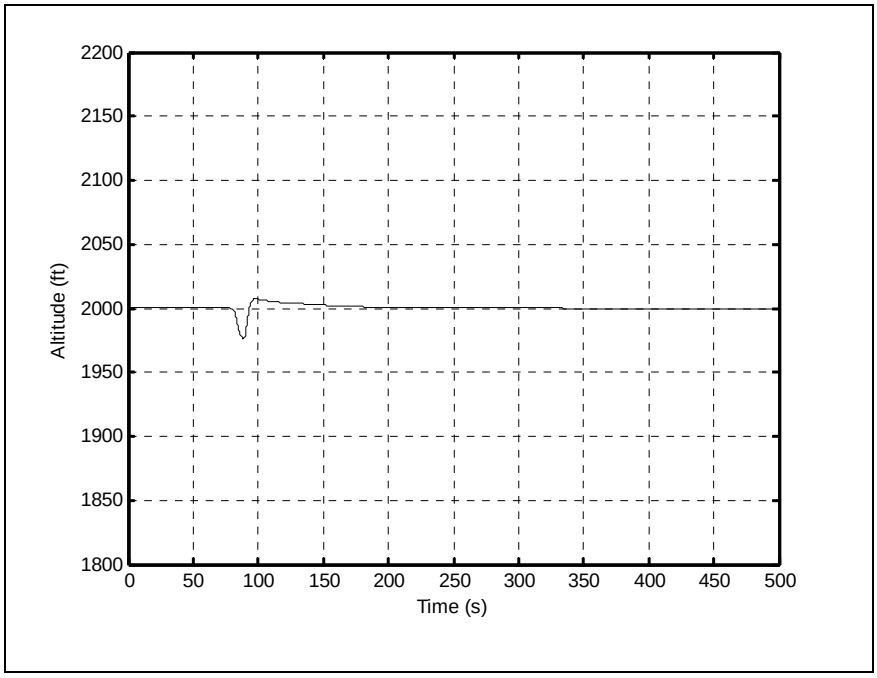

(k) Altitude (ft)

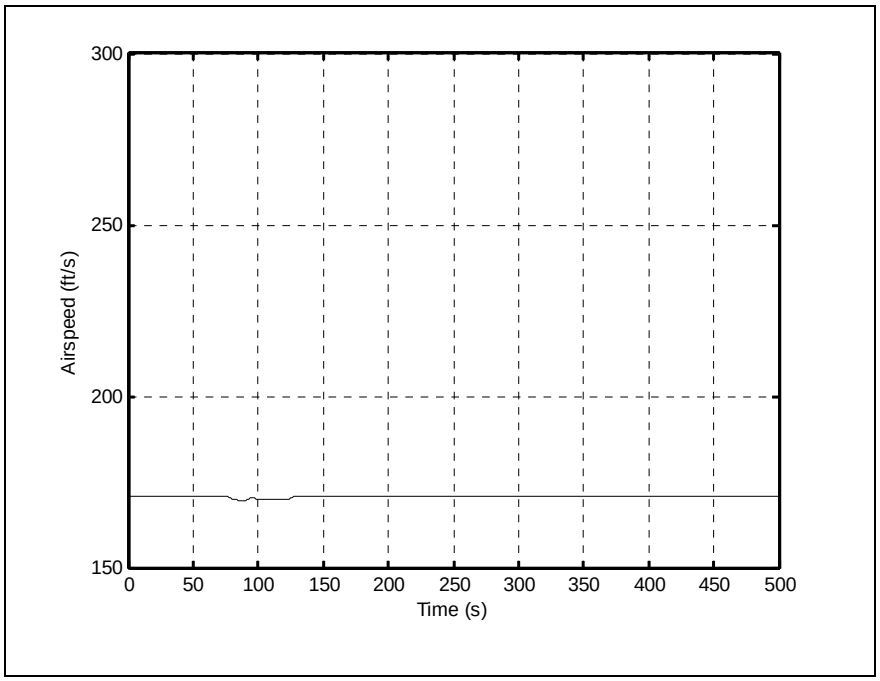

(l) Airspeed (ft/s)

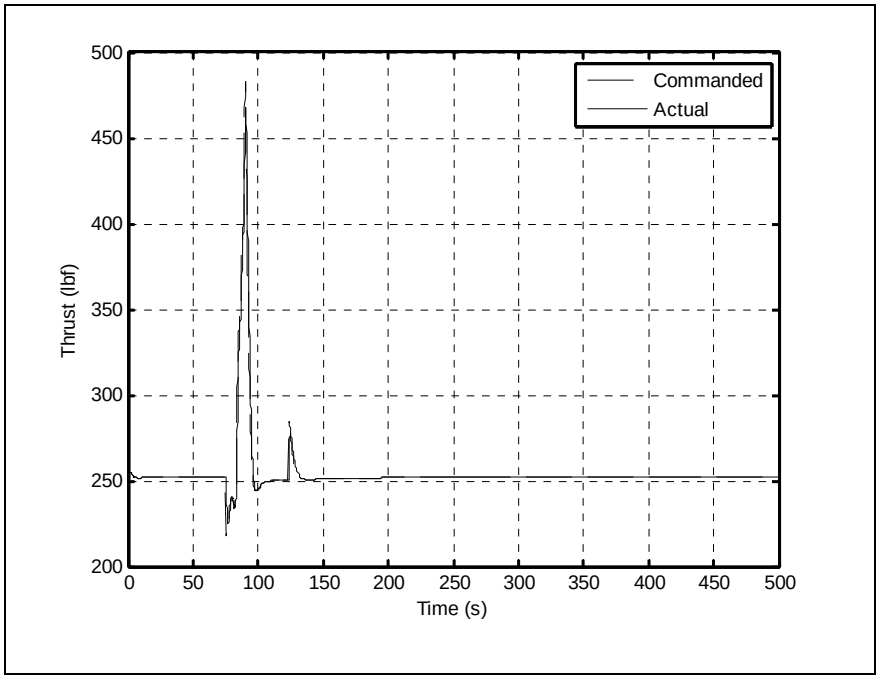

(m) Thrust (lbf)

Figure 4-1 Aircraft Trajectory and state variables for case 1

4.2.2. Case 2

The purpose of this maneuver was to show that the controller did not have a preferred direction. This approach was very similar to the previous case, except now the flight path placed the aircraft slightly to the right of the center of the restricted zone. Therefore, the controller commanded a positive bank angle to avoid an intercept. All other parameters were exactly the same as those of the previous case and the results are shown in Figures 4-2(a) through (m). The flight trajectory relative to the size of the restricted zone is shown in Figure 4-2(a), while the close-up view of the maneuver is given in Figure 4-2(b).

Again, times histories of the angle of attack, the sideslip angle, and the elevator deflection angle are given in Figures 4-2(c) and (d). It is obvious that the angle of attack and the elevator deflection behaved identically to the previous case because they were insensitive to the direction of the turn. However, the sideslip angle was opposite to that of the Case 1. The same behavior was also observed in other lateral-directional parameters, such as aileron deflection angle and the corresponding bank angle, shown in Figures 4-2(f) and (g), as well as rudder deflection angle and the corresponding change in the heading, given in Figures 4-2(h) and (i).

Again, the AFCS kept the altitude to within 50 feet of the commanded value, even though the climb angle had momentary changes as large as 3 degrees. This is shown in Figures 4-2(j) and (k). Likewise, the airspeed remained nearly constant throughout, owing to the change in thrust as depicted in Figures 4-2(l) and (m).

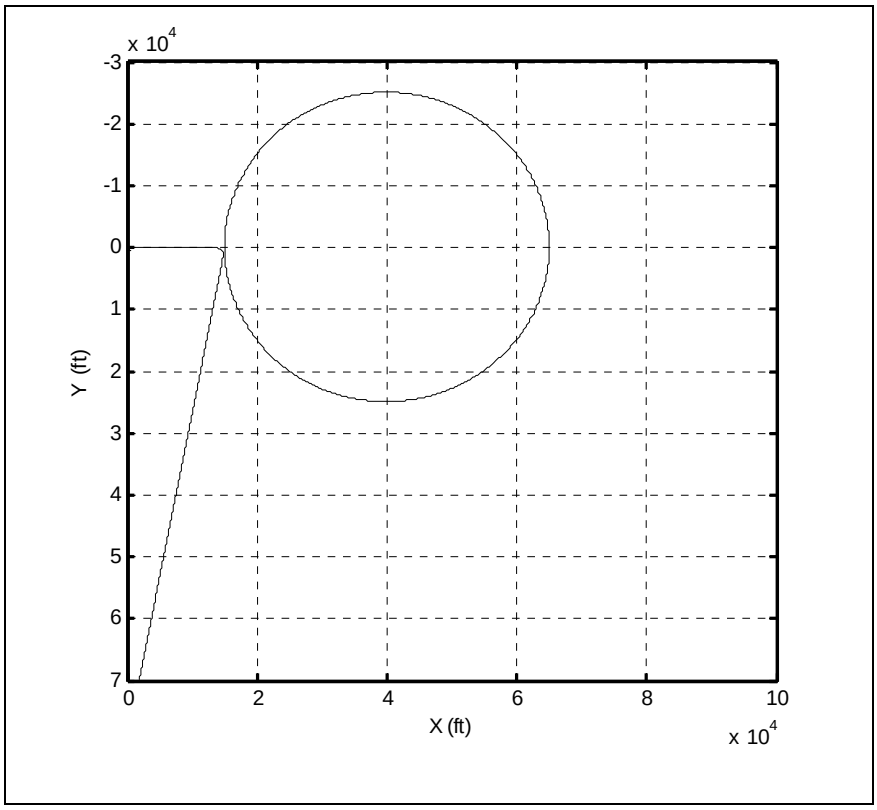

(a) Trajectory and restricted zone

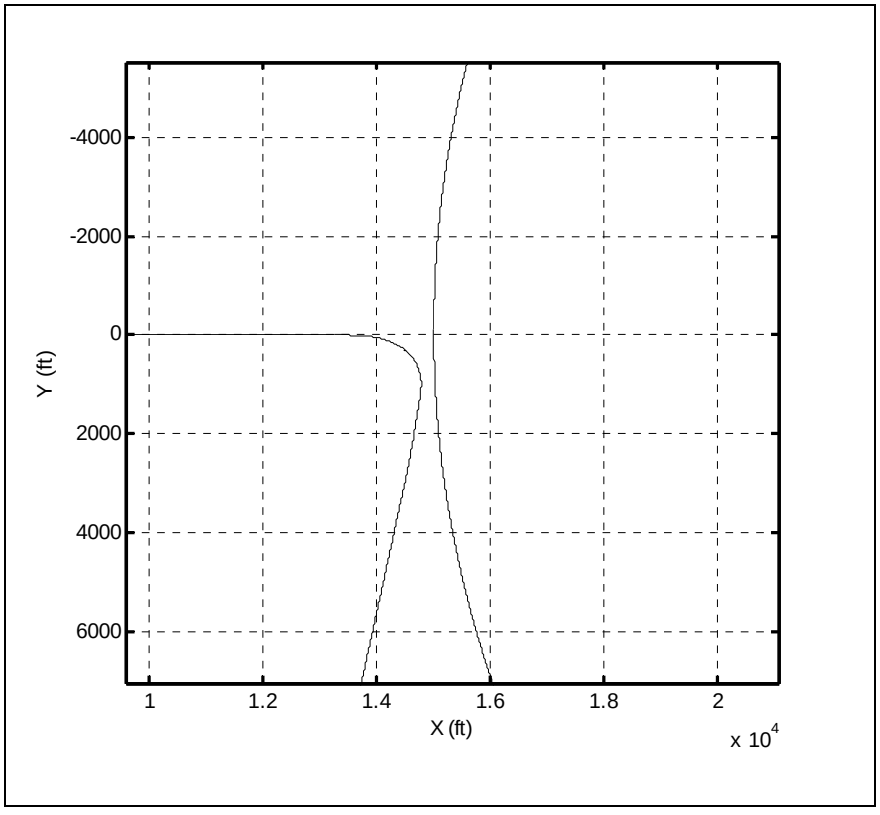

(b) Closeup view

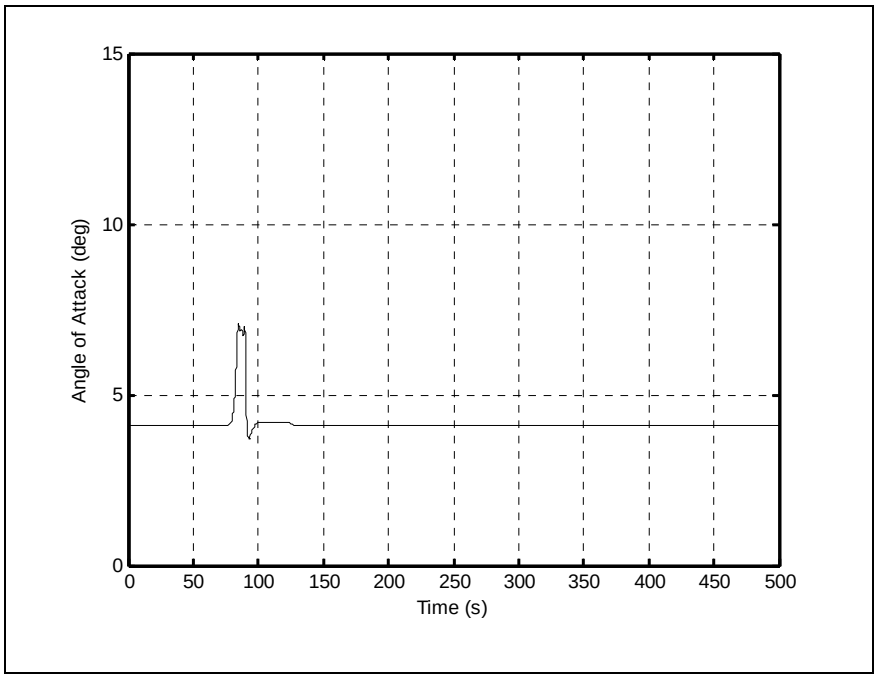

(c) Angle of Attack (deg)

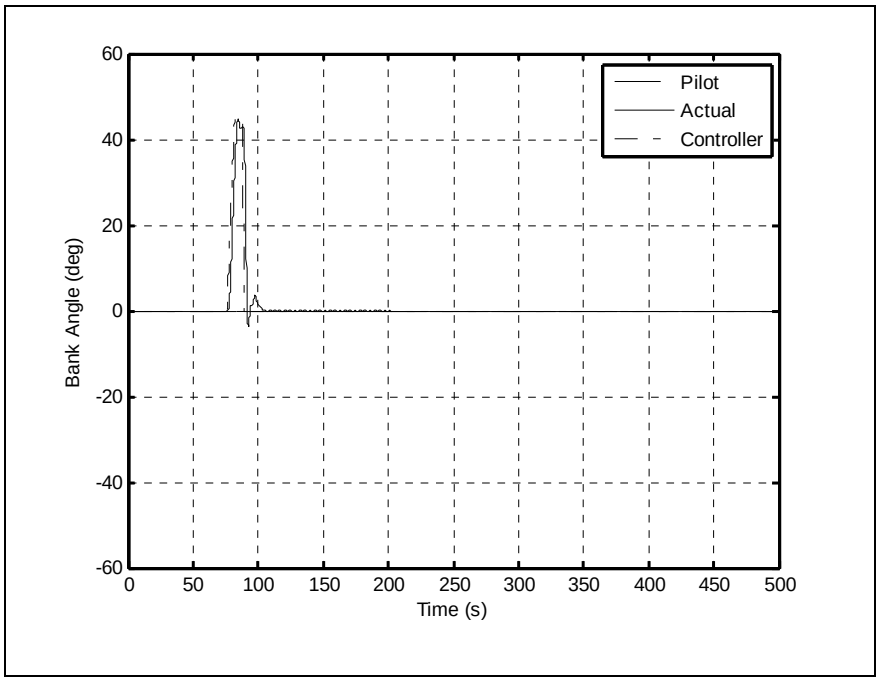

(d) Sideslip Angle (deg)

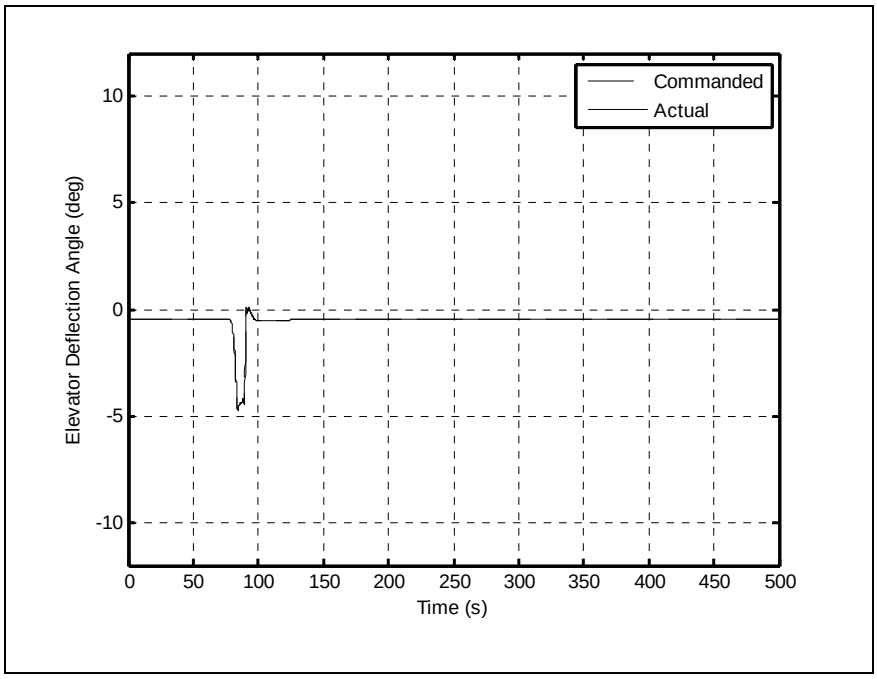

(e) Elevator Deflection Angle (deg)

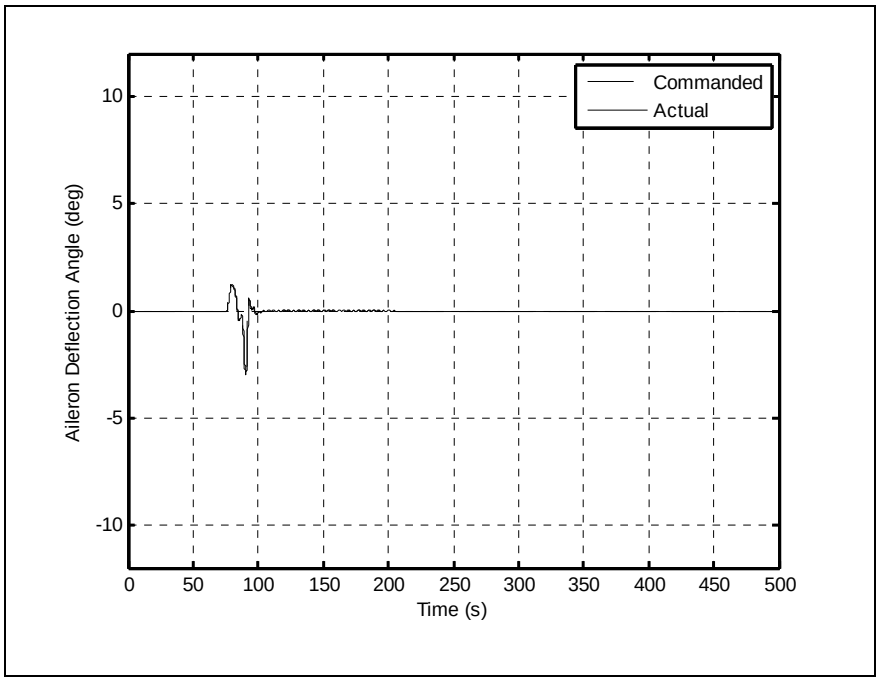

(f) Aileron Deflection Angle (deg)

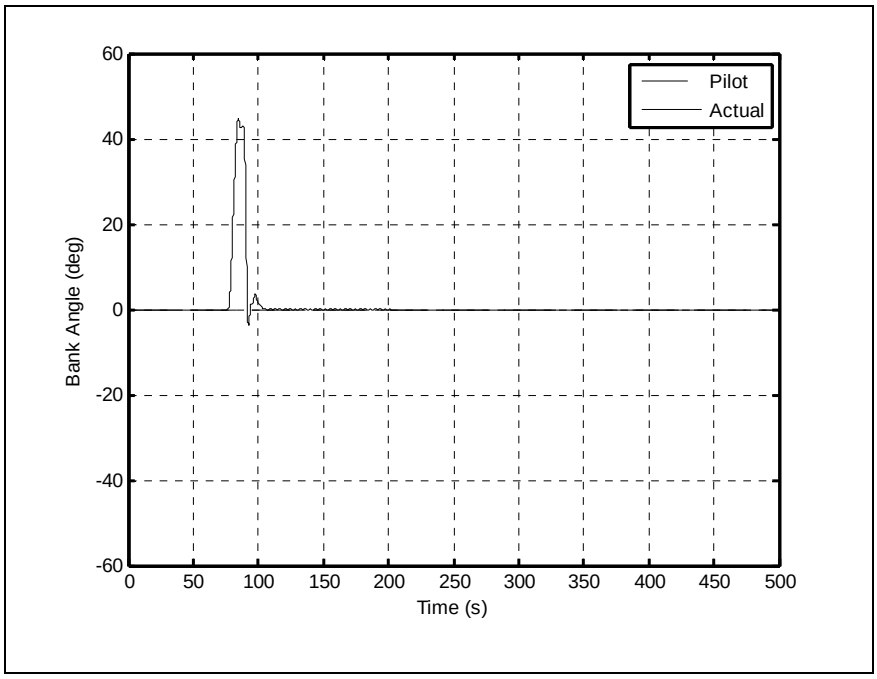

(g) Bank Angle (deg)

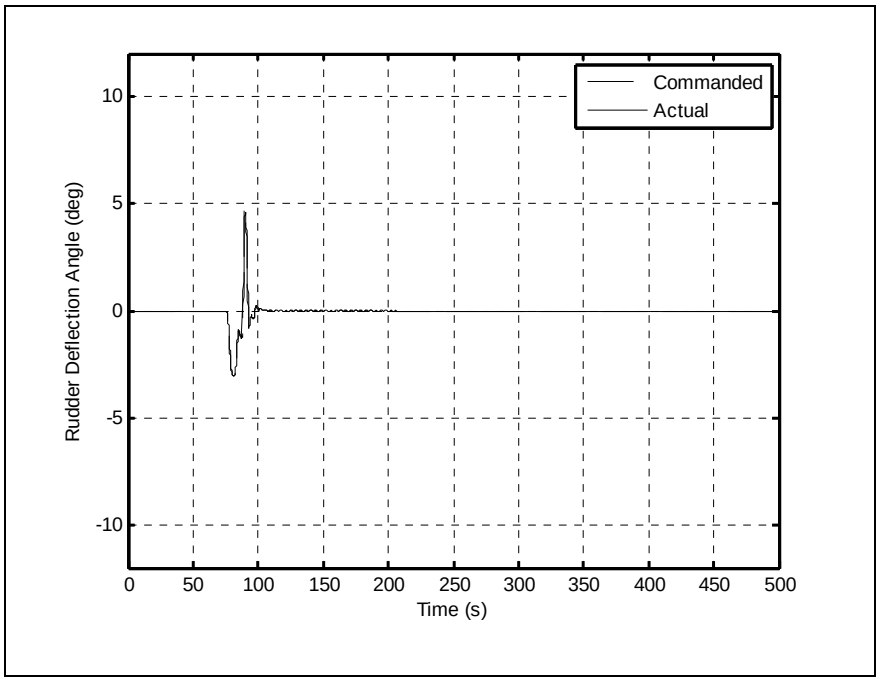

(h) Rudder Deflection Angle (deg)

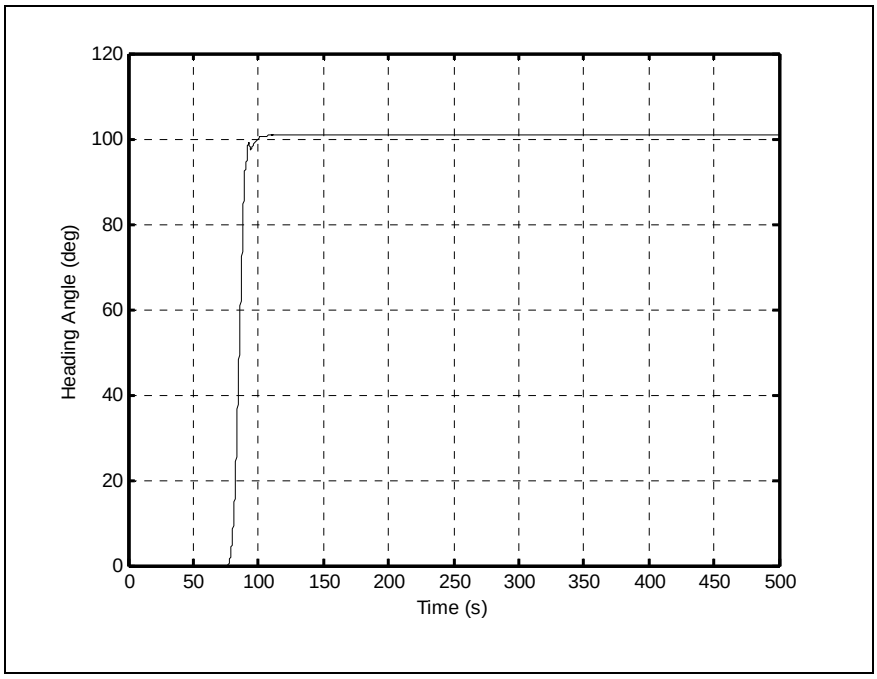

(i) Heading Angle (deg)

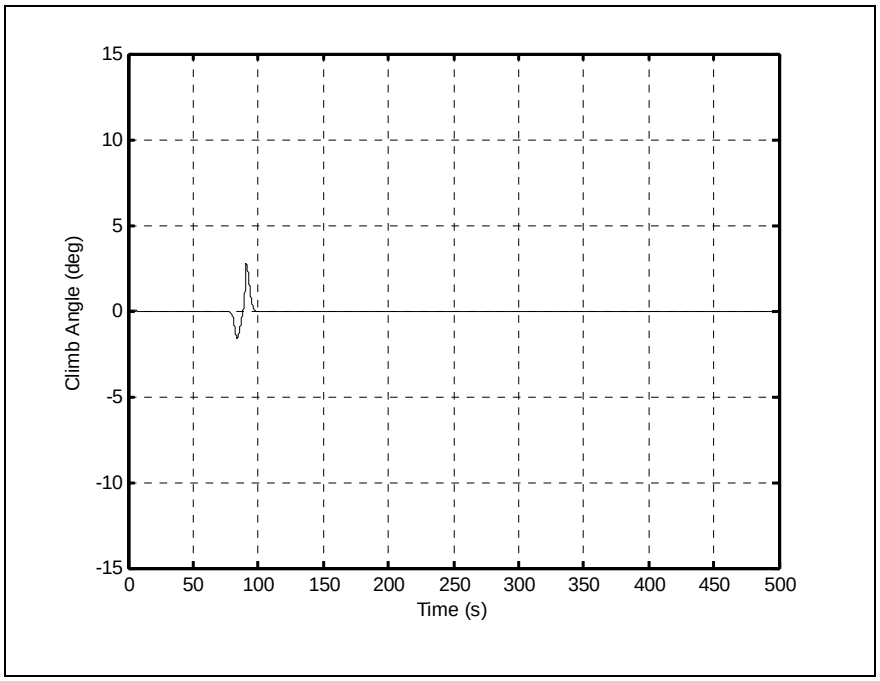

(j) Climb Angle (deg)

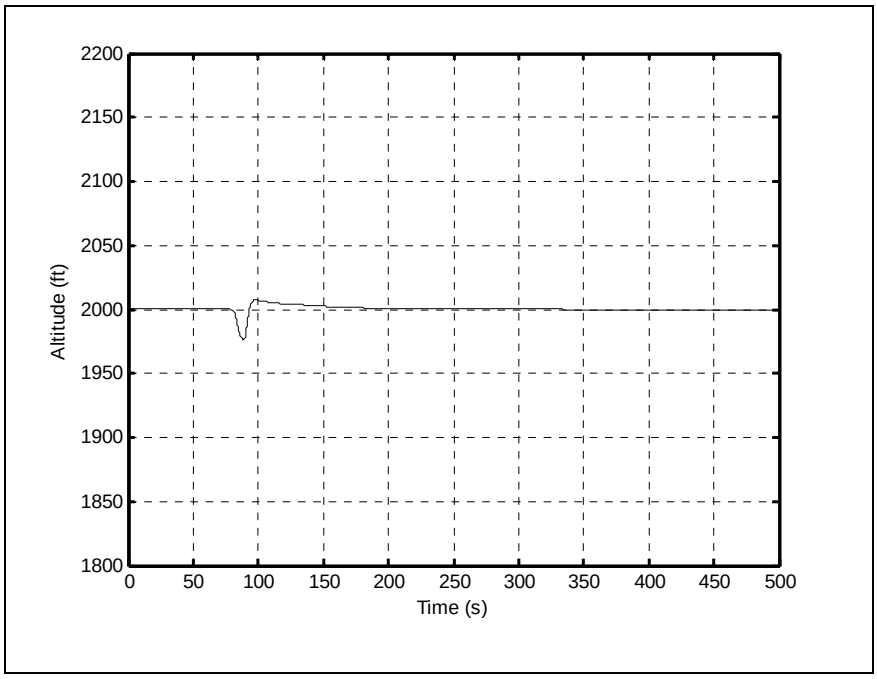

(k) Altitude (ft)

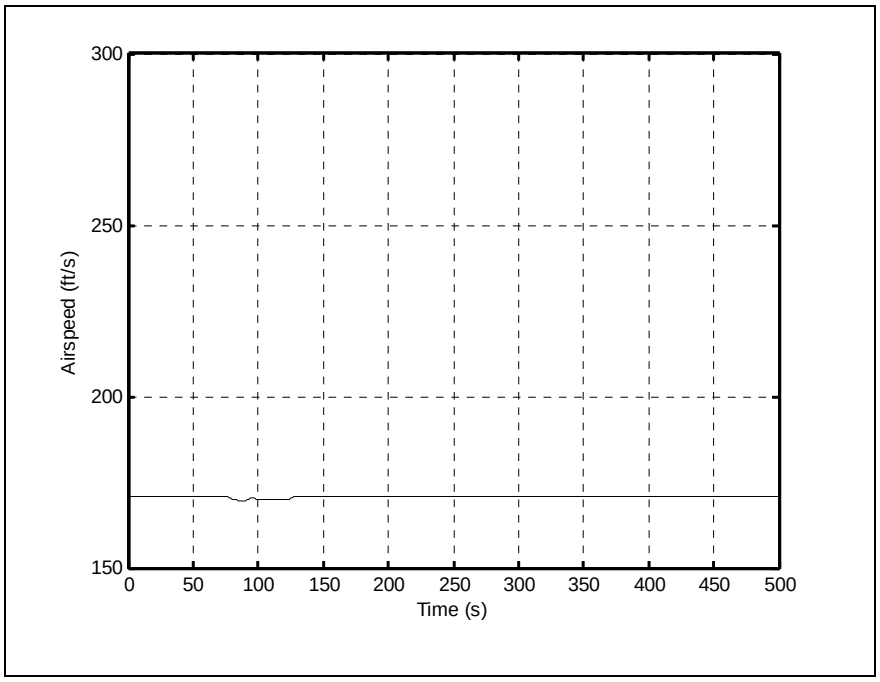

(l) Airspeed (ft/s)

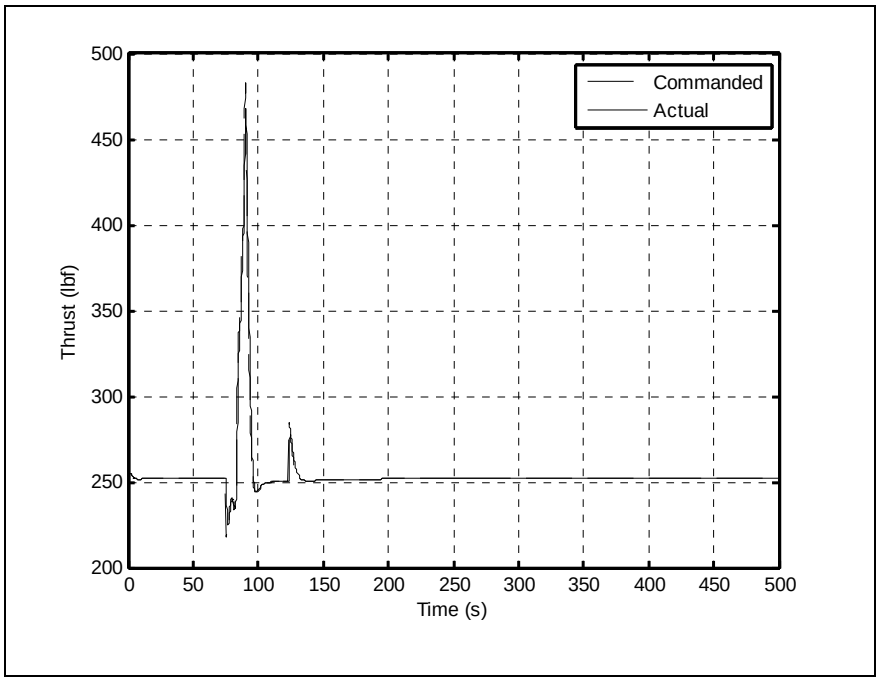

(m) Thrust (lbf)

Figure 4-2 Aircraft Trajectory and state variables for case 2

4.2.3. Case 3

The purpose of this case was to validate the performance of the algorithm and the AFCS in the presence of a crosswind. Therefore, different from the first two cases, a wind directed to the north with magnitude 50 ft/s was added to Case 2. The flight trajectory relative to the location and the size of the restricted zone is shown in Figure 4-3(a) with the close-up of the flight path in Figure 4-3(b). As in first two cases, initially aircraft was flying towards east (i.e. from left to right in Figure 4-3), but the crosswind tried to carry the aircraft north (i.e. from bottom to top in Figure 4-3).

In this case, since the flight path was slightly to the right of the centerline of the restricted zone, the aircraft was required to turn south to avoid a collision (i.e. right turn). This turned the aircraft into the crosswind. Consequently, the angle of attack and the sideslip angle, shown in Figure 4-3(c) and (d) became somewhat larger than those of

Case 2. However, the values still remained reasonable, considering the strength of the crosswind. Likewise, since the maneuver accompanied a slightly steeper turn because of wind, it required a larger deflection of the elevator, aileron, and the bank angle. These quantities are shown in Figures 4-3(e) through (g). At this writing, the source of the small oscillations in the initial sideslip and bank angles is not known. Nonetheless, the amplitudes of these oscillations are so small that their presence can be neglected.

Because of the crosswind, the initial yaw angle was not zero, even though there was no initial sideslip. It is important to note that in the initial phase of this maneuver when the aircraft flew rectilinearly, it yawed sufficiently for the trajectory to remain straight and pointed to the east. Therefore, the accompanying sideslip angle was zero with non-zero heading angle. The time histories of the rudder deflection and the heading angles are shown in Figures 4-3(h) and (i). Again, the minimum distance between aircraft and the edge of the zone remained larger than 300 ft.

Much like in the previous cases, the AFCS allowed performing the maneuver with little change in altitude and airspeed as shown in Figures 4-3(k) and (l). The accompanying climb angle that is shown in Figure 4-3(j) was inline with that of previous cases. However, in this case the commanded thrust was rather large, as indicated in Figure 4-3 (m). Nonetheless, the reader is cautioned that the actual thrust was limited by the engine model therefore; the commanded peak value was not used.

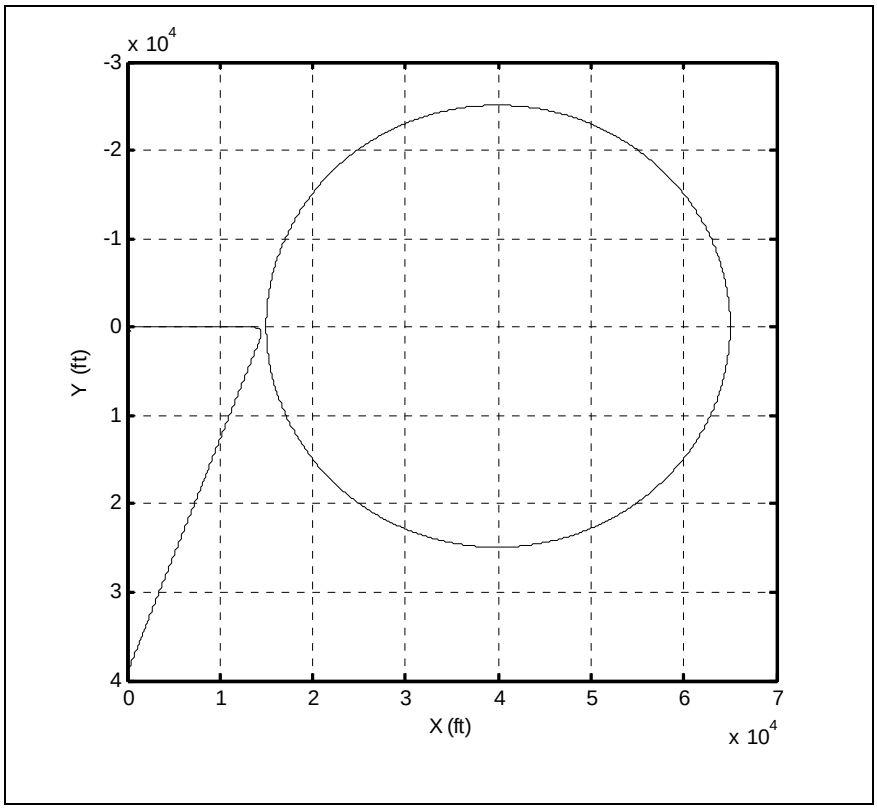

(a) Trajectory and restricted zone

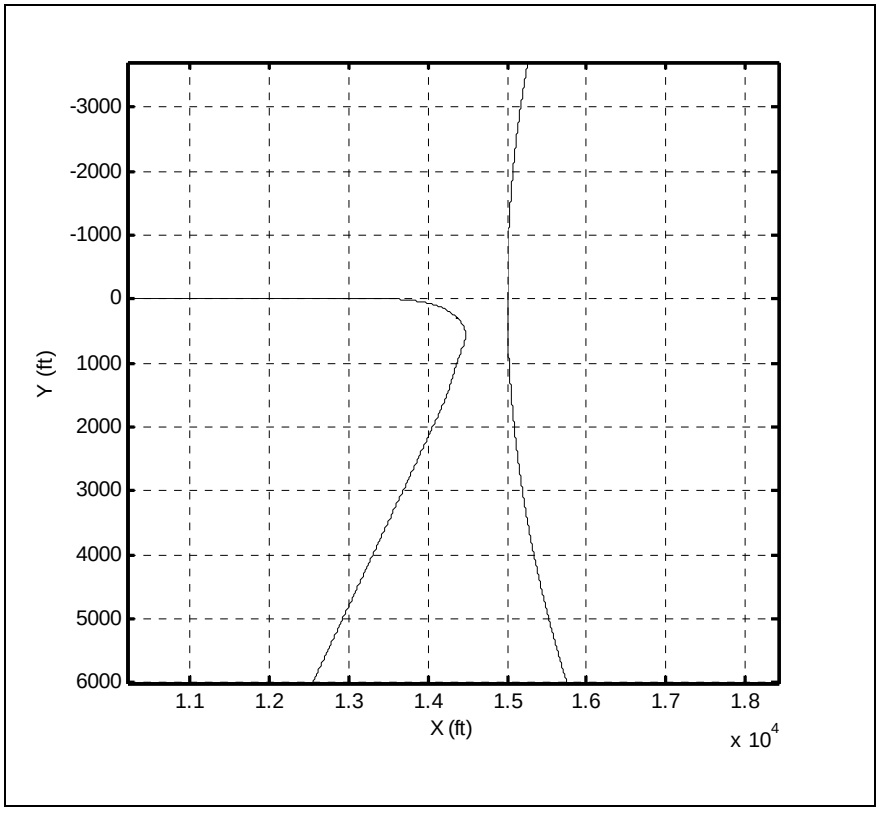

(b) Closeup view

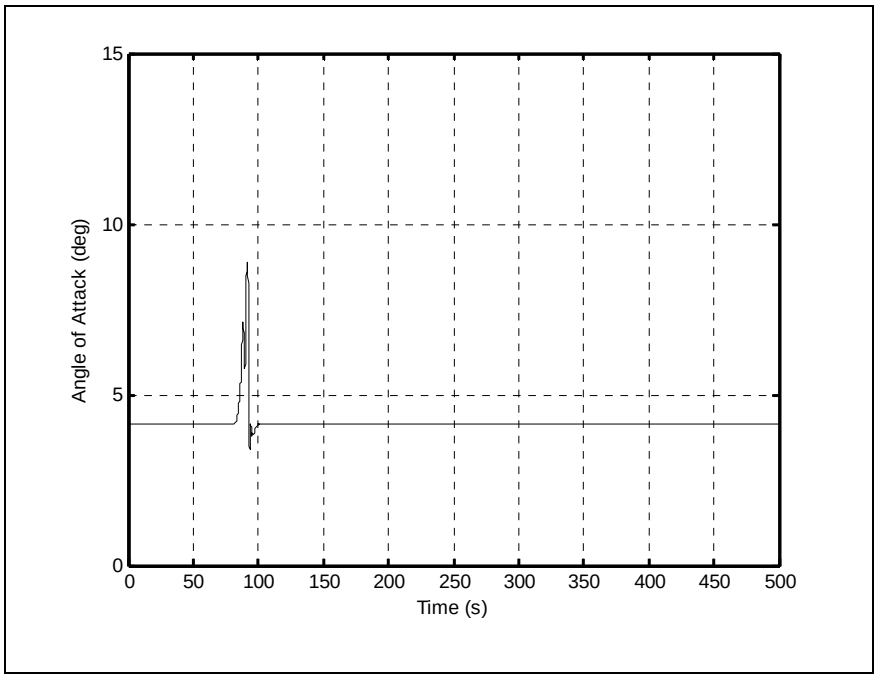

(c) Angle of Attack (deg)

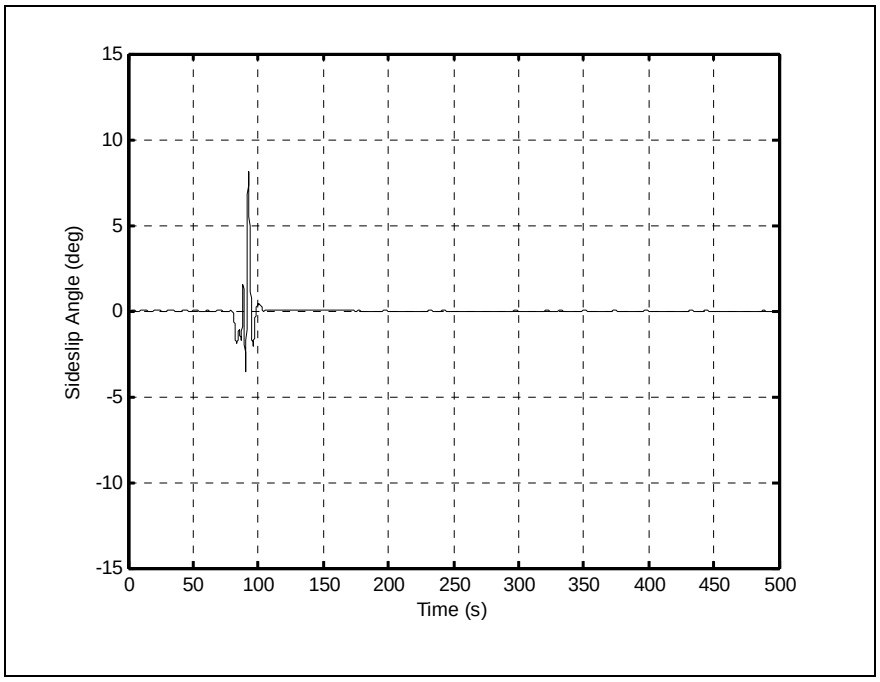

(d) Sideslip Angle (deg)

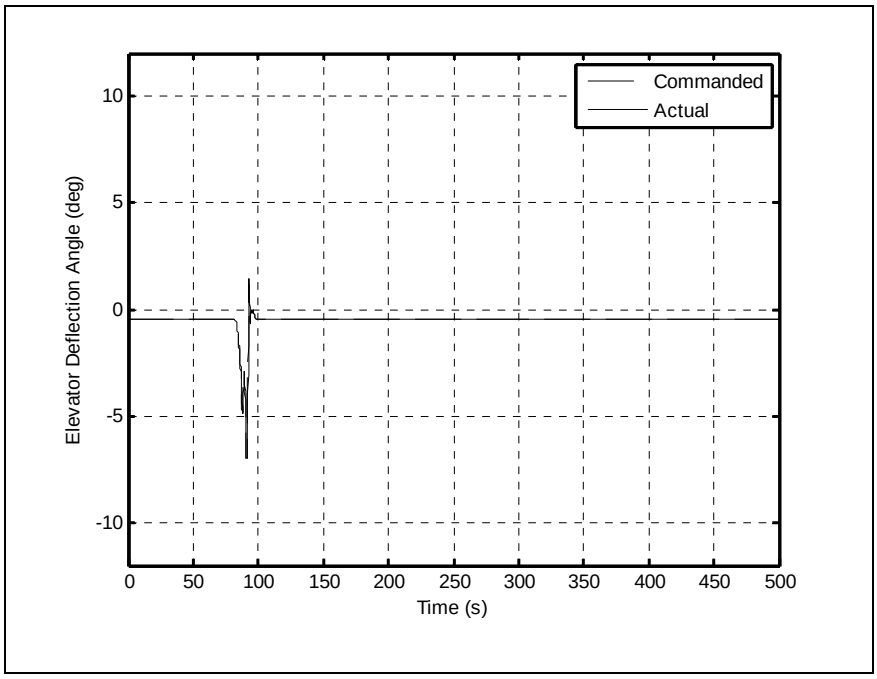

(e) Elevator Deflection Angle (deg)

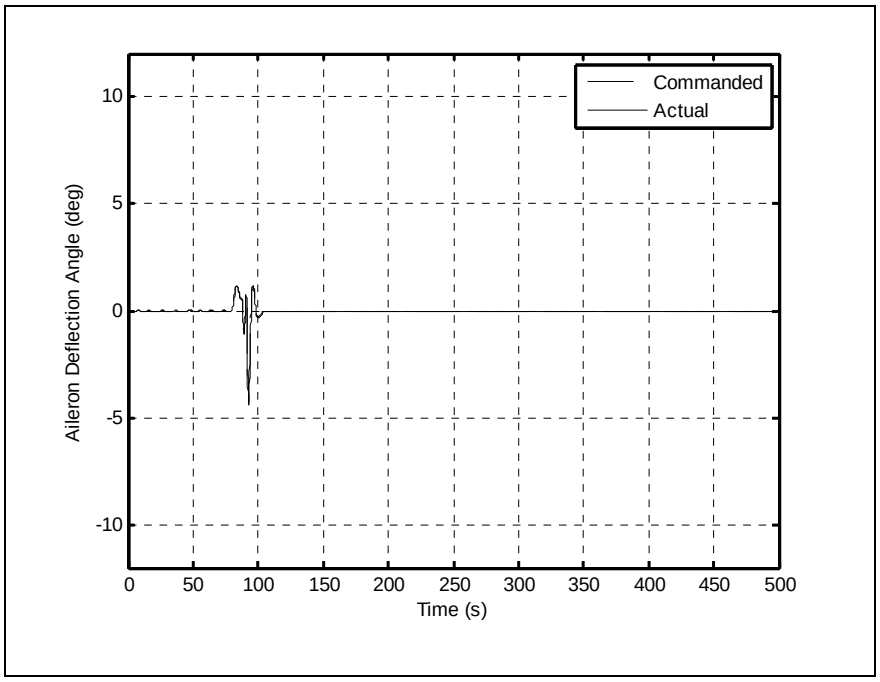

(f) Aileron Deflection Angle (deg)

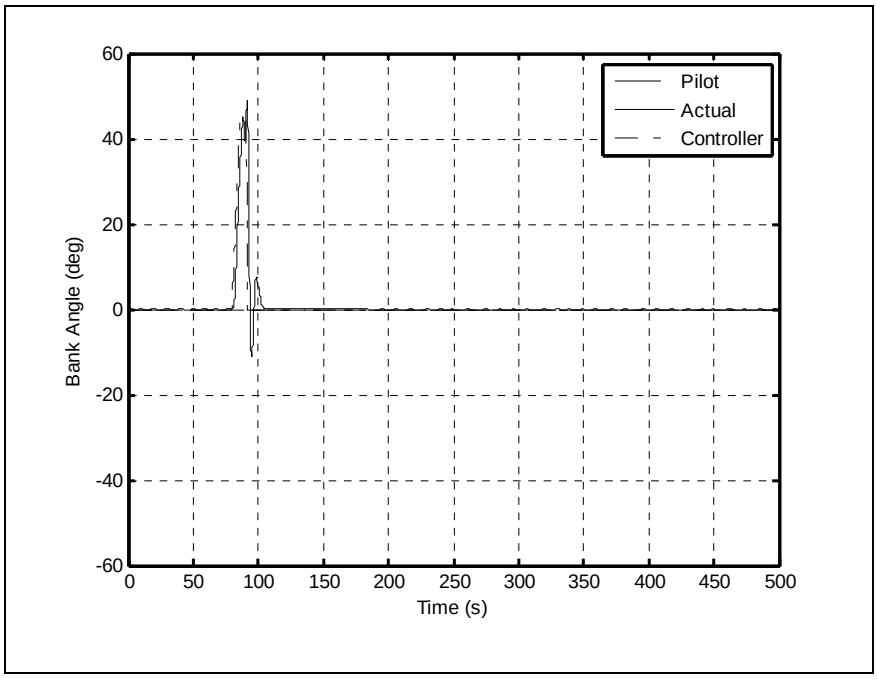

(g) Bank Angle (deg)

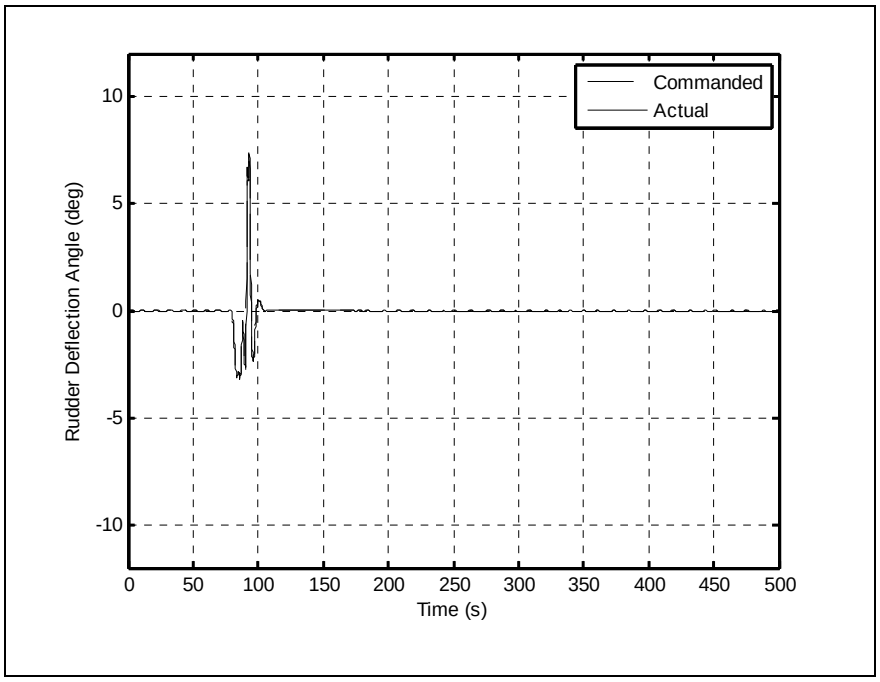

(h) Rudder Deflection Angle (deg)

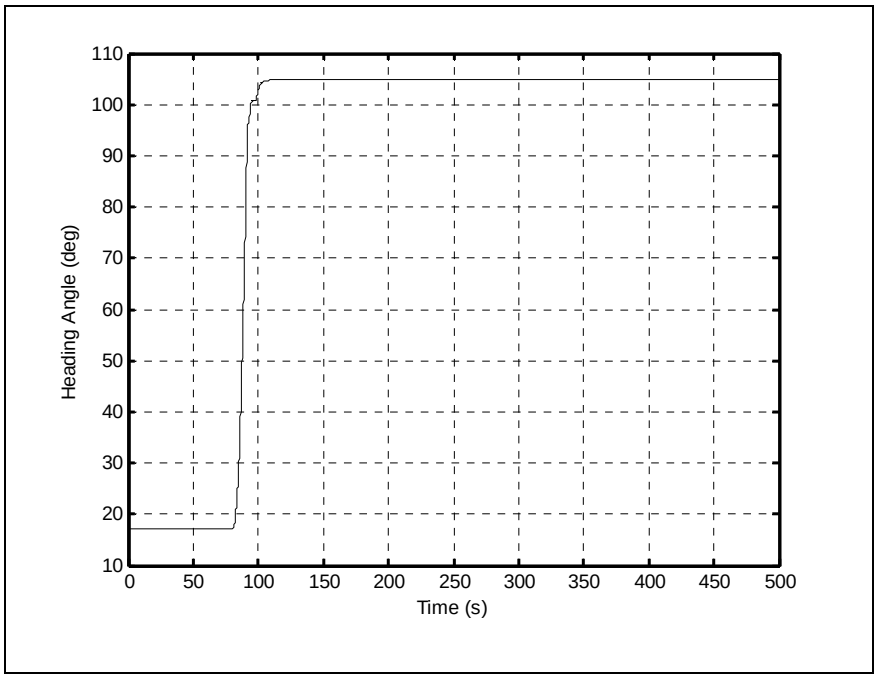

(i) Heading Angle (deg)

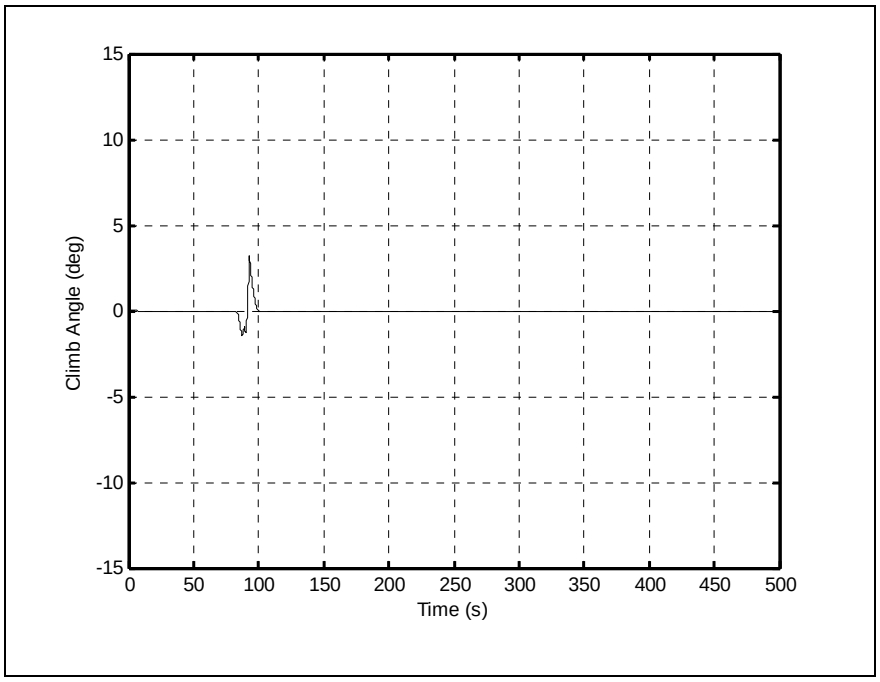

(j) Climb Angle (deg)

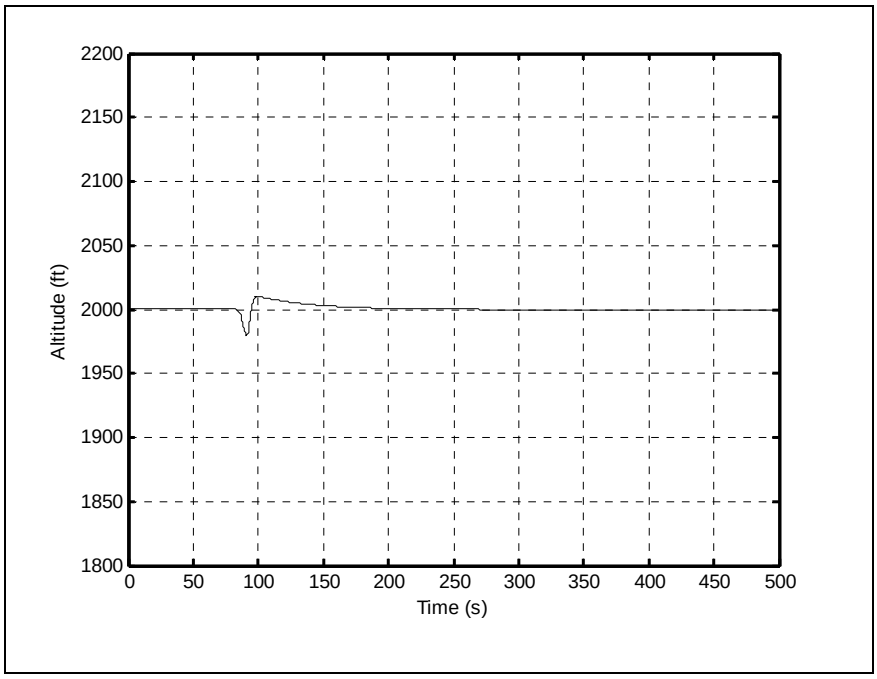

(k) Altitude (ft)

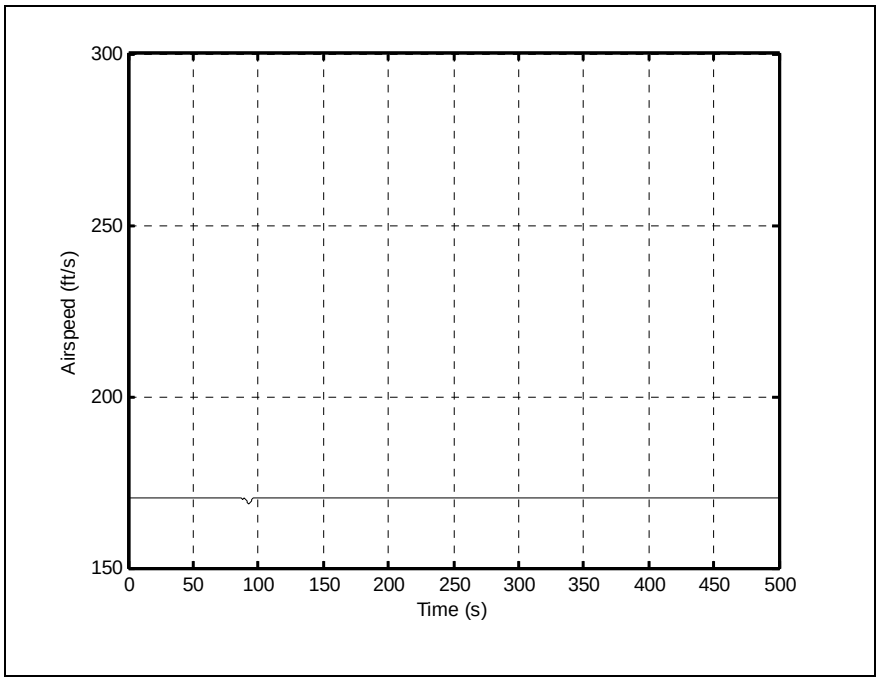

(l) Airspeed (ft/s)

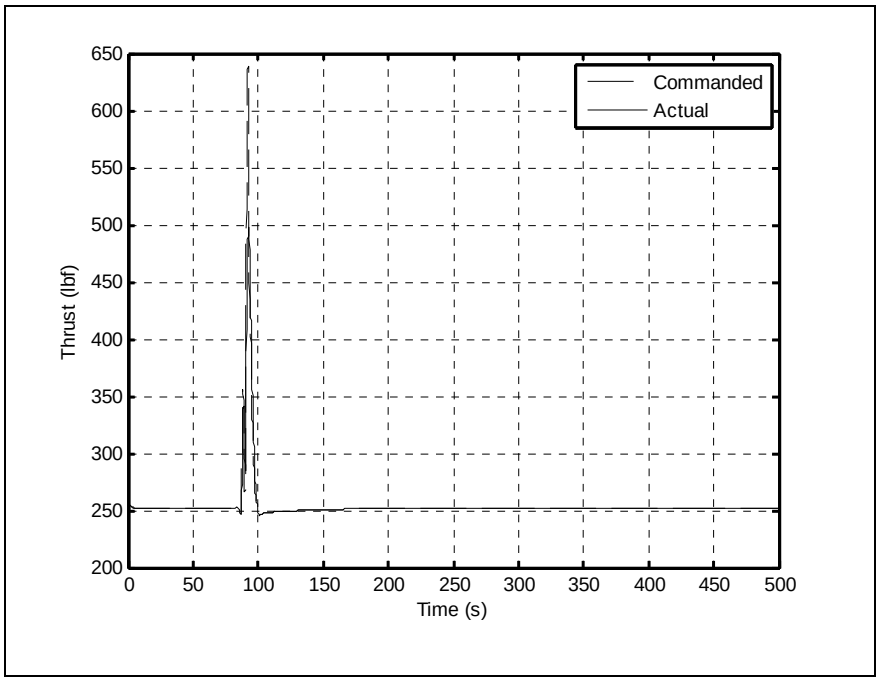

(m) Thrust (lbf)

Figure 4-3 Aircraft Trajectory and state variables for case 3

4.2.4. Case 4

It was shown in an earlier chapter that the turn radius would increase with the square of the airspeed. Likewise the turn rate was shown to decrease with the increasing the bank angle. If the turn radius associated with the highest airspeed was used to establish the size of the aircraft domain, it would result in too large of a region. Furthermore, a sharper turn could be performed at lower airspeeds. For these reasons, a limit was place on the airspeed. The purpose of the present case was to validate the implementation of this strategy.

The present maneuver was the same as that of Case 1, except the approach speed was increased to 250 ft/s, while an airspeed limit of 170 ft/s was imposed on the aircraft when in close vicinity of the restricted zone.

Again, the flight path and its relationship with the size and the placement of the restricted zone is shown in Figures 4-4(a) and (b). Much like in the previous cases, the minimum distance between the aircraft and the edge of the restricted zone remained within 300 feet. The time histories of the remaining variables are shown in Figures 4-4(c) through (m).

As the aircraft approached the restricted zone, the controller began to reduce the airspeed, resulting in a larger angle of attack required to maintain level flight. This is shown in Figure 4-4(c) for times between approximately 25 and 60 seconds. This was accomplished without any commanded bank angle. When the edge of the aircraft zone became in contact with that of the restricted zone, the controller commanded an evasive bank angle, resulting in changes in the aircraft states, as indicated in Figures 4-4(d) through (m). As long as the airspeed remained at 170 ft/s, the aircraft response was exactly the same as that of Case 1. Elevator angle changed commensurate with the reduction in airspeed and increased angle of attack, as shown in Figure 4-4(e). The aileron deflection remained reasonable and the maximum bank angle reached the limit of 45 degrees, as evident from Figures 4-4(f) and (g).

Rudder deflection angle remained within 5 degrees and the heading angle changed until the aircraft was no longer a threat to the restricted zone. These quantities are plotted in Figures 4-4 (h) and (i). Once the turn was accomplished and the aircraft resumed level flight, the controller maintained the airspeed of 170 ft/s until the aircraft was sufficiently far from the restricted zone. At that point, it allowed the airspeed to build up to that commanded by the pilot, which was 250 ft/s, as shown in Figure 4-4(l). The variations in altitude were somewhat larger in this case than in previous cases.

Nonetheless, the maneuver was performed with very reasonable excursions of altitude and climb angle, as depicted in Figures 4-4(j) and (k). The thrust required to perform the evasive operation exceeded the available threshold, as shown in Figure 4-4(m). However, the present results indicate that thrust saturation did not affect the system's performance adversely.

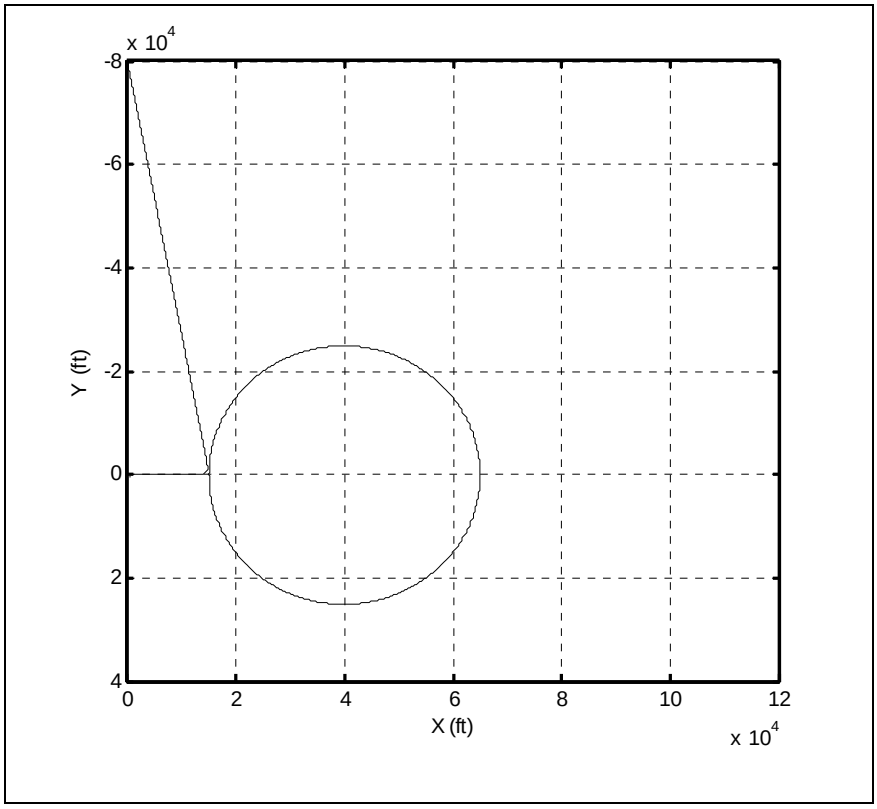

(a) Trajectory and restricted zone

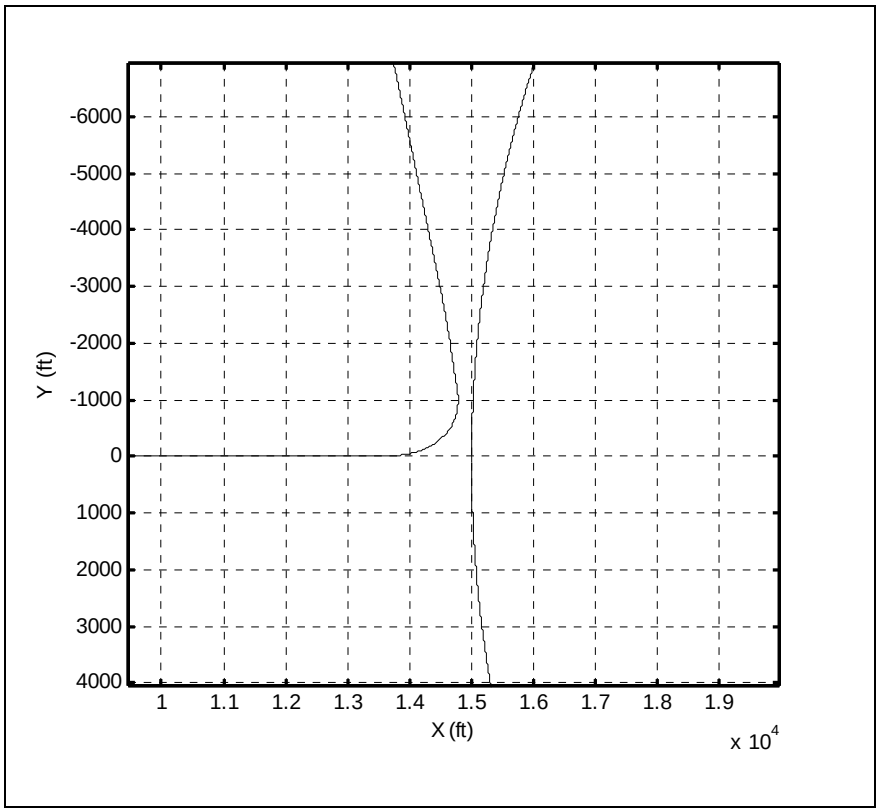

(b) Closeup view

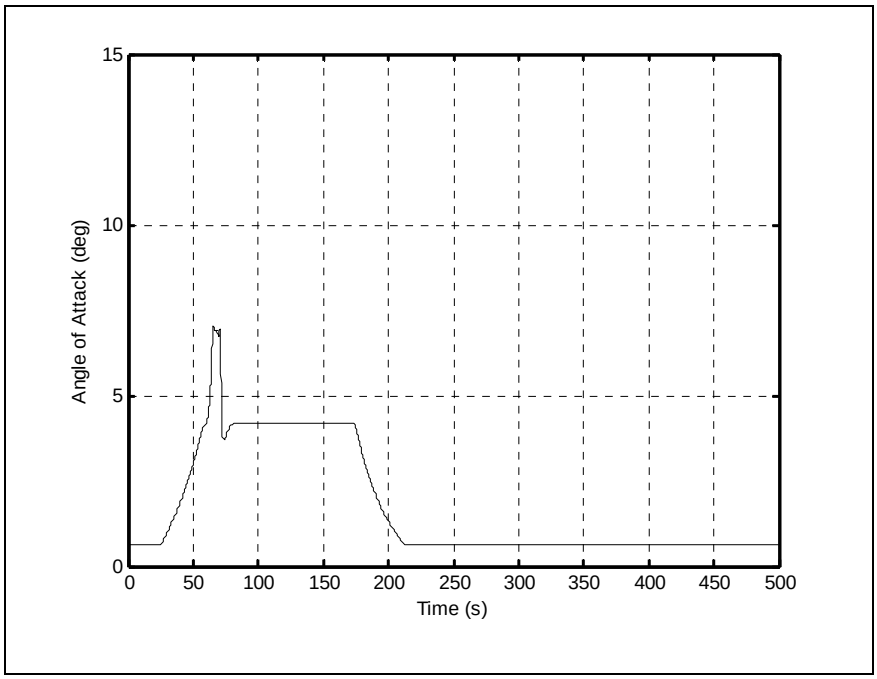

(c) Angle of Attack (deg)

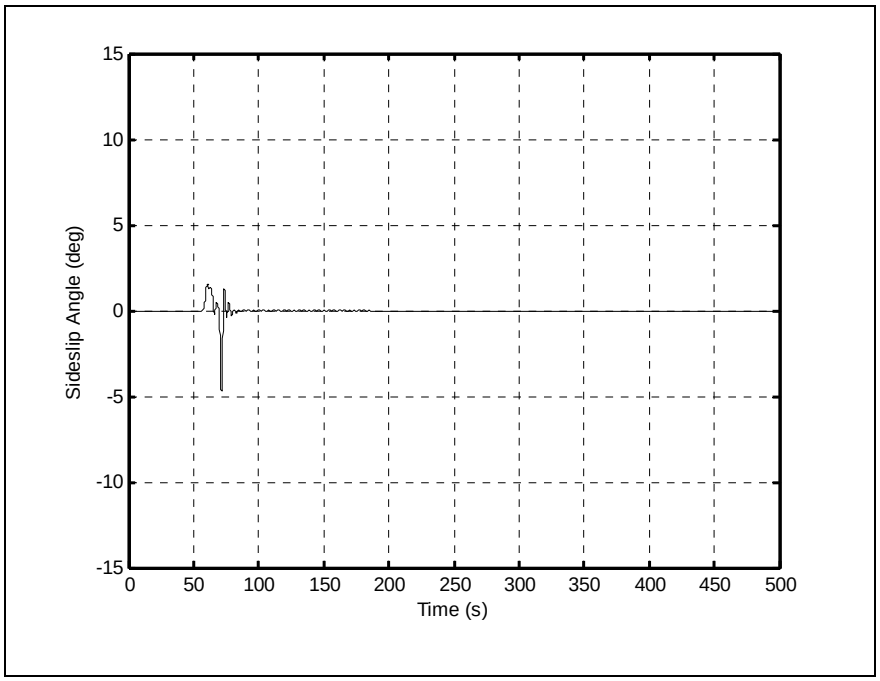

(d) Sideslip Angle (deg)

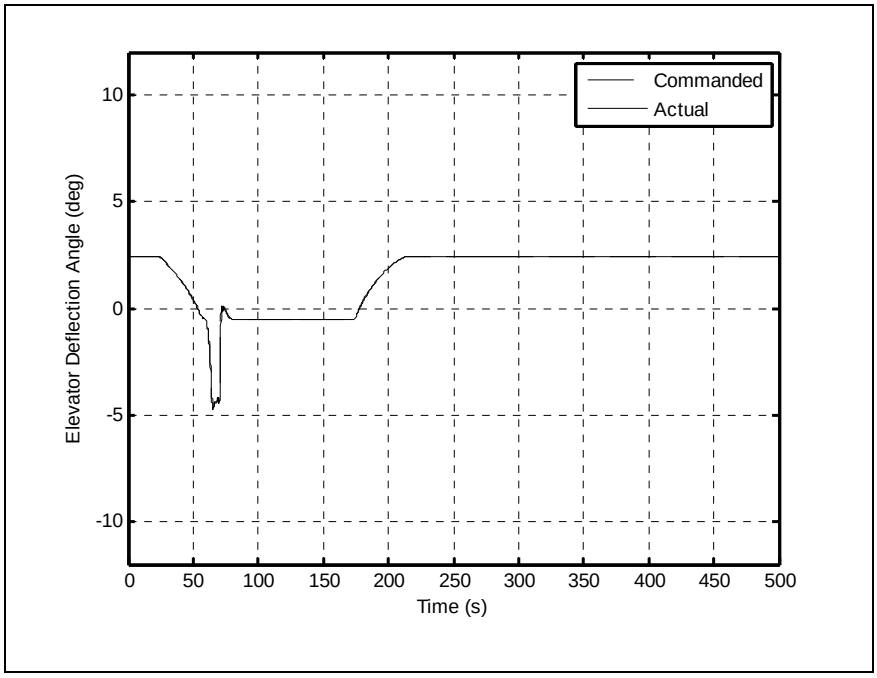

(e) Elevator Deflection Angle (deg)

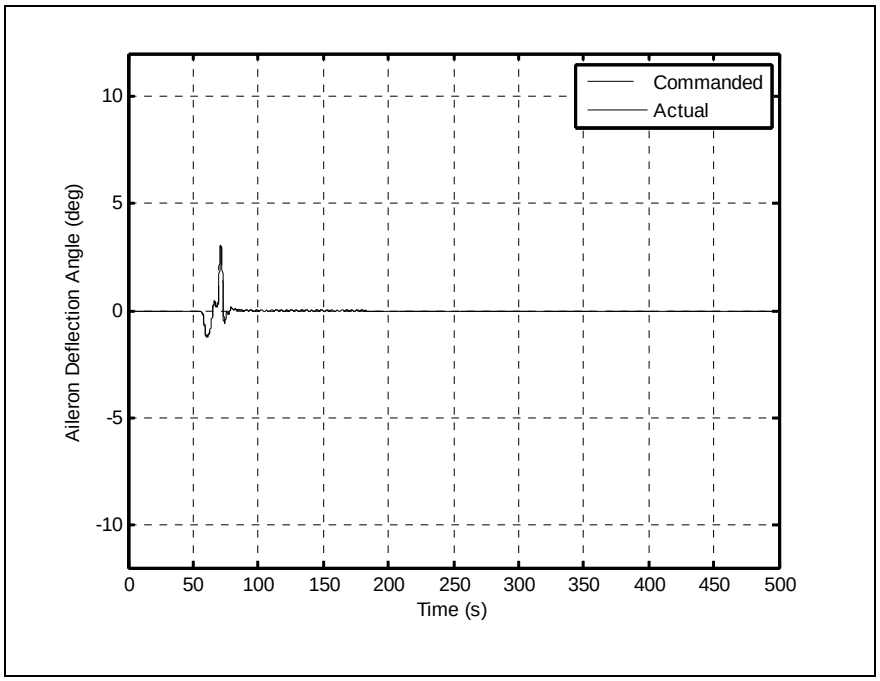

(f) Aileron Deflection Angle (deg)

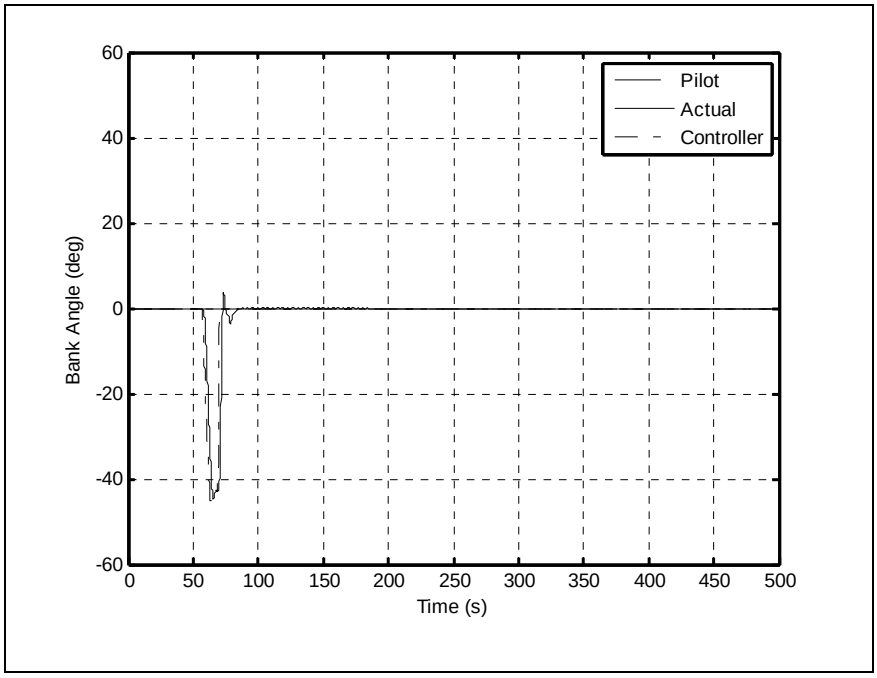

(g) Bank Angle (deg)

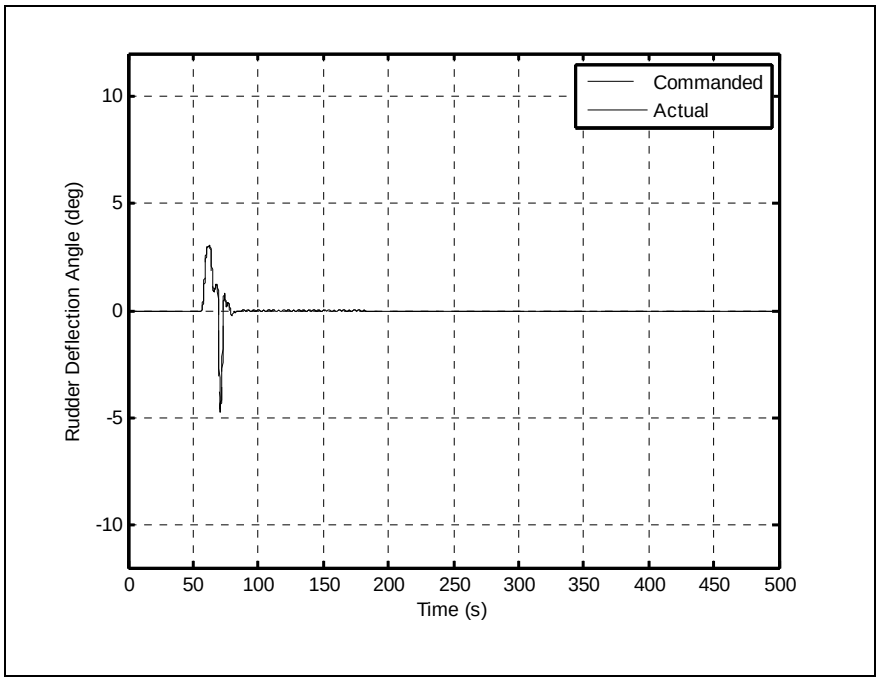

(h) Rudder Deflection Angle (deg)

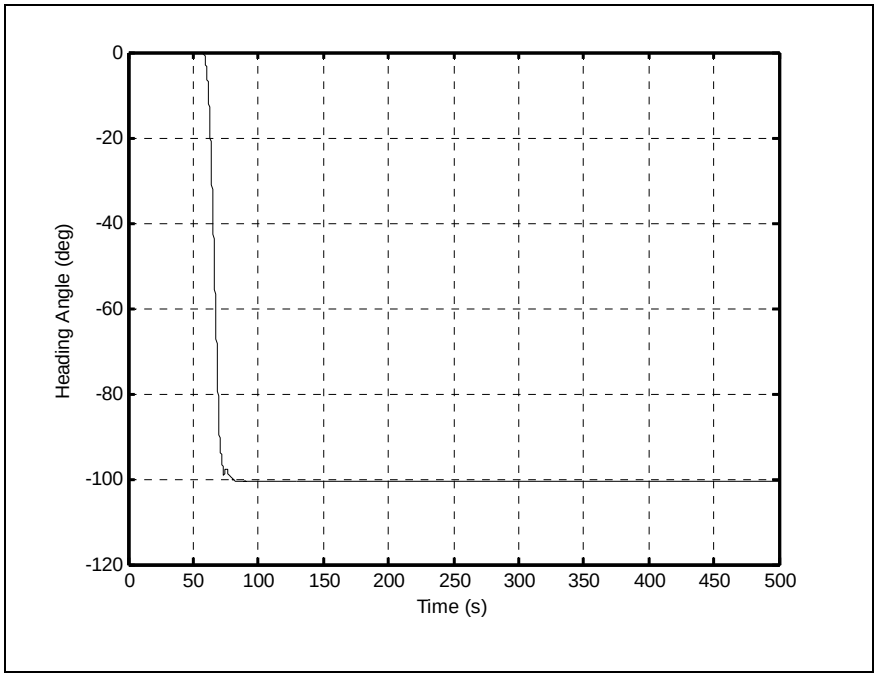

(i) Heading Angle (deg)

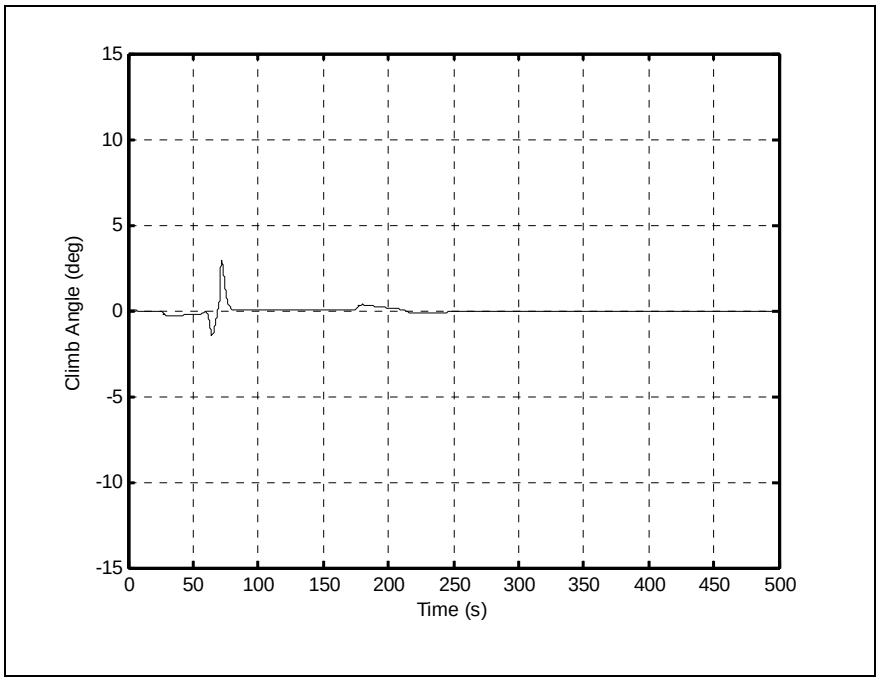

(j) Climb Angle (deg)

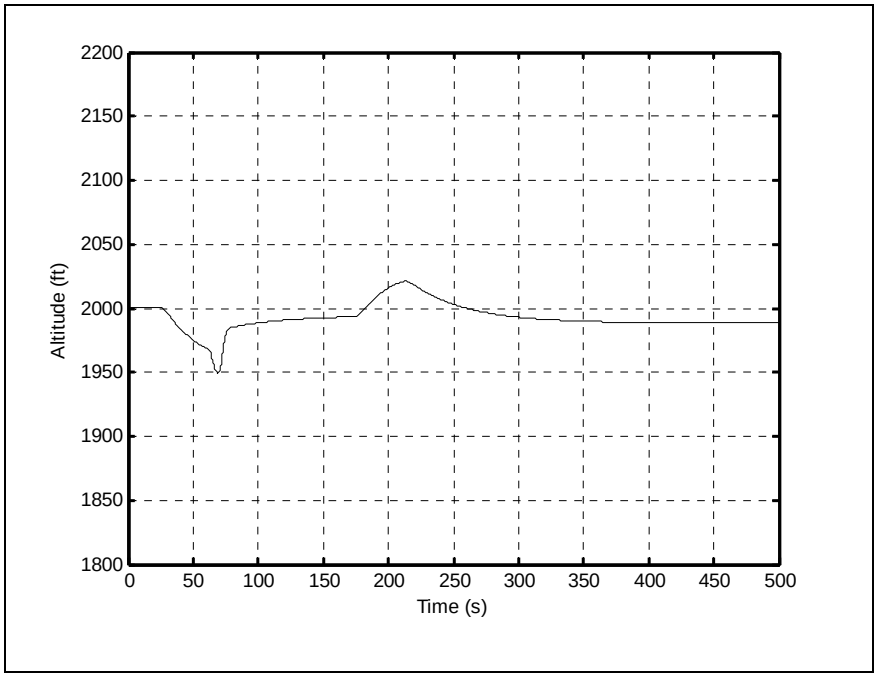

(k) Altitude (ft)

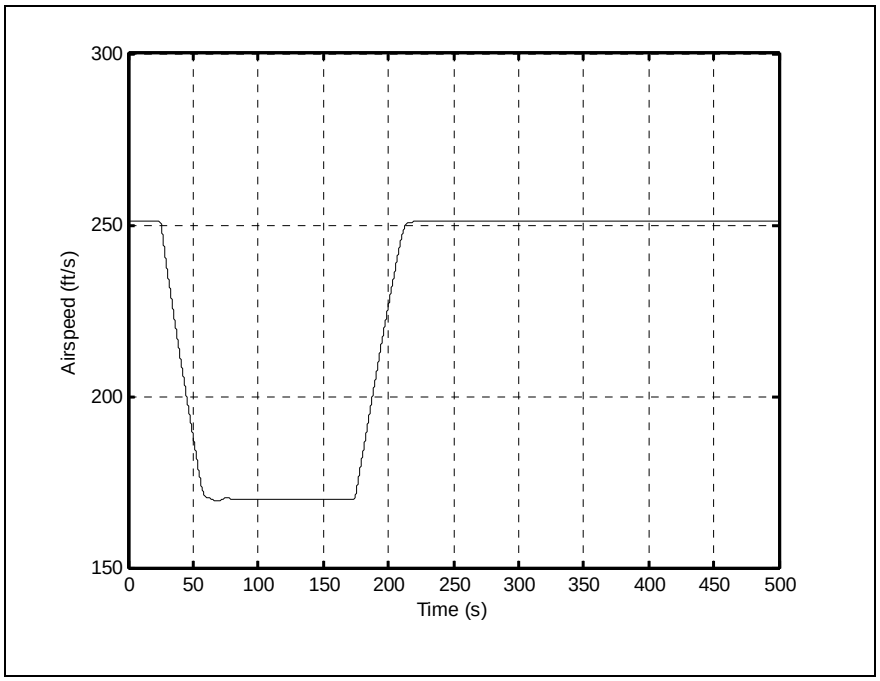

(l) Airspeed (ft/s)

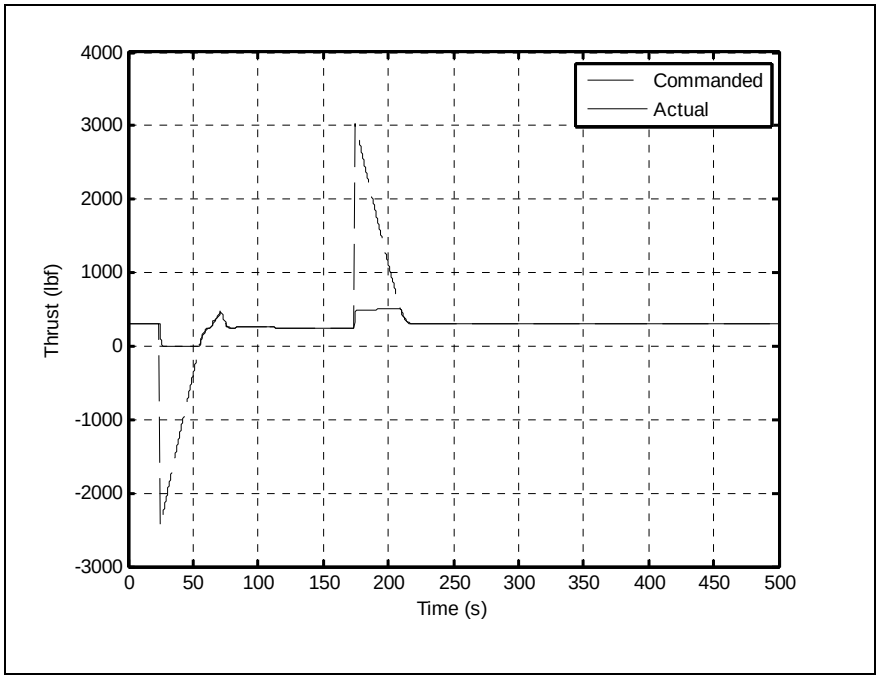

(m) Thrust (lbf)

Figure 4-4 Aircraft Trajectory and state variables for case 4

4.2.5. Case 5

In this case, it was assumed that the pilot would try to enter the restricted area intentionally by approaching the zone at an angle and trying to bank hard to the right and into this region. It is important to note that during this maneuver the pilot-commanded bank angle remained at 45 degrees for time greater than 77 seconds. The fact that the pilot did not alter his/her input is especially important in understanding the response once the avoidance operation started to take place.

The aircraft trajectory is shown in Figures 4-5(a) and (b). The aircraft approached the zone rectilinearly, but 77 seconds later, the pilot commanded a 45-degree bank turn to the right. The controller commanded a further increase in the bank angle to prevent collision of the two paths. However, the controller input was nullified when the angle between the velocity vector and the tangent to the edge of the restricted zone became larger than 90 degrees. At this moment, the full control authority returned to the pilot who tried to enter the zone again through a 45-degree bank right turn. This sequence of events was repeated once again. However, coming out of the second turn and by the time the avoidance scheme started to become active, the velocity vector was pointed to the left of the center of the restricted zone. Therefore, for the third evasive maneuver, the controller commanded a 45-dgree bank ***left*** turn. Beyond this point, the flight path started to follow the perimeter of the zone with the pilot trying hard to enter the zone by commanding a right turn.

Throughout the remainder of the maneuver, the full control authority switched abruptly between the pilot and the controller depending on the direction of the velocity vector. This was primarily due to the treatment of the approach angle, ζ. In the present

form of the algorithm, there is no smooth switching of the controls based on this angle. When the aircraft is close to restricted zone, the avoidance algorithm is either on or off, depending on whether this angle is less than or greater than ninety degrees. Therefore, every the velocity vector pointed away from the edge of the zone, the full authority was returned to the pilot, while the controller took complete control each time the velocity vector pointed towards the zone. The cyclic switching of the controls resulted in oscillations of the flight path angle and all of the other variables, as shown in Figures 4-5(c) through (m). Nevertheless, the controller was successful in preventing the aircraft from entering the zone. The scheduling of the switching of the control authority between the pilot and the controller in this case is an area that needs to be investigated further.

Examining these figures reveals that despite the severe oscillations in the controls, the aircraft performed this maneuver without much gain in altitude or loss of airspeed.

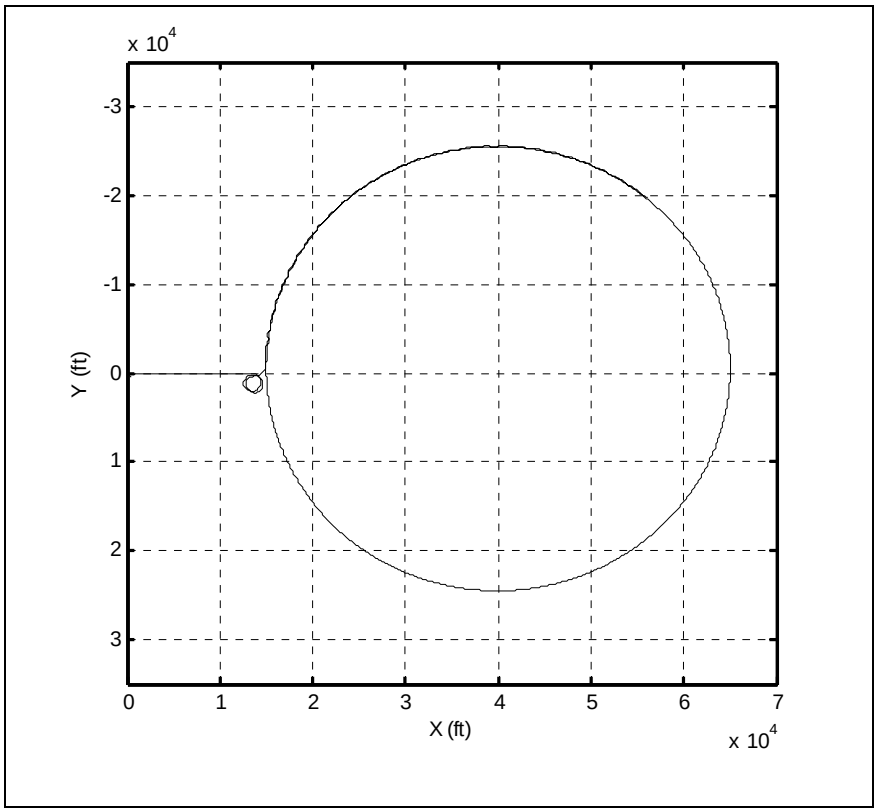

(a) Trajectory and restricted zone

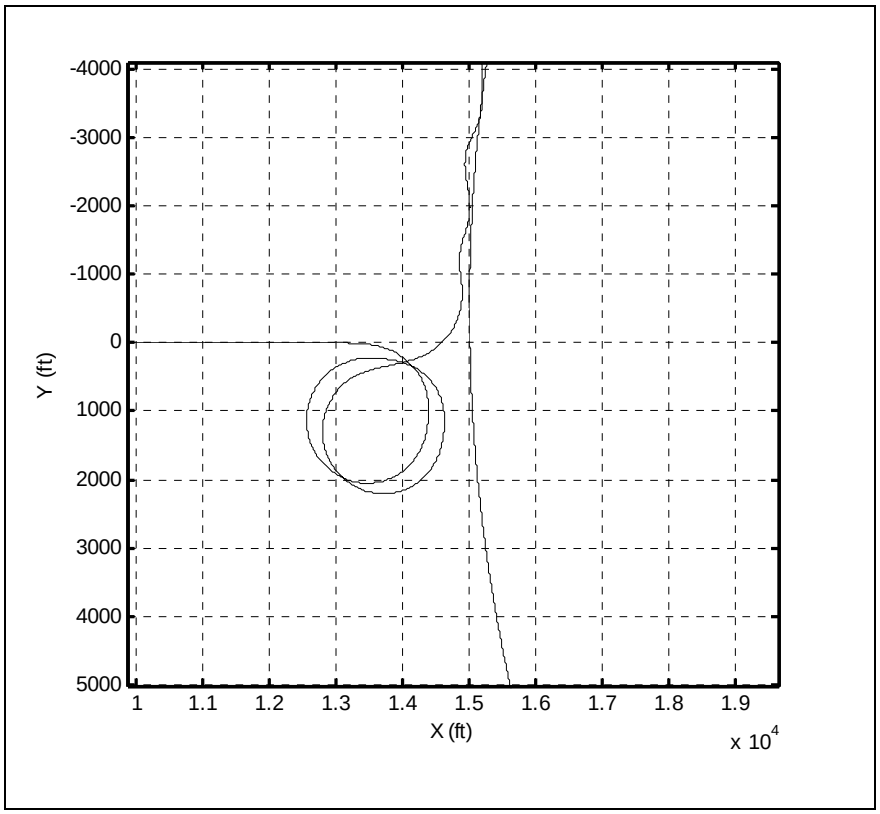

(b) Closeup view

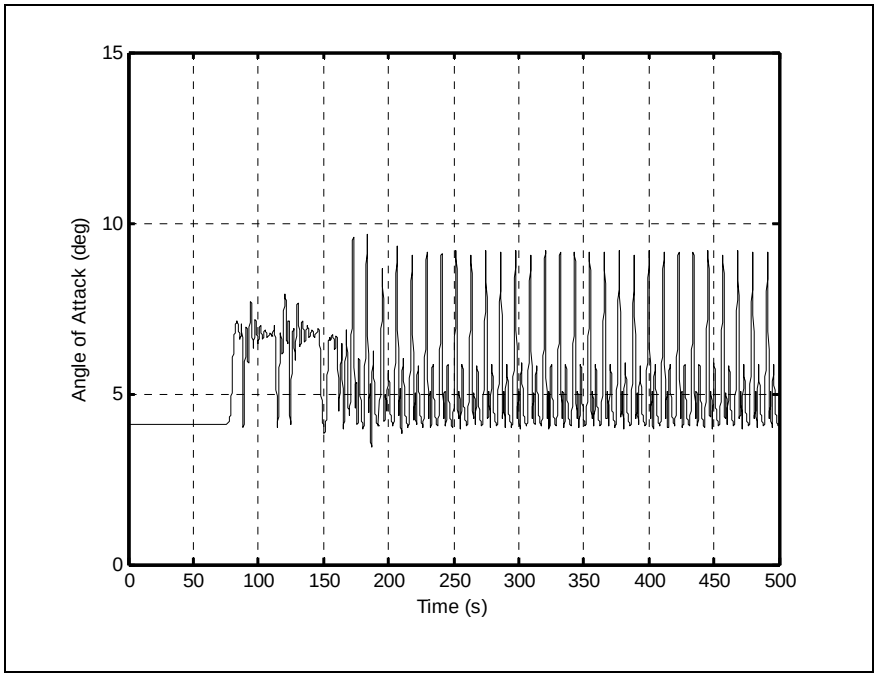

(c) Angle of Attack (deg)

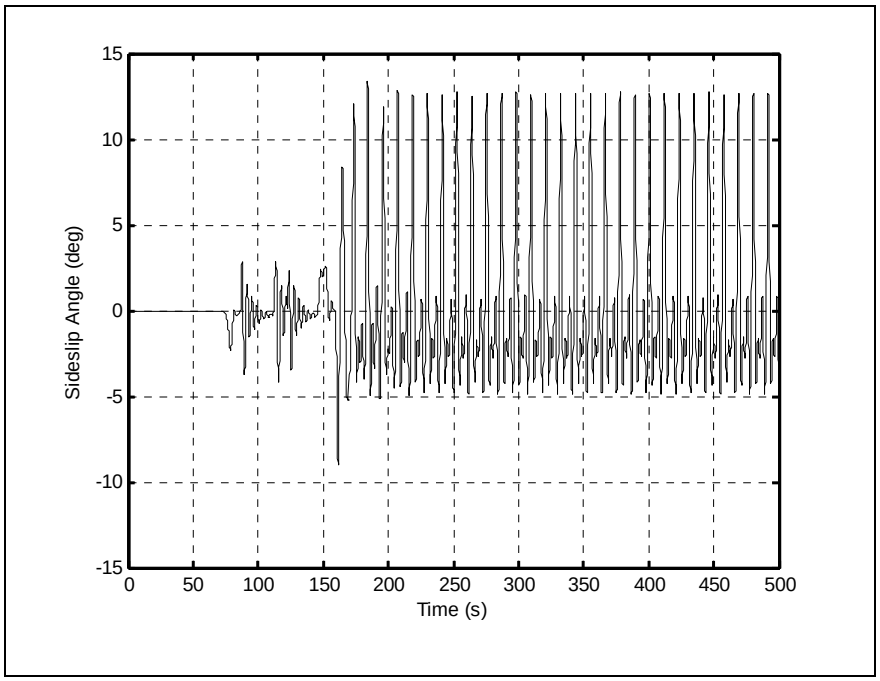

(d) Sideslip Angle (deg)

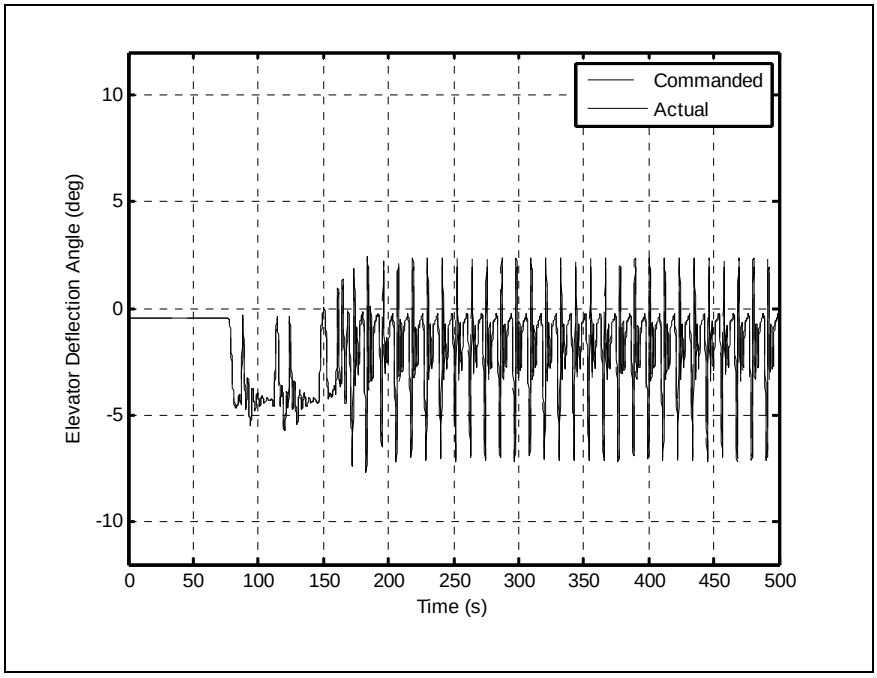

(e) Elevator Deflection Angle (deg)

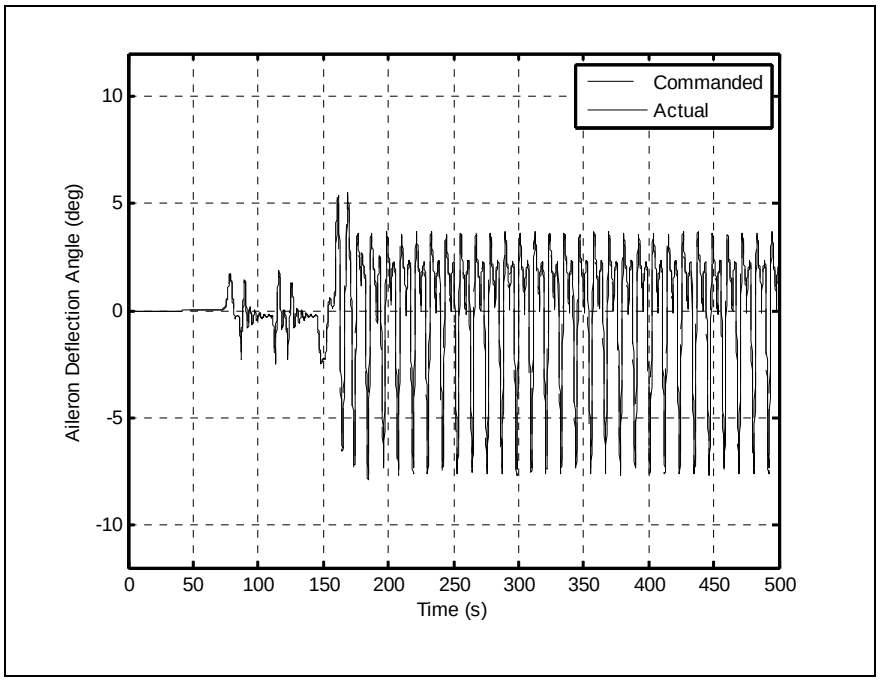

(f) Aileron Deflection Angle (deg)

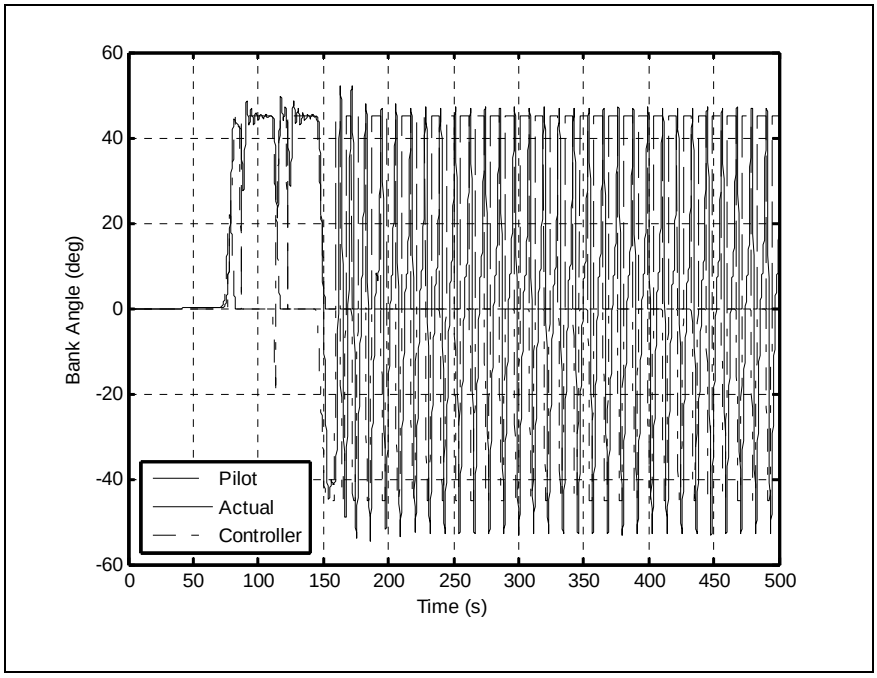

(g) Bank Angle (deg)

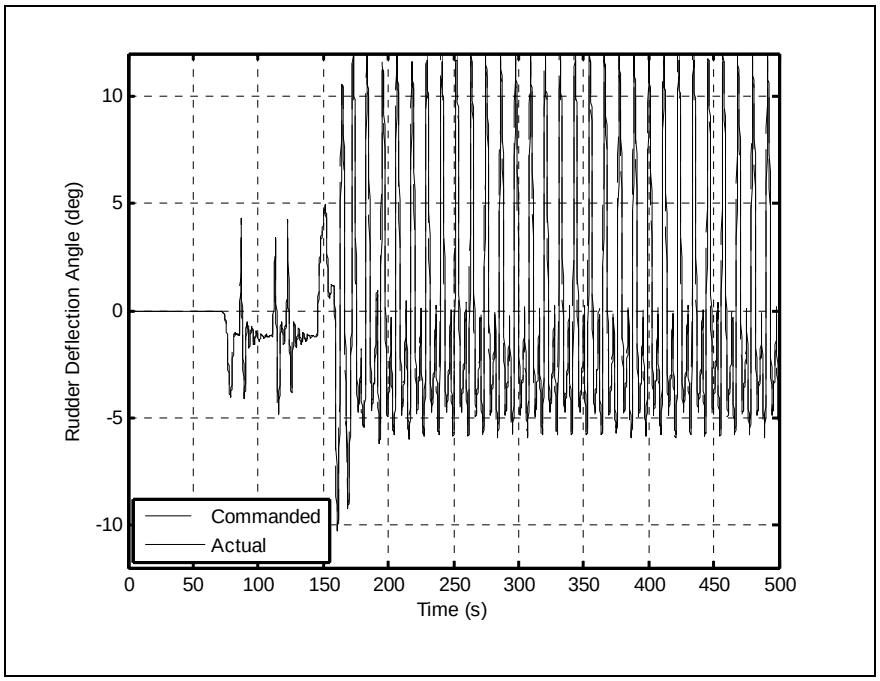

(h) Rudder Deflection Angle (deg)

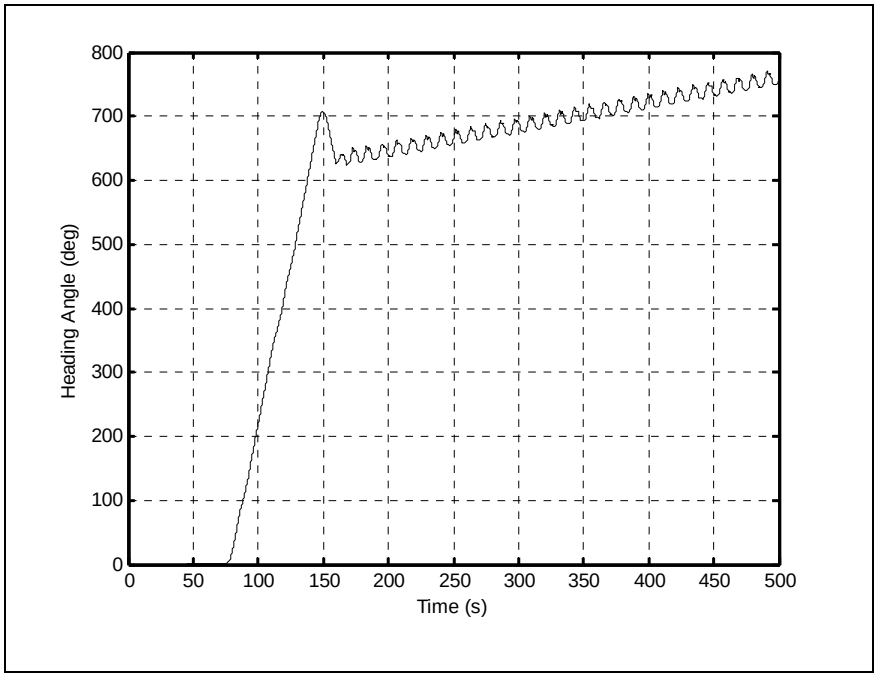

(i) Heading Angle (deg)

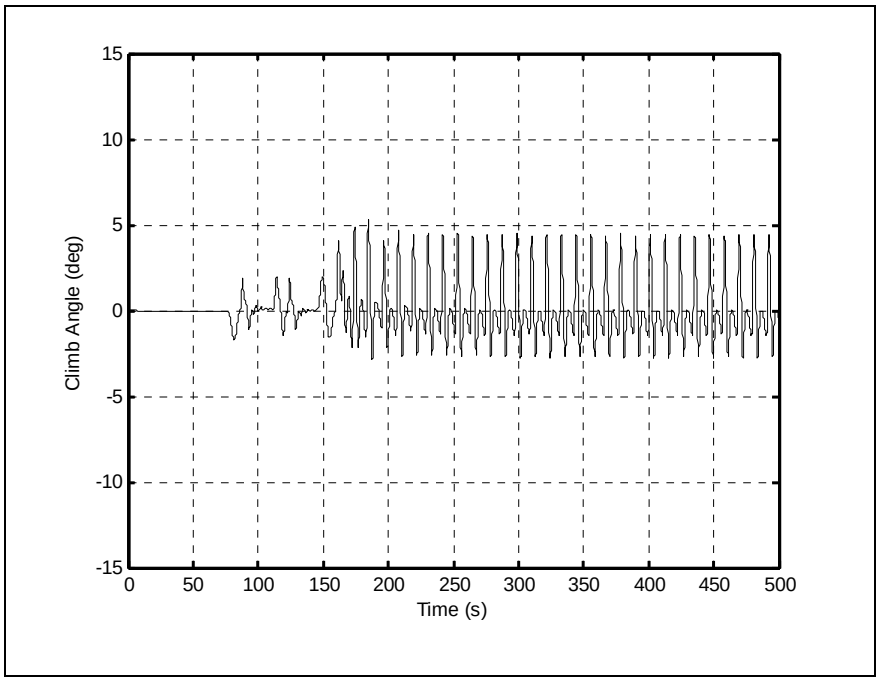

(j) Climb Angle (deg)

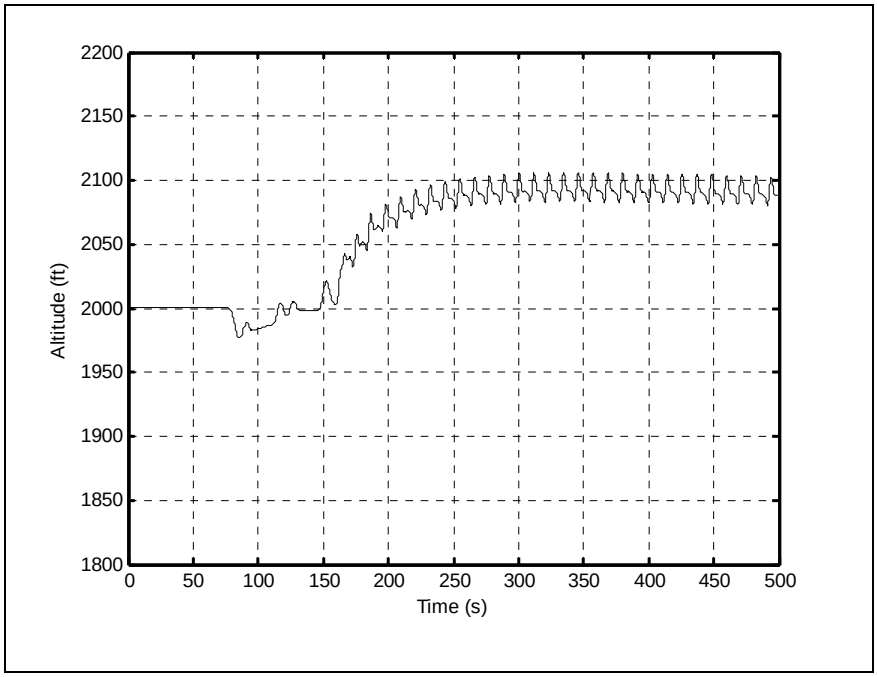

(k) Altitude (ft)

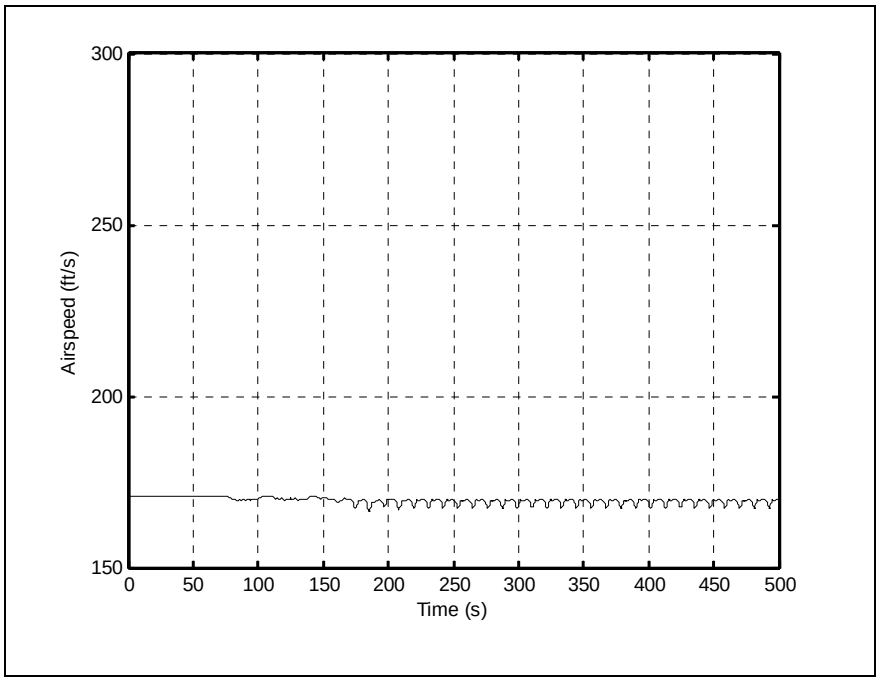

(l) Airspeed (ft/s)

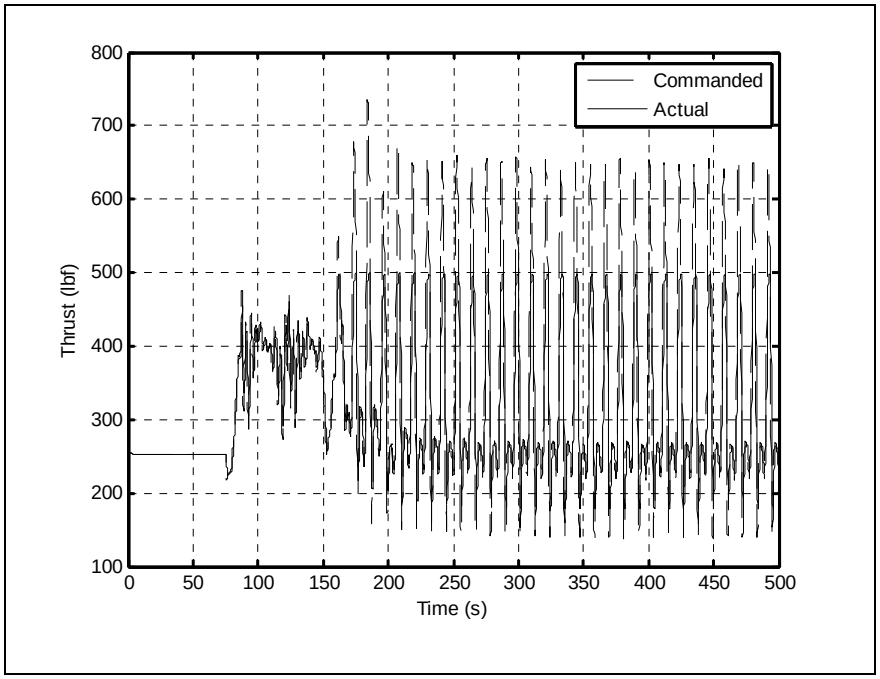

(m) Thrust (lbf)

Figure 4-5 Aircraft Trajectory and state variables for case 5

4.2.6. Case 6

This is the final single-zone case shown in this document and is almost identical to the previous case, except the initial approach was made at 250 ft/s. As a result of this, controller decreased the velocity to 170 ft/s before getting near to the zone

Again, the flight trajectory and its close-up view are given in Figures 4-6(a) and (b). Much like in the previous cases, the aircraft approached the zone rectilinearly and the controller started reducing the airspeed. However, this time when the control was returned to the pilot after the first turn, the velocity vector was pointed to the left of the center of the restricted zone. Therefore, for the second evasive maneuver, the controller commanded a left turn. Beyond this point, the response was very similar to that of the previous case, as shown in Figures 4-6(c) through (m). The reader is cautioned that although these plots show radical oscillations in the commanded values of the controls, the actual values were significantly smoother. The actuator models and the saturations of the controls and the thrust prevented large oscillations in these values from being introduced in the equations of motion. Nevertheless, oscillation of the order of 5 degrees in angle of attack and 20 degrees in sideslip angle are not deemed acceptable at this writing. Furthermore, the behavior of the altitude needs to be examined more closely as part of the refinement of this algorithm. One possible area of future investigation would be the introduction of the artificial neural networks back into the flight control system. At this point, the reader is reminded that throughout the above cases, all artificial neural networks were removed from the AFCS.

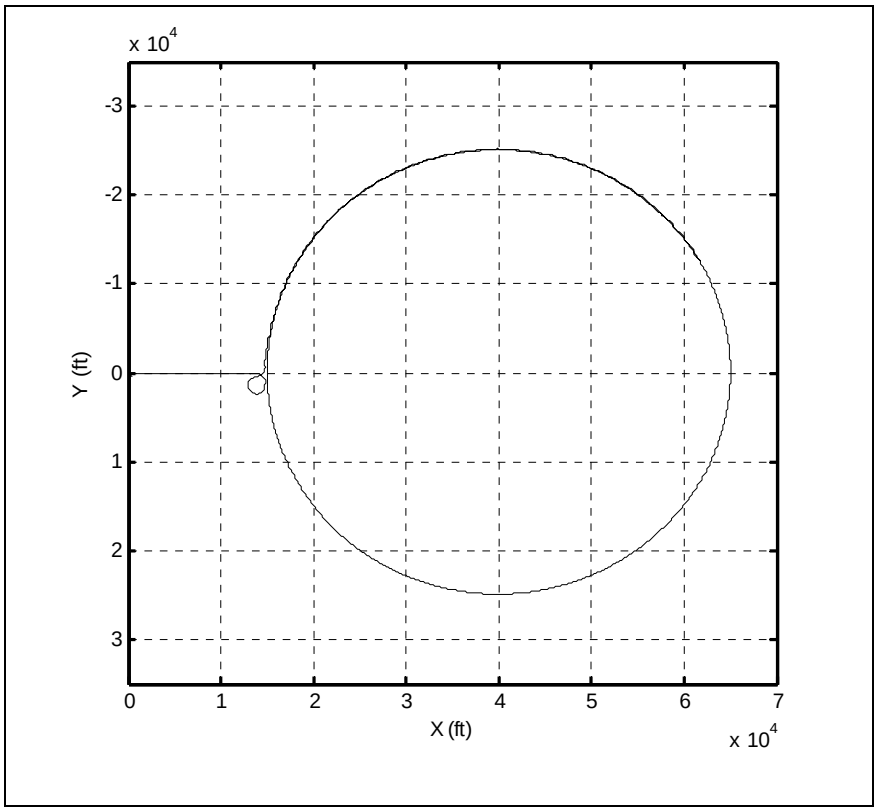

(a) Trajectory and restricted zone

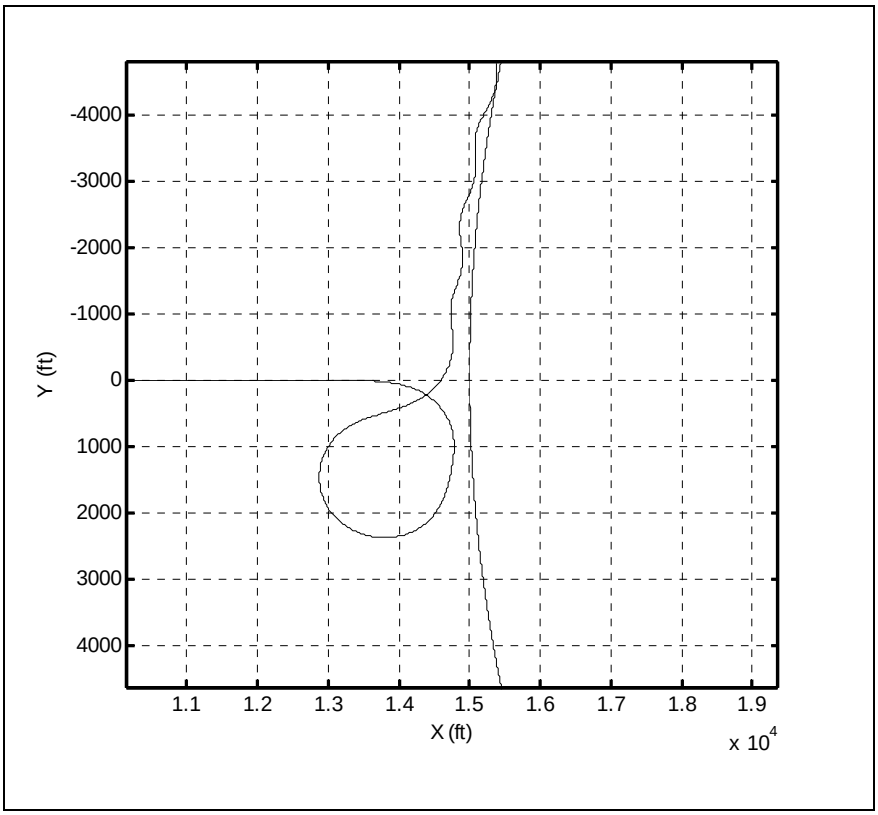

(b) Closeup view

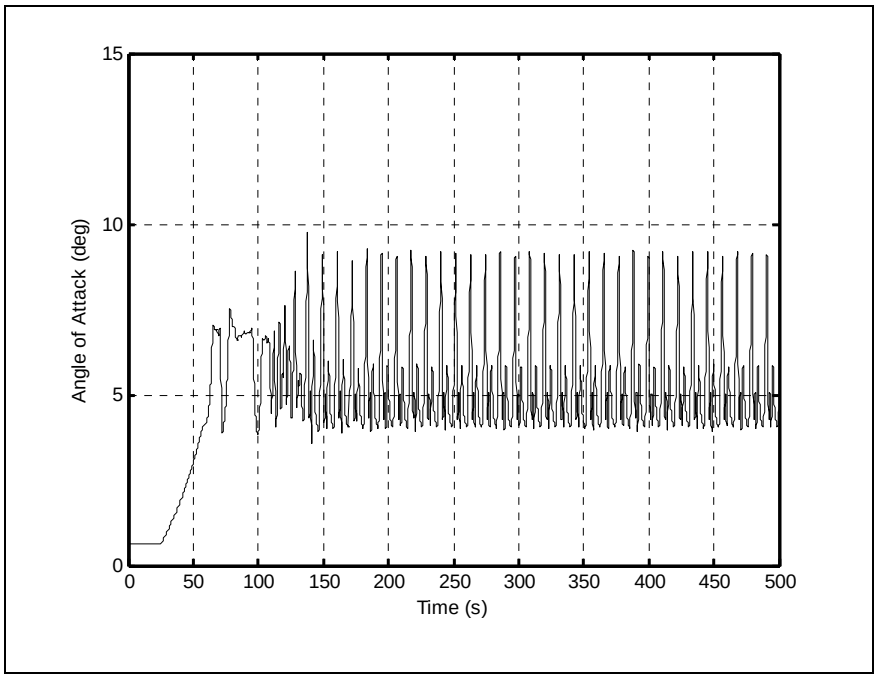

(c) Angle of Attack (deg)

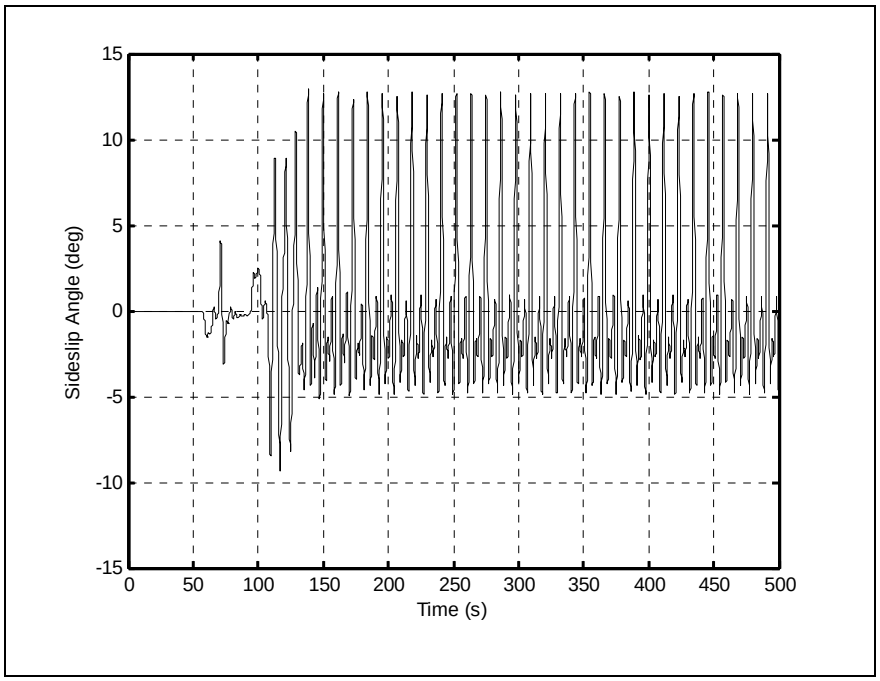

(d) Sideslip Angle (deg)

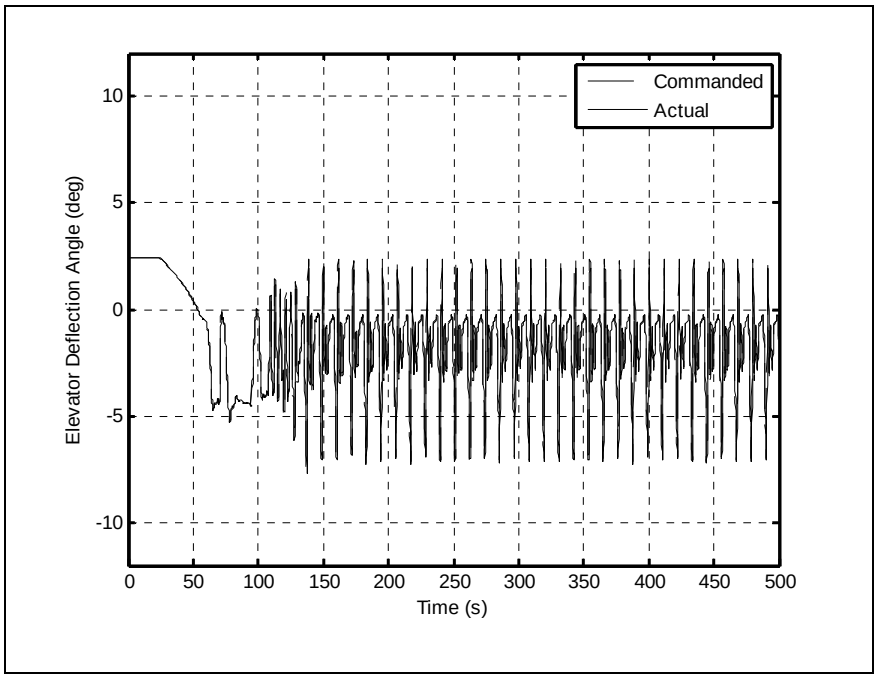

(e) Elevator Deflection Angle (deg)

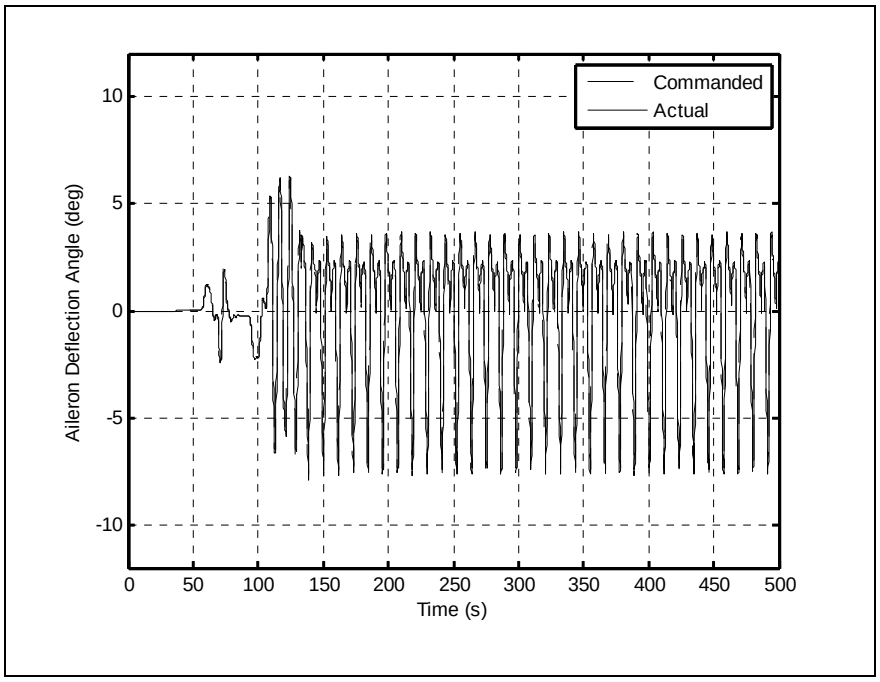

(f) Aileron Deflection Angle (deg)

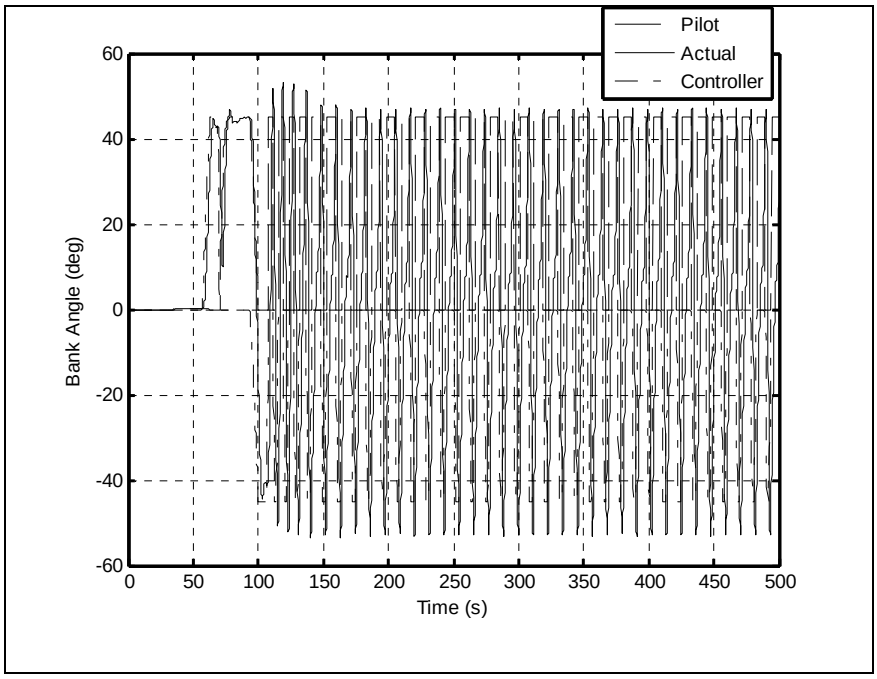

(g) Bank Angle (deg)

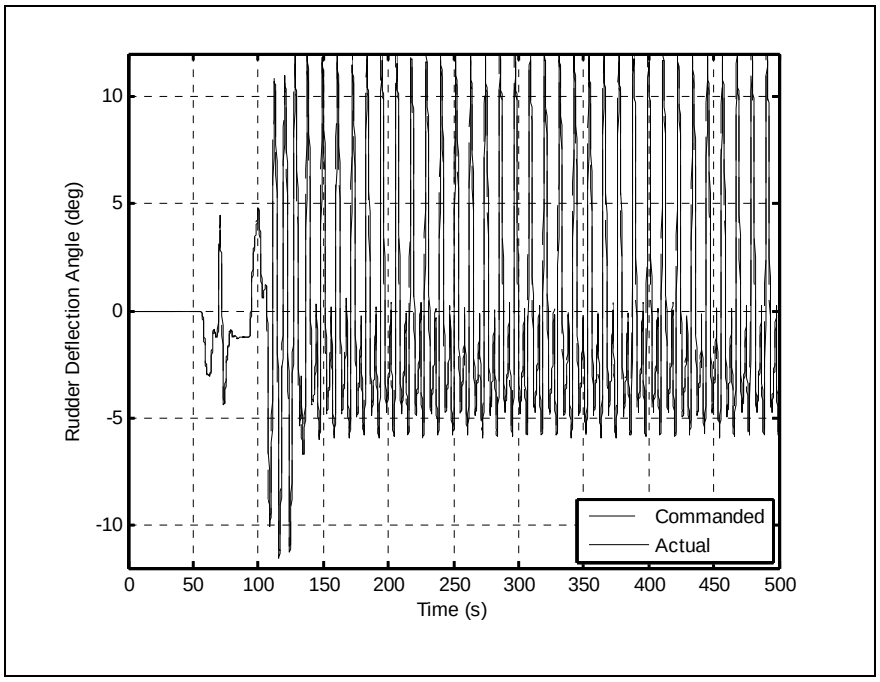

(h) Rudder Deflection Angle (deg)

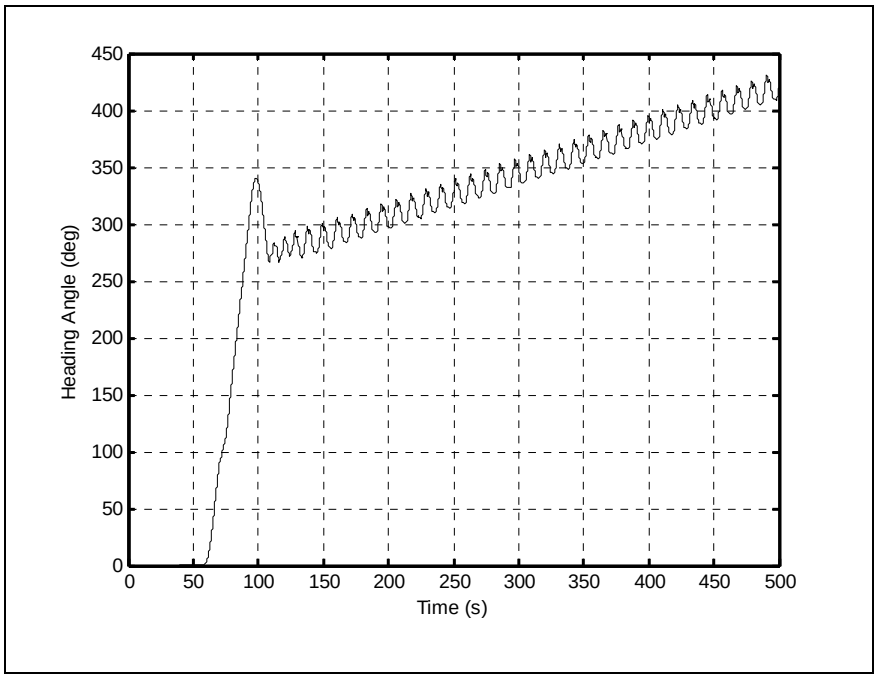

(i) Heading Angle (deg)

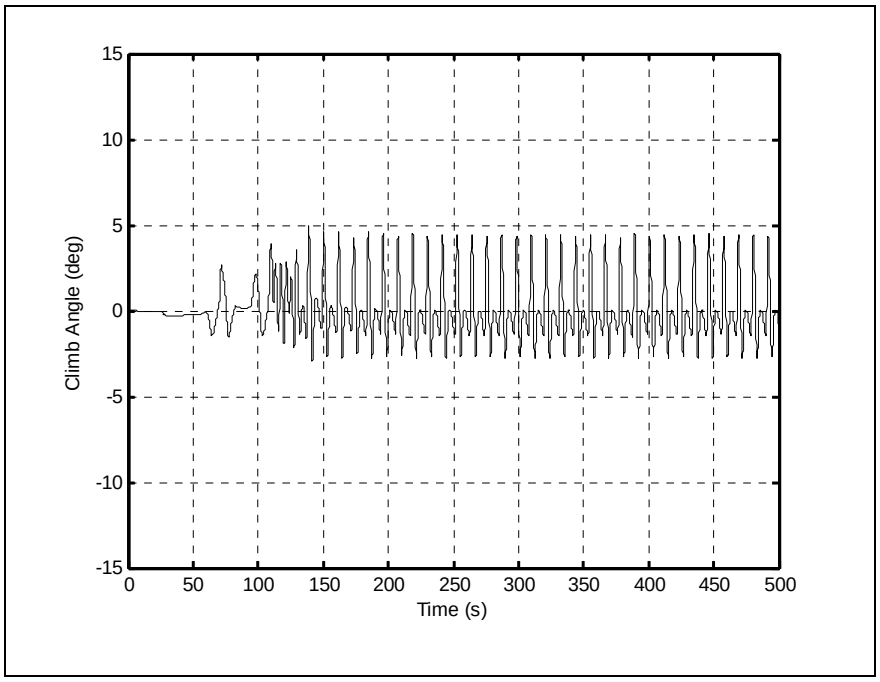

(j) Climb Angle (deg)

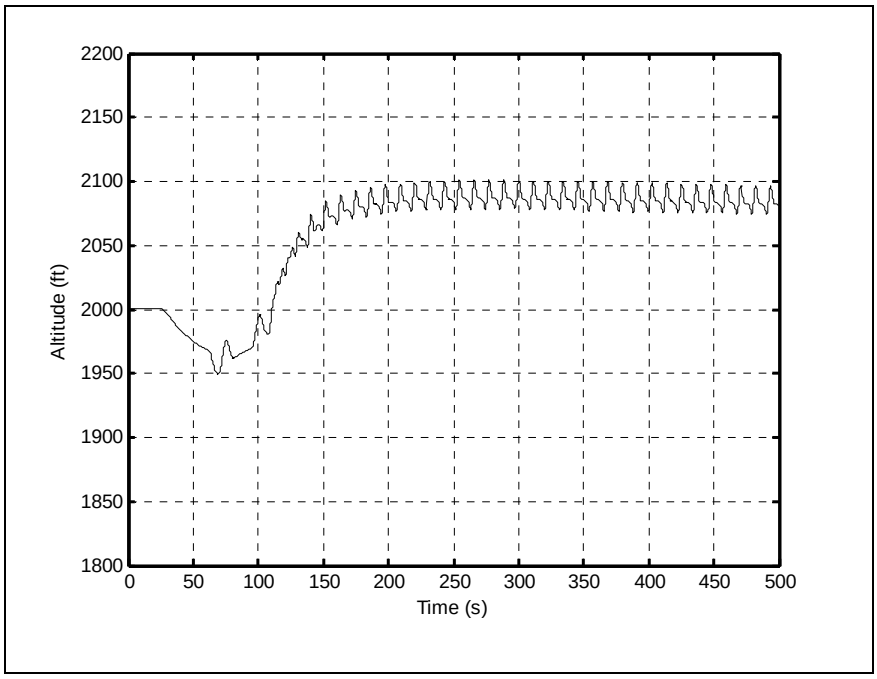

(k) Altitude (ft)

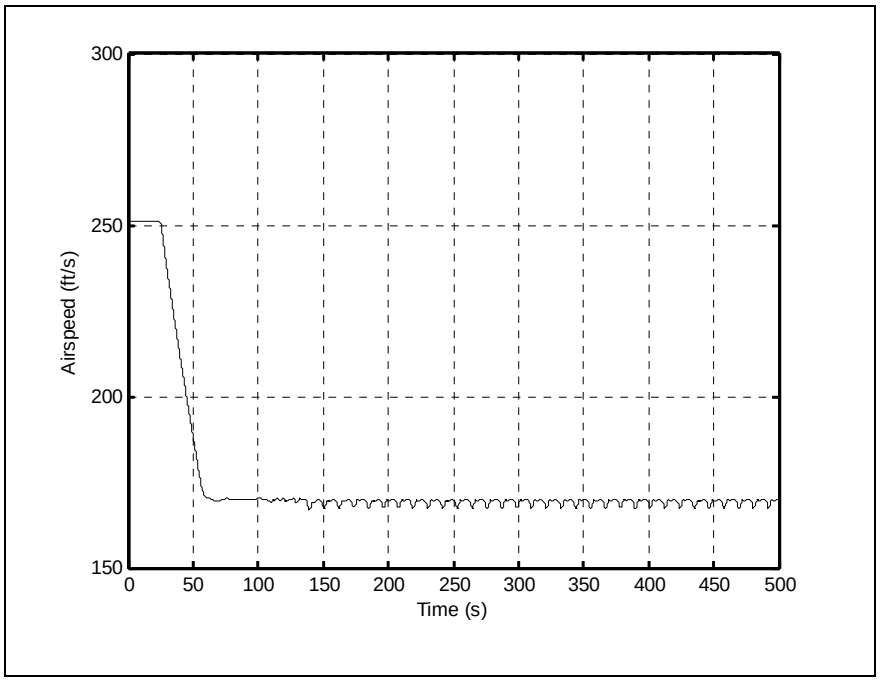

(l) Airspeed (ft/s)

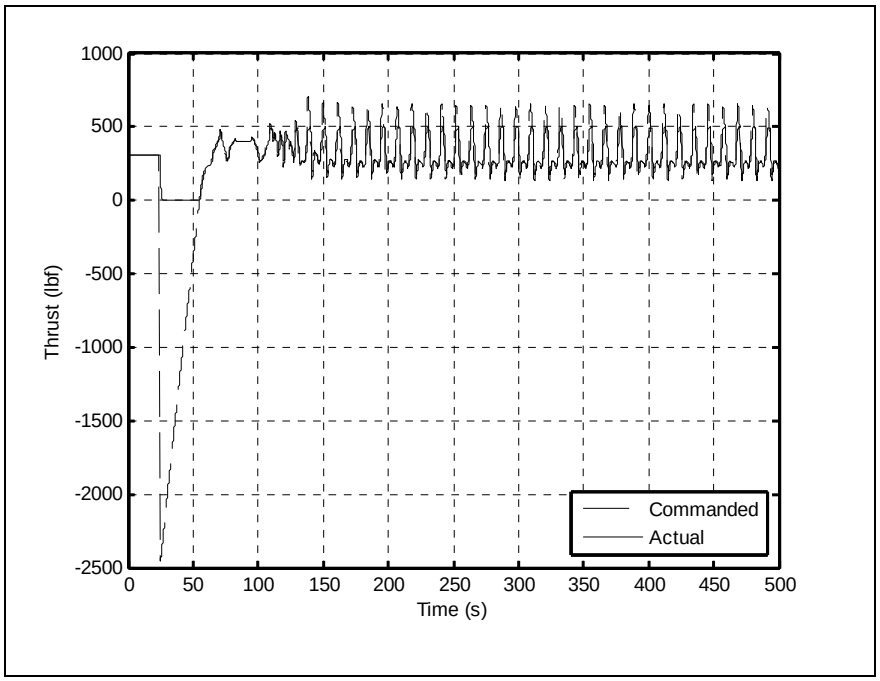

(m) Thrust (lbf)

Figure 4-6 Aircraft Trajectory and state variables for case 6

4.3. Multiple Zones

The only multiple-zone case considered for demonstration was that of an airspace cluttered with eleven (11) restricted zones of equal size. These regions did not overlap, but were placed randomly within the reach of the aircraft. The distribution of the zones, the aircraft trajectory, and its close-up are shown in Figures 4-7(a) and (b). The initial approach was made at 250 ft/s with the controller reducing the airspeed to 170 ft/s when the aircraft reached close to any of the zones. There was no pilot input in this case in that the intended flight path was steady and level.

The time histories of angle of attack, the sideslip angle, and the elevator deflection angle are shown in Figures 4-7(c) through (e). From these figures, it is clear that every time the controller changed the airspeed, the angle of attack and the elevator deflection angle also changed commensurately. Furthermore, the sideslip angle remained

within reasonable bounds. Figures 4-7(f) and (g) show clearly that the controller turned the aircraft enough to avoid each zone separately. Once the danger of the collision with a zone was over, the aircraft returned to level flight and if the distances allowed, the airspeed built up to its intended value.

Examining the results in Figures 4-7(h) and (i) reveals clearly that the system maneuvered the aircraft successfully through the collection of the restricted zones by applying the correct combination of speed control and commanded bank angle. Also, Figures 4-7(j) and (k) show how this operation was performed while keeping the altitude within 100 feet of its intended value.

From the discussions presented above, it is obvious that the presented algorithm was successful in automatic avoidance of restricted zones in many cases. It is equally evident from this material that there is need for further improvements of this technique for the purpose of better tuning. Examples include smoother switching tied to changes in the approach steepness angle, ζ, as well as inclusion of the artificial neural networks for better tracking. In the present implementation, the inverse model was that of the exact aircraft, without any nonlinearity. The influence of nonlinear effects on the system performance is also an area that needs to be investigated in further detail.

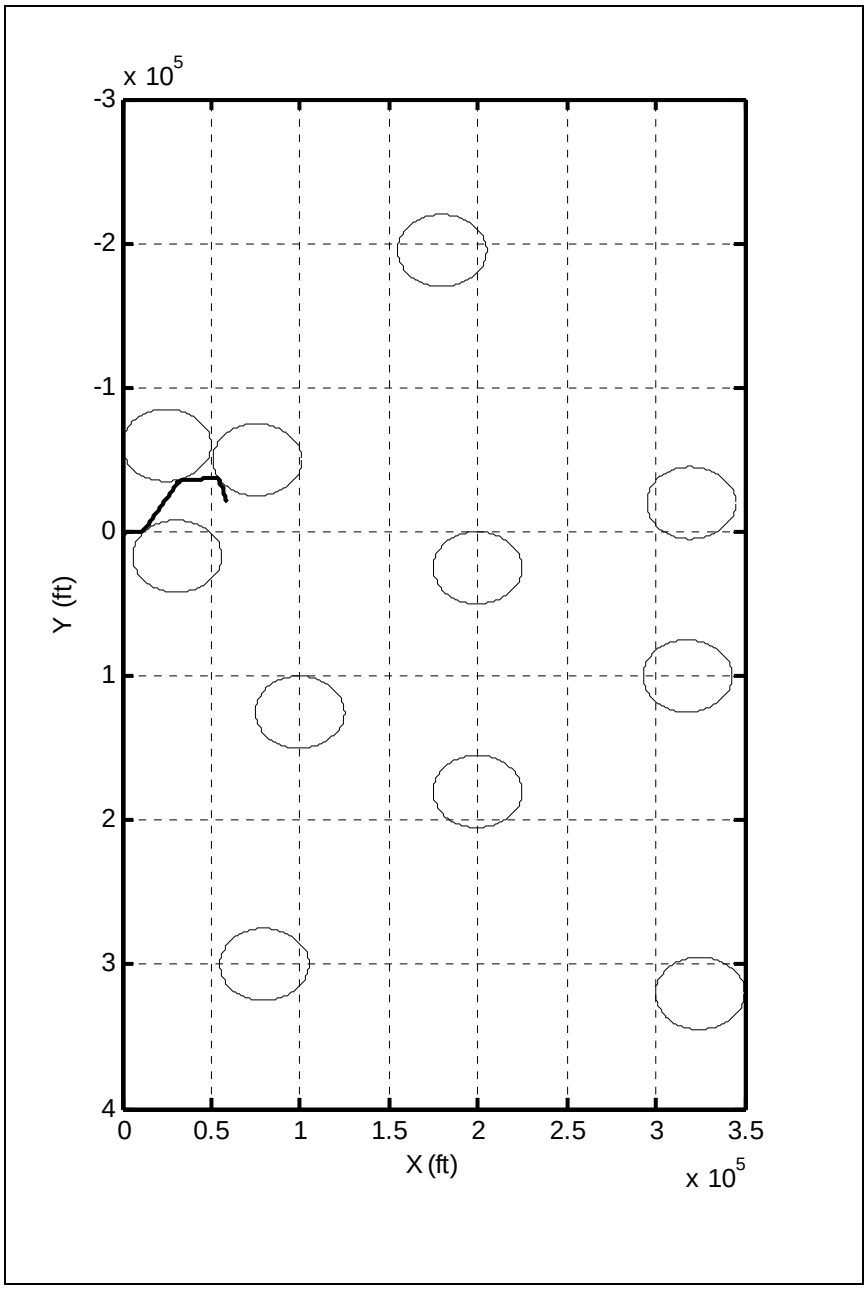

(a) Trajectory and restricted zones

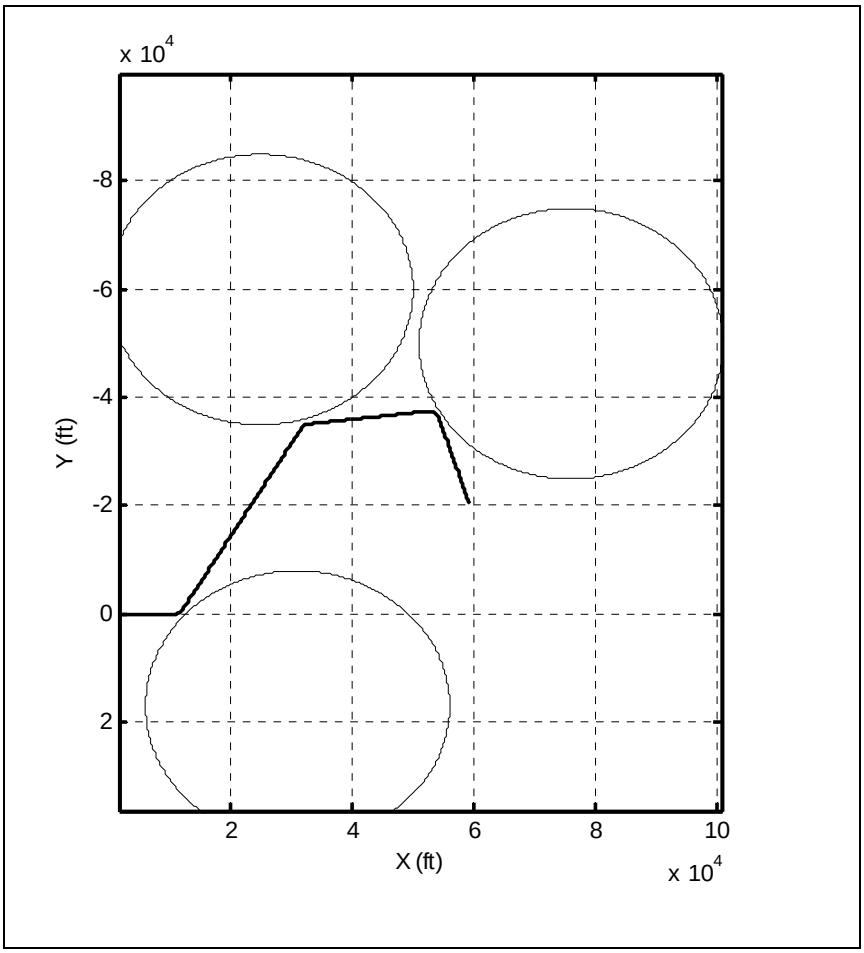

(b) Closeup view

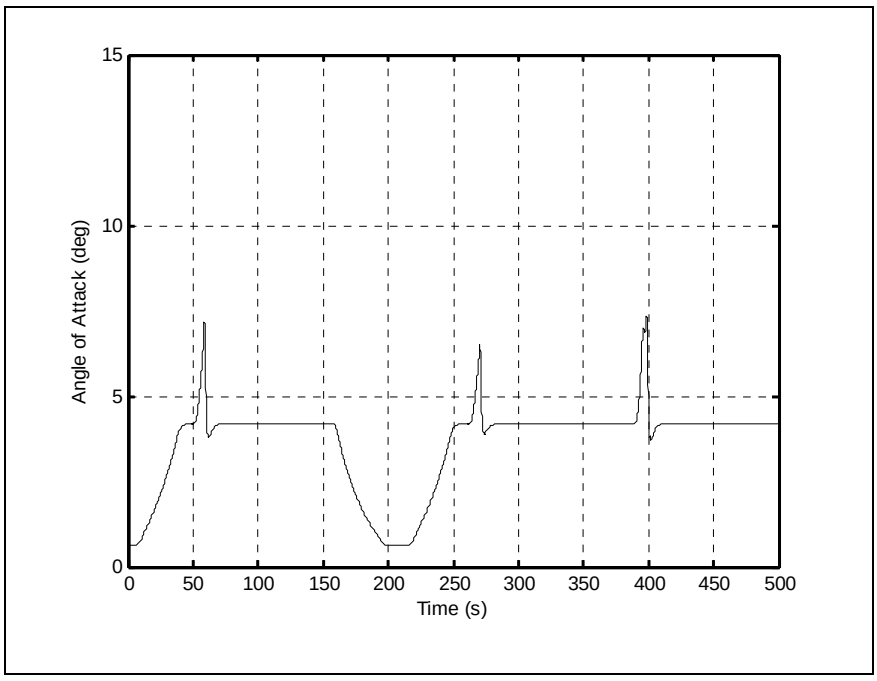

(c) Angle of Attack (deg)

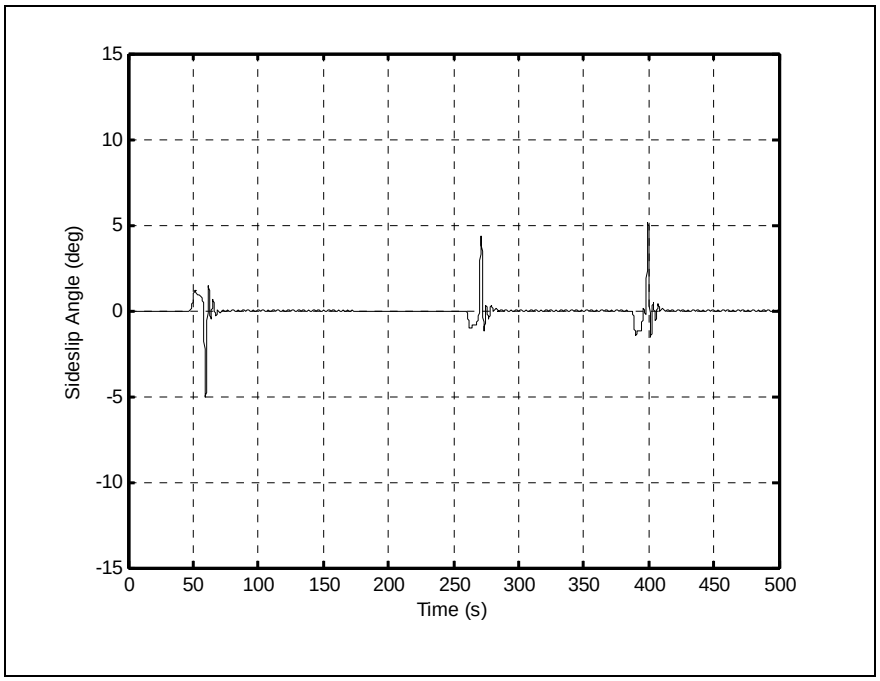

(d) Sideslip Angle (deg)

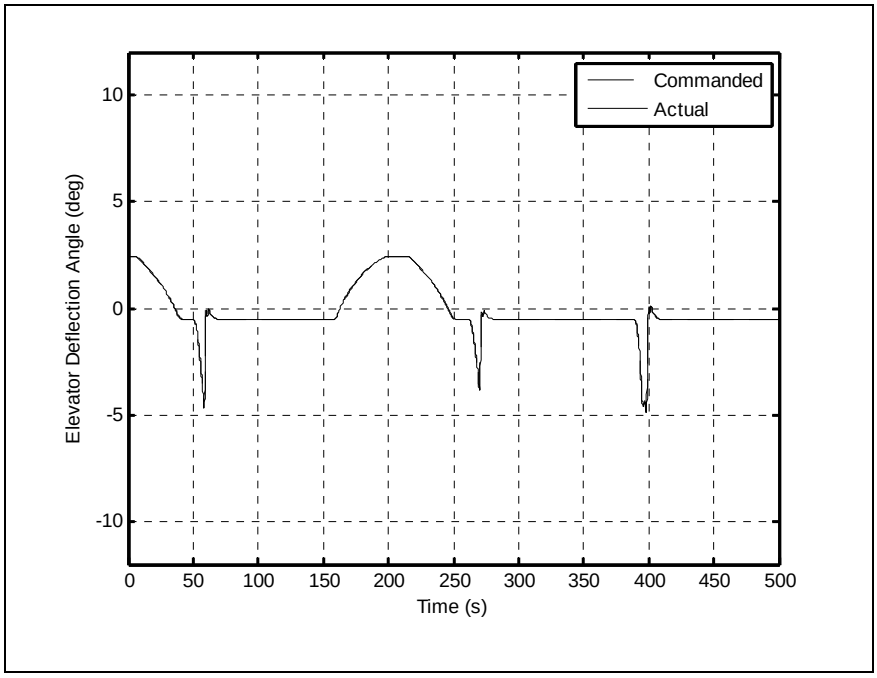

(e) Elevator Deflection Angle (deg)

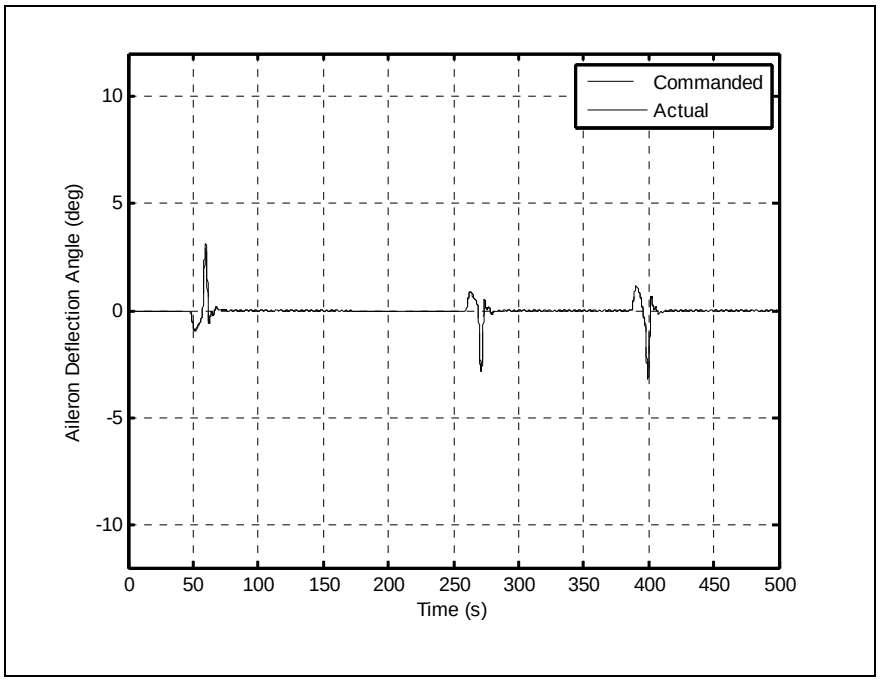

(f) Aileron Deflection Angle (deg)

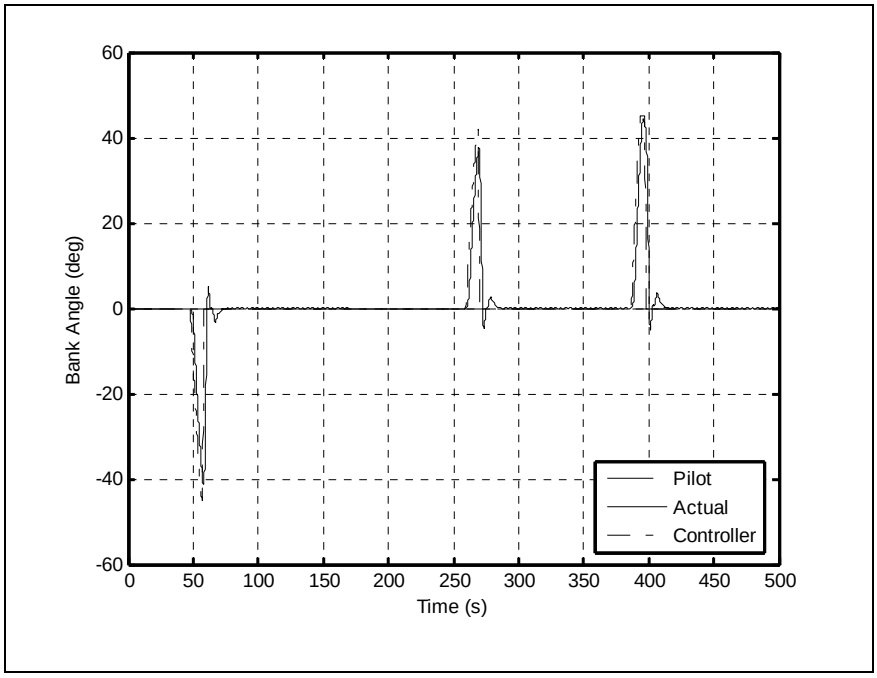

(g) Bank Angle (deg)

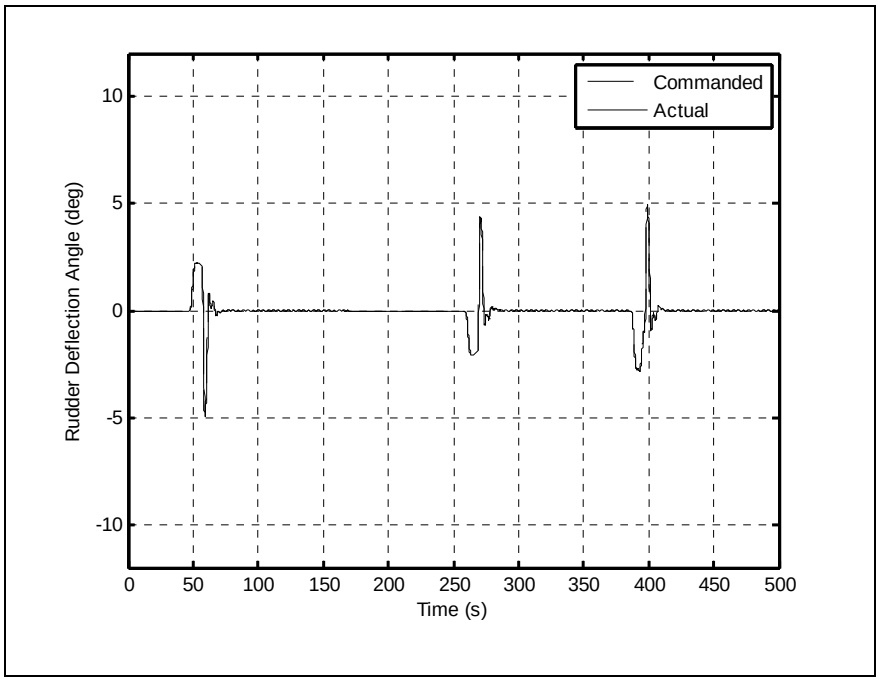

(h) Rudder Deflection Angle (deg)

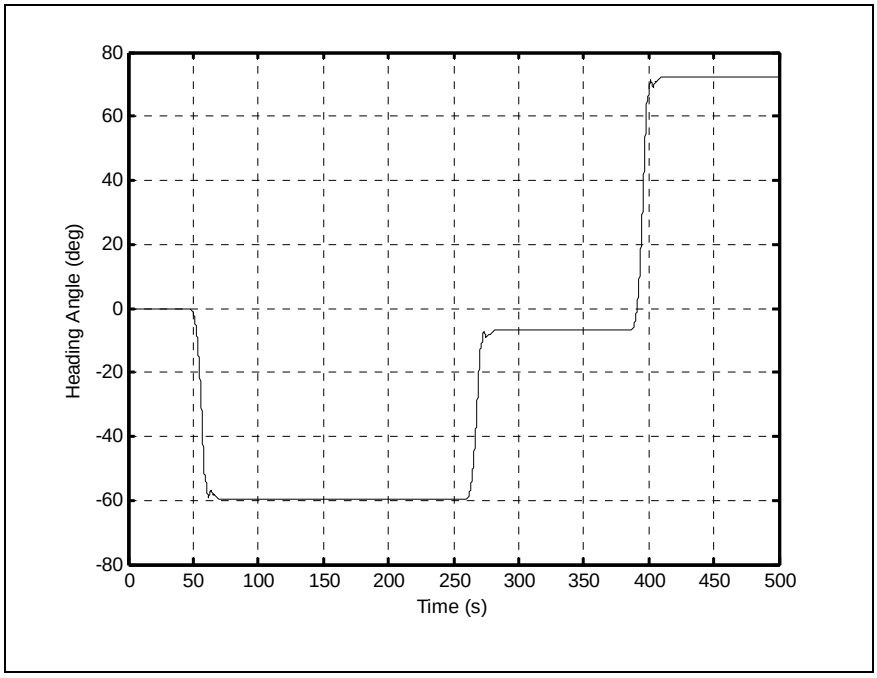

(i) Heading Angle (deg)

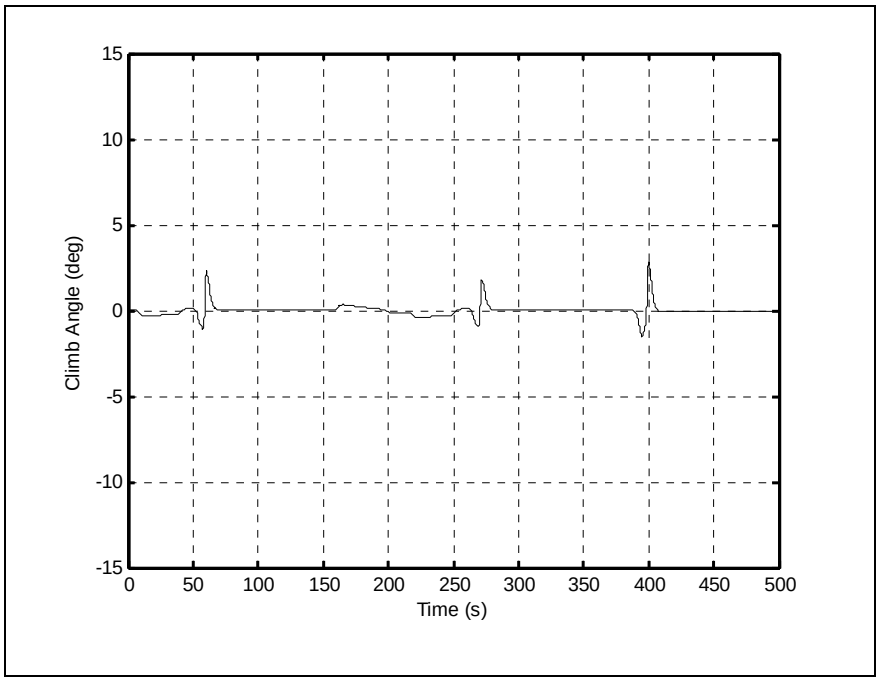

(j) Climb Angle (deg)

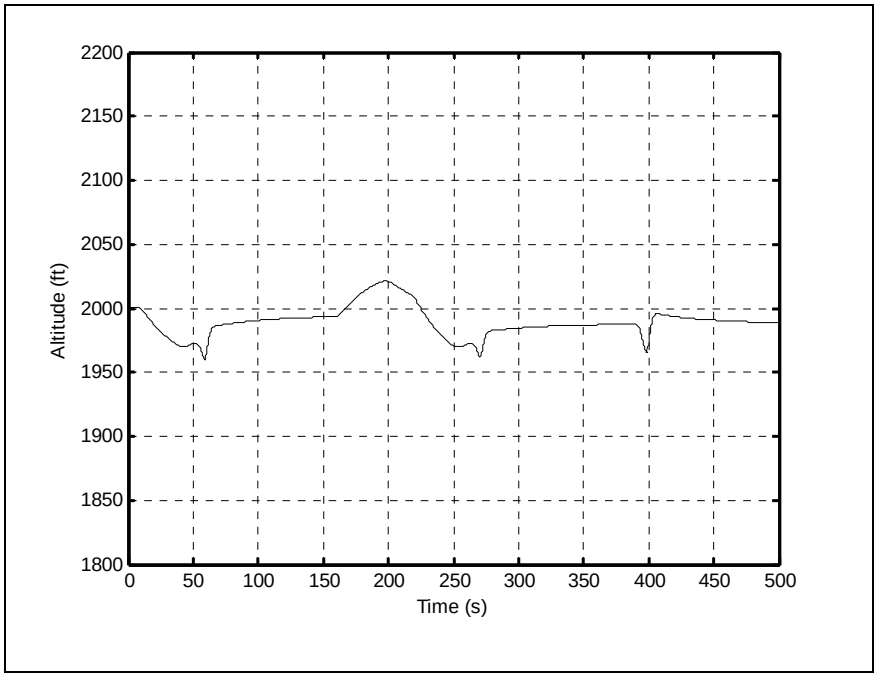

(k) Altitude (ft)

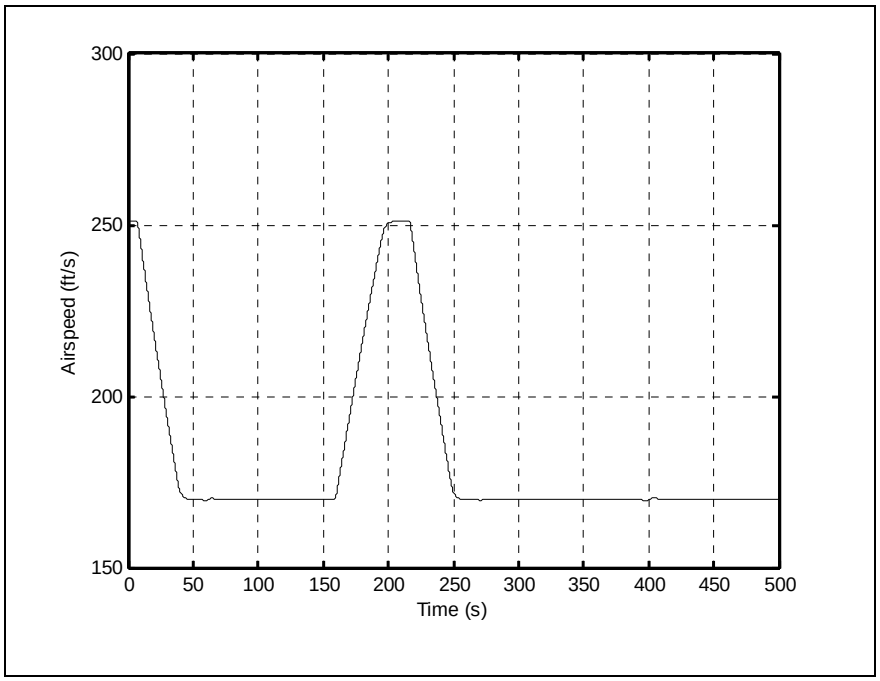

(l) Airspeed (ft/s)

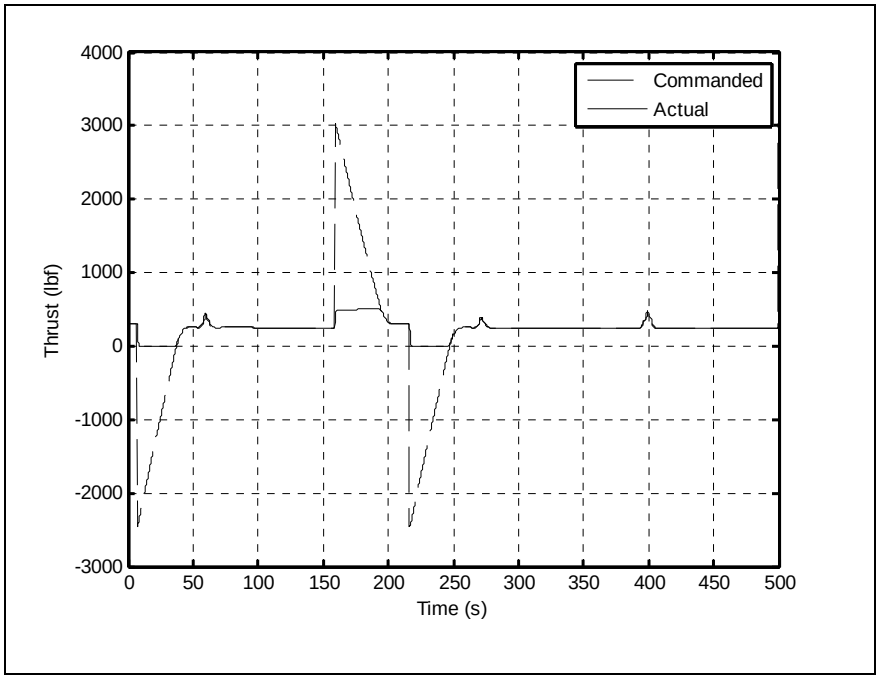

(m) Thrust (lbf)

Figure 4-7 Aircraft Trajectory and state variables for case 7

CHAPTER 5

CONCLUSION

An algorithm was developed and described for automatic avoidance of restricted airspaces. This method was developed specifically in conjunction with an advanced flight control system to keep a general aviation aircraft away from such restricted zones. Unlike other similar efforts, the present airspace avoidance system implemented two inputs to the aircraft; the bank angle required for a coordinated level turn, and the airspeed. Also, unlike the traditional safety systems such as TCAS that act in an advisory role, the current algorithm was designed to shift the burden of the aircraft control gradually away from the pilot and on to the automatic controller.

It was demonstrated that in order to implement this technique, the aircraft must be assigned an immediate domain whose size would have to depend on the aircraft performance and flight conditions. The algorithm was designed such that as the domain surrounding the aircraft approached that of the restricted airspace, aircraft control would switch gradually away from the pilot and to the controller, which would undertake an evasive maneuver. The degree of relative control was made dependant on the steepness of approach and the extent of the overlap between the aircraft domain and the restricted space. With this aim, the algorithm is developed first for avoidance of a single zone and later modified to handle multiple zones.

The implementation of the method was on a light single-engine general aviation aircraft was demonstrated. The aircraft was modeled in six degrees of freedom, including the effects of wind. All simulations were performed in Matlab/Simulink™ environment.

Simulation results were presented for six cases involving single zones and one case in the presence of multiple zones. The aircraft was made to approach the restricted zones with various airspeeds and attitudes with and without crosswind. It was shown that the controller would effectively prevent the aircraft from penetrating the prohibited area, while leaving the pilot some level of control.

In the course of this investigation, two major issues were identified for further research. The first pertained to the angle of approach. The algorithm described in this thesis employed an on/off technique for switching of the avoidance logic. This resulted in severe oscillations of the controls in some cases. A smoother switching of the control is thought to alleviate this problem and should be investigated further. The second item involves simultaneous control of the airspeed and the bank angle. While both parameters were employed in the algorithm presented in this document, no attempt was made at simultaneous optimization of the combination of the two. Investigation of such an optimization is very much in order to render the techniques truly multi-input/multi-output.

REFERENCES

LIST OF REFERENCES

1. Haines, T. B., "Flight of Mistakes," *AOPA Pilot*, Vol. 49, No. 1, January 2006, pp. 71-76.
2. "Homeland Security: Agency Resources Address Violations of Restricted Airspace, but Management Improvements Are Needed," GAO Report Number GAO-05-928T, July 21, 2005.
3. Evans, D., "Kudos for TCAS Stance," *Avionics Magazine*, Vol. 26, No. 1, Jan. 2002, pp. 44–46.
4. Cooper, J., "Controlled Flight into terrain," *Aerospace (UK) (0305-0831)*, Vol. 22, No. 2, Feb. 1995, pp. 16–19.
5. Snow, M. P. and Moroze, M. L., "Causes and Remedies of Controlled Flight Into Terrain in Military and Civil Aviation," Tech. rep., Vol.2, Air Force Research Laboratory, Wright-Patterson Air Force Base, Dayton OH, 1999, pp. 1143-1149.
6. Scott, W. B., "Automatic GCAS: 'You Can't Fly Any Lower'," *Aviation Week and Space Technology*, Vol. 150, No. 5, Feb. 1999, pp. 76–79.
7. Evans, D., "Anti-Hijacking Avionics," *Avionics Magazine*, Vol. 25, No. 11, Nov. 2001, pp. 53–54.
8. Evans, D., "Robolander Revisited," *Avionics Magazine*, Vol. 26, No. 3, March 2002, pp. 45–46.
9. Lee, E. A., "Soft Walls – Modifying Flight Control Systems to Limit the Flight Space of Commercial Aircraft – Draft 2," Revised from UCB/ERL Memorandum M001/31, University of California – Berkeley, October 2001.

10. Cataldo, J. A., Lee, E. A., and Liu, X., "Preliminary Version of a Two-Dimensional Technical Specification for SoftWalls," Technical Memorandum UCB/ERL M02/9, University of California – Berkeley, April 2002.

11. Cataldo, J. A., "Control Algorithms for Soft Walls," M.S. Research Project Report, Department of Electrical Engineering and Computer Sciences, University of California – Berkeley, January 2004.

12. Tomlin, C., Pappas, G. and Sastry, S., "Conflict Resolution in Air Traffic Management: A Study in Multi-Agent Hybrid Systems," *IEEE Transactions on Automatic Control*, Vol. 43, No. 4, April 1998, pp. 509–521.

13. Grootendorst, F. H., Brouwer, D. I. K., van Paassen, M. M. and Mulder, M., "Design of a Safety Augmentation System for Commercial Aircraft". *AIAA Guidance, Navigation, and Control Conference and Exhibit,* 16-19 August 2004.

14. Steck, J. E., Rokhsaz, K., Pesonen, U. J., and Duerksen, N., "An Advanced Flight Control System for General Aviation Application," SAE 2004-01-1807, *2005 SAE Aerospace Transactions*, July 2005, pp. 27-36.

15. Pesonen, U. J., Steck, J. E., Rokhsaz, K., Bruner, S., and Duerksen, N., "Adaptive Neural Network Inverse Controller for General Aviation Safety," *AIAA Journal of Guidance, Control, and Dynamics,* Vol. 27, No. 3, 2004.

16. Roskam, J., Airplane *Flight Dynamics and Automatic Flight Controls – Second Edition, DARcorporation,* 1995, pp. 21.

17. Anderson, J. D., *Introduction to Flight – Fifth Edition*, McGraw Hill, 2005, pp. 467.

18. Watanabe, Y., Calise, A., Johnson, E., Evers, J., "Minimum- Effort Guidance for Vision- Based Collision Avoidance," *AIAA Guidance, Navigation, and Control Conference and Exhibit*, Keystone, Colorado, August 21-24, 2006.